Design Analog FIR Filter for UWB Frequency Band

Von der Fakultät für Ingenieurwissenschaften
Abteilung Elektrotechnik und Informationstechnik
der Universität Duisburg-Essen
zur Erlangung des akademischen Grades
Doktor der Ingenieurwissenschaften
genehmigte Dissertation

von

Saeed Arafat

aus

Khan Younis

Gutachter: **Prof. Dr.-Ing. Klaus Solbach**
Gutachter: **Prof. Dr.-Ing. Ingolf Willms**

Tag der mündlichen Prüfung: 18.12.2014

To the memory of Tala & Rolf.

ACKNOWLEDGMENT

This Thesis has been developed and written during my time as research assistant (wissenschaftlicher Mitarbeiter) at Fachgebiet Hochfrequenztechnik (Institute of Microwave and RF Technology) at Universität Duisburg-Essen and was partially supported by the German Research Foundation (DFG) under the UKoLoS program.
Foremost, I would like to express my sincere gratitude to my supervisor Prof.Dr.-Ing. Klaus Solbach for the continuous support of my thesis and research, for his motivation, enthusiasm, and immense knowledge. His guidance helped me in all the time of research and writing of this thesis. For me, he is more than supervisor.
I am also grateful to Prof.Dr.-Ing. Ingolf Willms for his willingness to be part of the examination committee and for the time and effort he invested.
Moreover, I want to thank all members of the (Institute of Microwave and RF Technology) for providing an excellent and inspiring working atmosphere and in particular my room colleague Adam for the nice discussion not only about Antennas, Microwave, and RF Technology but also about other important things in life. A special thanks goes to the secretary of our institute Sabine. I would also like to thank Dr.Ing Markus Neinhüs for introducing me to this topic
I would also like to express my great thanks to my parents, for supporting me spiritually throughout my life. I will never truly be able to express my sincere appreciation to both of you. Also I cordially thank brothers and sisters and their families for their moral support, and prayers. Last, but certainly not least, I would like to thank my lovely wife for her continuous help, unfailing love and patience.

Saeed Arafat

Duisburg, August 2014

ABSTRACT

UWB technology has drawn great attention after it was regulated in February 2002 in the USA by the FCC[1] and in February 2007 in the EU[2]. What makes UWB systems unique is their large instantaneous bandwidth where up to 7.5 GHz in the USA or 2.5 GHz in the EU are license-free operation for commercial systems. In recent years, more interest has been put into UWB technology worldwide from both industrial and academic research. However, there are still challenges in making this technology live up to its full potential. The FIR filter principle is widely used in DSP[3], for the realization of filter responses with prescribed frequency behavior. But only relatively few efforts have been made to produce a broadband **analog** FIR filter circuit for the microwave frequency range.The objective of this thesis is to develop a principle design of an analog FIR filter, which operates over the complete UWB band. In the course of the research different FIR filter concepts were studied and as a result several microwave components for UWB wireless communications applications were developed, in particular the new active node topology which replaces the earlier traveling wave topology in our FIR filter circuit. The final design was fabricated in MIC technology, and measurement results proved the possibility of building analog FIR filters in this technology and also validated the simulation results. Based on the characterization results for the active node prototype, designs for different applications for the analog FIR filter are presented such as adaptive analog filtering where a tunable analog filter is designed which operates over the complete UWB band and supports all filter types (highpass,lowpass, bandpass and bandstop). Each filter type is proven with a design example which tries to achieve useful results with a minimum filter order, thus keeping the circuit layout compact: The weighting coefficients with small values (close to 0) are omitted, but the delay line continues for the next nonzero coefficients. Another application is in transmit pulse shaping to fulfill the UWB spectrum mask requirements, with an extension to notch filters for transmit and receive which relieve the coexistence with existing narrowband radio systems and at the same time, protect the UWB receiver against interference coming from these. Additional degrees of freedom can be afforded when analog FIR filters are integrated in UWB antenna array beamforming networks: As one example for the more general concept of adaptive antenna, the generation of a frequency invariant radiation pattern for the EU UWB frequency band is presented and one example design proves the ability of insertion of frequency invariant pattern nulls in prescribed directions which can minimize (null) the received power from one or more interference sources.

[1]Federal Communications Commission
[2]European Union
[3]Digital Signal Processing

CONTENTS

Acknowledgment v

Abstract vi

List of Figures x

List of Tables xv

Acronyms and Symbols xvi

1 Introduction 1
- 1.1 UWB Technology . . . 1
- 1.2 State of the Art . . . 2
- 1.3 Objectives of the Thesis . . . 4
- 1.4 Thesis Organization . . . 4

2 Theoretical Background 6
- 2.1 Basics of Ultra-Wide Bandwidth Radio . . . 6
- 2.2 UWB Communication System . . . 7
  - 2.2.1 Carrier-based UWB (CB-UWB) . . . 7
  - 2.2.2 Impulse-radio UWB IR-UWB[4] . . . 8
  - 2.2.3 UWB Signal and Spectrum . . . 8
- 2.3 Finite Impulse Response Filter (FIR) . . . 11
  - 2.3.1 FIR filter . . . 11
  - 2.3.2 FIR Filter Characteristics . . . 12
  - 2.3.3 Translation of Digital to Analog FIR Filter . . . 12
  - 2.3.4 Why Analog FIR Filter . . . 13

3 Practical Realization 14
- 3.1 Introduction . . . 14
  - 3.1.1 Grounded CoPlanar WaveGuide (GCPWG) . . . 15
  - 3.1.2 TRL Calibration . . . 16
- 3.2 Analog UWB FIR Filter . . . 17

[4]Impulse Radio Ultra Wideband

3.2.1 FIR Filter Components . . . 17
3.2.1.1 Bi-phase divider . . . 17
3.3 Triple Line Analog UWB FIR Filter . . . 20
3.3.1 Weighting Stage . . . 21
3.3.1.1 High Input Impedance . . . 22
3.3.1.2 Amplitude Control Unit . . . 22
3.3.1.3 High Output Impedance . . . 22
3.4 Triple Line Active Node Topology . . . 24
3.4.1 Active Node Concept Components . . . 24
3.4.1.1 Bi-Phase Divider . . . 25
3.5 FIR Single Tap . . . 31
3.5.1 FIR Single Tap Measurements . . . 32
3.5.2 From Measurements to Simulation . . . 34
3.5.2.1 Generating ADS Model for Measurement Data . . . 34
3.5.3 Advantages of Using the Node Concept . . . 35

4 FIR Adaptive Filter 36
4.1 Introduction . . . 36
4.1.1 Filter Types . . . 36
4.1.1.1 Lowpass Filter LPF: . . . 38
4.1.1.2 Highpass Filters HPF . . . 38
4.1.1.3 Bandpass Filters BPF: . . . 38
4.1.1.4 Bandstop Filters BSF: . . . 38
4.1.2 Group Delay . . . 39
4.2 Ideal Analog FIR Filter . . . 40
4.2.1 Ideal Analog FIR Filter Implemented in ADS Circuit Simulator . . . 40
4.2.2 Ideal FIR Tap Filter versus Measured One . . . 42
4.3 Adaptive FIR Filter . . . 44
4.4 Optimization of Filter Coefficients . . . 45
4.5 FIR Filter as Lowpass Filter . . . 45
4.5.1 FIR as Tunable Lowpass Filter . . . 49
4.5.2 Compactness Design of LPF Filter . . . 51
4.6 FIR Filter as Bandpass Filter . . . 52
4.6.1 UWB Bandpass Filter . . . 53
4.6.1.1 Tunable Bandpass Filter . . . 54
4.6.1.2 Combined Bandpass Filter . . . 55
4.7 FIR Filter as Highpass Filter . . . 56
4.8 FIR Filter as Notch Filter . . . 59
4.8.1 Single Notch Frequency . . . 60
4.8.1.1 Dual Notch Filter . . . 63

5 Pulse Shaping Network 64
5.1 Introduction . . . 64
5.2 Gaussian Derivative Pulse Shaping . . . 65
5.2.1 First Derivative Gaussian Pulse . . . 65
5.2.2 Higher Order Gaussian Derivative . . . 66
5.3 Transversal Filter Pulse Shaping . . . 67
5.4 FIR Filter Pulse Shaping . . . 70
5.4.1 Ideal FIR Filter . . . 70
5.4.2 UWB FIR Pulse Shaper Design Exercise . . . 74

6 Antennas and FIR Filter **77**
6.1 Introduction . . . 77
6.2 UWB Antenna and Antenna Array . . . 77
6.2.1 Polarization . . . 78
6.2.2 Half-Power Beamwidth (HPBW), Sidelobe Level (SLL), and Nulls . 78
6.2.3 Directivity and Gain . . . 78
6.2.4 Mutual Coupling . . . 79
6.3 Antenna Array . . . 79
6.3.1 Introduction . . . 79
6.3.2 Array Types . . . 80
6.3.2.1 Linear Array (LA) . . . 80
6.3.2.2 Circular Array (CA) . . . 82
6.3.2.3 Different Array Geometries . . . 83
6.4 Phased Array . . . 84
6.4.1 Amplitude Weighting: . . . 86
6.4.2 Null Steering . . . 89
6.4.3 Design Procedure for wideband Array . . . 91
6.4.4 Design Example . . . 91
6.5 Beamforming . . . 96
6.5.1 Applications of Beamforming . . . 97
6.5.2 Beamforming Types . . . 98
6.5.2.1 Analog or Digital . . . 98
6.5.2.2 Fixed and Adaptive Beamforming. . . . 99
6.5.2.3 Narrowband and Wideband Beamforming . . . 100
6.6 Beamforming using FIR Filter . . . 102
6.6.1 FIR as Beamformer . . . 102
6.6.2 Calculating the Filter Coefficients: . . . 105
6.6.3 Design Example . . . 106

7 Conclusion and Future Work **110**

Bibliography **112**

LIST OF FIGURES

1.1 A history of UWB developments in the USA and the EU [Nek11]. 1
1.2 FCC and EC UWB mask. 2
1.3 Diagram of thesis organization. 5

2.1 UWB spectrum division into 14 sub-bands of 528 MHz each [Roh14]. . . . 7
2.2 An example of an IR-UWB based transceiver architecture. 8
2.3 (a) Time domain Gaussian pulse and its derivative (b) The equivalent power spectrum density with respect to the FCC power mask. 9
2.4 Comparison of (a) OOK[5], (b) PAM[6], (c) BPSK[7], and (d) PPM[8] [Pat03]. . 10
2.5 Principle block diagram of a FIR filter. 11
2.6 Translation of digital filter components to analog filter components. 13

3.1 Principle design of analog FIR filter 14
3.2 Single weighting unit [Nei08] 15
3.3 Top view (a) and cross section of the CBCPW (b) 16
3.4 TRL calibration standards used in all measurement at this work 17
3.5 Circuit design of FET transistor as bi-phase divider 18
3.6 Amplitude and phase imbalance 18
3.7 (a) Ring diode mixer circuit (b) In-phase and Out-phase output according to DC sign 19
3.8 (a) Insertion losses (b) Phase imbalance when applying different DC setting 19
3.9 (a) Insertion Losses (b) Phase Imbalance at different input power setting . 19
3.10 Bi-Phase power divider 20
3.11 Bi-Phase power divider amplitude and phase imbalance 20
3.12 Modified triple line analog UWB FIR filter 21
3.13 Single weighting stage components 21
3.14 Variable Voltage Attenuator (VVA) layout 22
3.15 Variable amplitude attenuation and relative phase 22
3.16 Measured S_{11} of low noise HEMT transistor 23
3.17 Manufactured single tap triple line analog UWB FIR filter 23

[5]On-off Keying
[6]Pulse Amplitude Modulation
[7]Binary Phase Shift Keying
[8]Pulse position Modulation

3.18 New implementation of UWB FIR filter 24
3.19 Splitter node components 25
3.20 UWB amplifier gain block circuit concept layout, schematic and manufactured device 25
3.21 S-Parameter and group delay of manufactured UWB amplifier 26
3.22 Setup for pulse distortion test caused by UWB gain block 26
3.23 Voltage and PSD of 5^{th} derivative Gaussian before and after 26
3.24 Resistive power divider (A) Schematic (B) Layout (C) Symbol 27
3.25 S-Parameter of the resistive power divider 27
3.26 Delay line using CPWG and reference line 28
3.27 Delay line measurement S-Parameter 28
3.28 Time impulse response of two different transmission lines 28
3.29 Resistive power combiner (a) Schematic (b) Layout (c) Symbol 29
3.30 Combiner measurements S-Parameter 30
3.31 Pi Attenuator 31
3.32 S-Parameter of 1dB Pi attenuator 31
3.33 Final FIR single tap layout 31
3.34 Prototype single tap FIR filter 32
3.35 S-Parameter measurements of single FIR tap (Transmission S_{xy}) 32
3.36 S-Parameter measurements of single FIR tap (Transmission S_{xx}) 33
3.37 S-Parameter measurements of single FIR tap (transmission S_{xx}) 33
3.38 Transmission S_{xy} over frequency (different filter coefficient) 34
3.39 Convert 5 measurement files to single file 34
3.40 Symbol will be used later on for FIR tap 35
3.41 Circuit model for n^{th} order FIR filter 35

4.1 Low pass filter frequency response parameters 37
4.2 Filter effects on a sweep frequency signal input signal 37
4.3 HPF frequency response and its parameters 38
4.4 BPF frequency response and its parameters 38
4.5 BSF frequency response and its parameters 39
4.6 S-Parameter and GD at Different Filter Types 39
4.7 S-Parameter and GD at different filter order 40
4.8 S-Parameter and GD at same filter order and at different bandwidth 40
4.9 Ideal FIR filter implementation using ADS 41
4.10 Screenshot of filter design and analysis tool in Matlab for filter design . . . 41
4.11 Attenuation of both LPF and its complementary HPF. Ideal FIR tap filter versus measured one 42
4.12 Comparison between ideal tap and measured FIR tap where filter coefficient $a_0 = 1$ and L is electrical delay. 43
4.13 Amplitude and phase of the transmission coefficient of the ideal FIR tap and measured one. 43
4.14 Universal tunable analog FIR filter concept. 44
4.15 Flowchart for design of the adaptive FIR filter. 44
4.16 Schematic of LPF FIR filter $N = 11$, where goals are defined as limit1 and limit2. 46
4.17 Transmission and reflection coefficients of a LPF FIR filter $N = 11$. 46
4.18 Insertion phase of a LPF FIR filter $N = 11$. 46
4.19 LPF insertion loss for different FIR filter order. 47

4.20 GD (red) and insertion loss (black) of LPF FIR filter with different order. . 48
4.21 GD at different filter order. 48
4.22 Tunable LPF filter. 49
4.23 Filter coefficients for different cutoff frequencies. 50
4.24 Insertion loss of FIR filter for different cut-off frequencies. 50
4.25 LPF performance at different τ 50
4.26 Zero inserted for small filter coefficients, as shown in Table 4.5 52
4.27 FCC and EC UWB mask 52
4.28 Schematic design of FIR BPF for FCC and EC requirements 53
4.29 Transmission coefficient of an UWB BPF with bandpass from 4 to 9 GHz . 53
4.30 GD of FIR bandpass filter 54
4.31 Insertion loss for FIR filter of different passbands. 54
4.32 Insertion loss and GD for FIR BPF designs. 55
4.33 Parallel transmission lines as periodic bandpass filter schematic design and insertion loss. 56
4.34 BPF performance with and without supplementary section. 56
4.35 Highpass filter design. 57
4.36 Insertion loss of HPF at different Cut-off frequencies. 58
4.37 Insertion Loss of HPF with different filter orders at same Cut-off frequency. 58
4.38 GD of HPF at $f_c = 8GHz$ and different filter order FIR filter as notch filter 58
4.39 Transversal notch filter. 60
4.40 Design and optimization of a notch filter at different frequencies. 60
4.41 Insertion loss of notch filter at different frequencies. 61
4.42 GD of notch filter at different notch frequencies. 61
4.43 Notch frequencies at different electrical length of delay sections with fixed filter coefficients. 61
4.44 GD at different electrical length of delay sections with fixed filter coefficients. 62
4.45 GD and insertion loss of a notch filter for different design optimizations at the same frequency. 63
4.46 Dual notch using adaptive FIR filter. 63

5.1 (a) Gaussian pulse derivative design concept, (b) Implementation of pulse derivative in ADS. 65
5.2 Simulation Result of the Gaussian pulse differentiator: (a) Input and Output pulses, (b) PSD for Input and Output pulses, (c) Ideal 2^{nd} derivative Gaussian pulse and the generated one, (d) PSD for both in Part C. 66
5.3 Two cascaded pulse differentiators to generate the second derivative of an Input pulse. 66
5.4 Three cascaded pulse differatiators to generate the 3^{rd} derivative of an Input Gaussian pulse. 67
5.5 Conventional transversal filter (series structure). 68
5.6 Modified transversal filter (parallel structure). 68
5.7 Implementaion of transversal filter (parallel structure) in ADS with variable time delay t_i 69
5.8 Output pulse amplitude and PSD after applying the modified transversal filter. 69
5.9 An optimized pulse shape fulfils the EC requirement for PSD. 70
5.10 Ideal FIR filter implementation Using ADS. 70
5.11 Optimization of Ideal FIR filter in ADS. 71

5.12 (a) 1^{st} Derivative Gaussian pulse, (b) Generated pulse using FIR filter. . . 71
5.13 (a) PSD of 1^{st} derivative Gaussian pulse, (b) PSD of generated pulse using FIR filter . . . 71
5.14 (a) 3^{rd} Derivative Gaussian pulse, (b) Generated pulse using FIR filter. . . 72
5.15 (a) 3^{rd} Derivative Gaussian pulse, (b) Generated pulse using FIR filter. . . 72
5.16 Amplitude and PSD before and after using FIR pulse shaper. 72
5.17 Pulse shaping using FIR filter. 73
5.18 Definition of pulse width under ADS. 73
5.19 Pulse width definition. 73
5.20 Pulse shaper optimization wit FIR filter, $N = 5$. 74
5.21 Concept and simulation setup of UWB FIR pulse shaper. 75
5.22 UWB pulse shaper optimized for FCC regulation. 75
5.23 UWB pulse shaper result optimized for ECC regulation. 75
5.24 Compact pulse shaper with supplementary section to improve efficient use of ECC mask. 76
5.25 Improved UWB pulse shaper for ECC mask. 76
5.26 Comparison of PSD performance of pulse shaper with and without the supplementary BPF section. 76

6.1 Linear array geometry. 81
6.2 Circular array configuration. 82
6.3 Comparison between ULA (right) and UCA (left) with 5-element $\lambda/2$ spacing and different steering angles. 83
6.4 (a) Three-dimensional radiation pattern for a 6x4 rectangular patch array. (b) Hemispherical 27 patch elements array [GLW98]. 84
6.5 (a)Phased array principle with amplitude weighting (b) Technical realization of PS using meander transmission line. 85
6.6 Radiation Pattern for a 9-element LA with Uniform, Cosine, Cosine-Squared and Triangular Distribution. 87
6.7 Amplitude weights of 8-element ULA by applying various window functions. 87
6.8 Radiation pattern of 8-element LA under various window functions. 88
6.9 Comparison of radiation patterns of 8-element LA with different window functions. 88
6.10 Beamforming and null forming in interference directions. 89
6.11 Weighting vector w_n using the LCMV algorithm for wideband. 90
6.12 Reference patterns designed using LCMV beamforming with null steering at $60°$ and $-60°$ and different main beam direction. 90
6.13 Normalized 5-element reference pattern with two nulls at $60°$ and $-60°$. . . 91
6.14 Resulting radiation pattern for $N = 5$ and $M = 5$. 92
6.15 Resulting radiation pattern for $N = 5$ and $M = 7$. 92
6.16 Resulting radiation pattern for $N = 7$ and $M = 5$. 93
6.17 Resulting radiation pattern for $N = 9$ and $M = 9$. 93
6.18 Correlation between reference and optimized pattern at different N and M. 94
6.19 $FNBW/2$ for a ULA as function of antenna element number N and $d = \lambda/2$ 94
6.20 8-Element ULA with different null position 95
6.21 Creating wideband null. 95
6.22 ECC band frequency invariant with wideband null at $30°$. 96
6.23 Three-dimensional plot showing the frequency invariant behavior of the design example for the ECC frequency band. 96

6.24 Concept of Beamforming System. 97
6.25 (a) Analog Beamforming (ABF). (b) Digital Beamforming (DBF). 99
6.26 Advantage of using Adaptive beamforming in compare to switched beamforming. 99
6.27 (a) Adaptive Digital beamforming (b) Mixed Beamforming based on Analog FIR Filter. 100
6.28 Phase characteristic versus frequency: (a) PS (b) TTD 101
6.29 Wideband ($FBW = 10\%$) beamforming using (a) Phase shift by PS frequency independent (b)Frequency dependent phase shift by TTD. 101
6.30 UWB ($FBW = 25\%$) beamforming using (a)Frequency independent phase shift by PS (b)Frequency dependent phase shift by TTD. 102
6.31 Desired Amplitude and Phase response of weights in a 4-element Array beamformer. 102
6.32 (a) N-element ULA Beamforming Using FIR filter (b) structure of a single M order FIR Filter 103
6.33 Example average correlation coefficient as a function of array element number N and filter order M. 106
6.34 Correlation Coefficient as a function of frequency at different beam direction, optimization is done for frequency band [6 - 8.5]GHz. 106
6.35 Radiation Pattern of 9-element ULA using FIR BFN with $M = 9$ at different main beam directions. 107
6.36 Correlation Coefficient as a function of frequency at different beam direction, optimization are done for frequency band [5.5 - 9]GHz. 107
6.37 Correlation factor as a function of antenna element N and filter order M with fractional bandwidth $f_h/f_l = 2$. 108
6.38 Filter coefficients for N=*20* and M=*20* for a ULA at different beam direction. 108

7.1 Transpose Triple Line Analog UWB FIR Filter 111

LIST OF TABLES

3.1 Pi attenuator resistors 30

4.1 Filter characteristics and description 37
4.2 Filter coefficients for LPF and conversion to HPF;$N = 11$ 42
4.3 Summarizes the filter coefficient and resultant residual for different filter order. 47
4.4 Filter coefficients for different cutoff frequencies. 49
4.5 Zeros inserted for FIR coefficients with value close to zero. 51
4.6 FIR coefficient at different passband frequencies. 55
4.7 Optimized coefficients for HPF at different Cut-off frequencies. 57
4.8 Filter coefficients for HPF at $fc = 8\,\mathrm{GHz}$ and different filter order. 59
4.9 FIR filter coefficients for different notch frequencies. 60
4.10 Filter coefficients for notch filter. 62

5.1 Computed utilization efficiency compared to FCC mask. 74
5.2 Computed utilization efficiency for ECC mask. 76

6.1 Radiation Characteristics for linear antennas with Uniform, Cosine, Cosine-Squared and Triangular Distribution [Sol12] 86
6.2 Beamforming Types. 98
6.3 Design Parameter for EU-UWB beamforming. 106

ACRONYMS AND SYMBOLS

Acronyms

ABF Analog Beamforming

ADS Advanced Design System

ADC Analog-to-Digital Converter

AF Array Factor

AOA Angle of Arrival

ASP Analog Signal Processing

AUT Antenna under Test

BER Bit Error Rate

BFN Beamforming Network

BPF Bandpass Filter

BSF Bandstop Filter

CAD Computer Aided Design

BPSK Binary Phase Shift Keying

CMOS Complementary Metal Oxide Semiconductor

CPW Coplanar Waveguide

CPWG Grounded Coplanar Waveguide

DAC Digital-to-Analog Converter

DBF Digital Beamforming

DC Direct Current

DOA Direction of Arrival

DSP Digital Signal Processing

ECC Electronics Communications Committee

EIRP Equivalent Isotropic Radiated Power

EC European Commission

EM Electromagnetic

EU European Union

FBW Fractional Bandwidth

FCC Federal Communications Commission

FDTD Finite Difference Time Domain

FET Field-effect Transistor

FIR Finite Impulse Response

FNBW First Null Beamwidth

FWHM Full Width at Half Maximum

GL Grating Lobe

Gbps Gigabytes per Second

GPRS General Packet Radio Service

GPS Global Positioning System

GSM Global System for Mobile Communications

HPF Highpass Filter

HPBW Half-power Beamwidth

IC Integrated Circuit

IDFT Inverse Discrete Fourier Transformation

IEEE Institute of Electrical and Electronics Engineers

IF Intermediate Frequency

IIR Infinite Impulse Response

IR-UWB Impulse Radio Ultra Wideband

LAN Local Area Network

LCMV Linear Constrained Minimum

LNA Low Noise Amplifier

LOS Line of Sight

LPF Lowpass Filter

LPD Low Probability of Detection

LPI Low Probability of Interception

LTI Linear Time-Invariant

Mbps Megabit per Seconds

MC-UWB Multicarrier UWB

MIC Microwave Integrated Circuit

MIMO Multiple Input Multiple Output

MMIC Monolithic Microwave Integrated Circuit

NLOS Non Line of Sight

OFDM Orthogonal Frequency Division Multiplexing

OOK On-off Keying

PAM Pulse Amplitude Modulation

PCB Printed Circuit Board

PIN Positive Intrinsic Negative

PM Parks-McClellan

PPM Pulse position Modulation

PS Phase Shifter

PSD Power Spectral Density

RF Radio Frequency

RL Return Loss

RX,Rx Receiver

SIR Signal-to-Interference Ratio

SLL Sidelobe Level

SMD Surface Mounted device

SNR Signal-to-Noise-Ratio

TTD True-Time-Delay

TX,Tx Transmitter

UMTS Universal Mobile Telecommunications System

UCA Uniform Circular Array

ULA Uniform Linear Array

URA Uniform Rectangular Array

UWB Ultra Wideband

VGA Variable Gain Amplifier

VNA Vector Network Analyzer

VSWR Voltage Standing Wave Ratio

VVA Variable Voltage Amplifier

WBAN Wireless Body Area Networks

WLAN Wireless Local Area Network

WPAN Wireless Personal Area Network

Latin Symbols

a	Radius of circular antenna array
$\mathbf{A}$	Vector potential
A_θ, A_φ	Elevation and Azimuthal components of the vector potential
$\mathbf{A}_{\mathrm{SN}}$	Coefficient of beamforming network
a_m	Weighting coefficients
a_{nm}	FIR filter coefficients
B	Signal Bandwidth
d	Inter-element spacing for antenna array
D	Directivity
$\mathbf{e}_r$, $\mathbf{e}_\theta$, $\mathbf{e}_\varphi$	Unit vectors in spherical coordinates
$\mathbf{E}$	Electric field vector
f	Frequency
f_0	Center frequency
f_{H}	Higher cut-off frequency
f_{l}	Lower cut-off frequency
F	Array facor
G	Gain
h	Impulse response vector
H	Transfer function vector
h_{FIR}	FIR filter impulse response
H_{FIR}	FIR filter transfer function
H_{ref}	Reference transfer function
H_{SN}	Transfer function of beamforming network
j	Imaginary unit
k	Wave number
l_n	Delay line behind the nth antenna element
p	Pulse in time domain
P	Spectrum of pulse
p_n	Gauss pulse nth order in time domain
P_n	Gauss pulse nth order in frequency domain
M	Filter order
N	Number of antennas
r	Distance
S_{11}	Input reflection parameter
S_{21}	Forward transmission parameter
S_{12}	Reverse transmission parameter
S_{22}	Output reflection parameter
t	time
$t_{0,n}$	Spatial delay of the nth antenna element

T_P	Pulse width
w_n	Complex weighting coefficient for the nth antenna element
x, y, z	Cartesian coordination
x_n	Recived signal from the nth antenna element
y_n	Output signal of the nth filter
Z_0	Characteristics impedance

Greek Symbols

α	Attenuation
β	Phase coefficient
$\Delta\varphi$	Phase different
ε_r	Dielectric constant
$\varepsilon_\mathrm{r,eff}$	Effective dielectric constant
φ	Azimuth angle
φ_n	Angular position of the nth element
λ	Wavelength
μ	Permeability
θ	Elevation angle
ρ	Correlation coefficient
$\overline{\rho}$	Average correlation coefficient
σ	Stander deviation
τ	Time delay
τ	Discrete time delay for a filter
τ_n	Time delay after the nth element
ω	Angular frequency
ψ	Phase difference between antenna elements

Constants

c_0	$2,998 \cdot 10^8\,\mathrm{m/s}$	Velocity of light in vacuum
e	$2,718\ldots$	number of Euler
ε_0	$8,854\,\mathrm{As/Vm}$	Permittivity of the vacuum
μ_0	$4\pi \cdot 10^{-7}\,\mathrm{Vs/Am}$	Permeability of the vacuum
π	$3,14159\ldots$	

Operators and Mathematical Symbols

$\mathrm{cov}(\cdot)$	Covariance

$\mathrm{var}(\cdot)$	Variance
$\delta(\cdot)$	Dirac Delta Function
$(*)$	Convolution operator
$\mathrm{err}(\cdot)$	Error Function
$\mathcal{F}^{-1}$	Inverse Fourier transformation
$(\cdot)^H$	Hermitian (complex conjugate) transpose
max	Maximum
minimize	Main part of optimization problem
subject to	Constraints for optimization problem
$\mathrm{Re}\{\cdot\}$	Real part operator
$\propto$	Proportionality
∞	Infinity
$\forall$	for all

CHAPTER 1
INTRODUCTION

1.1 UWB Technology

UWB technology has drawn great attention after it was regulated in February 2002 in the USA by the FCC and the EU has also approved a UWB frequency spectrum. Fig 1.2 shows different frequency masks limits for the EU as well as the FCC. However, UWB radio has been used unintentionally over a hundred years ago, when Heinrich Hertz did his spark discharge experiment to transmit EM waves. Since then the use of sinusoidal carrier techniques was the dominant choice. UWB was not used again until the 1960s when the U.S. military used it for pulse transmission (impulse radio) for covert imaging, radar and stealth communications [ABS+05]. After the approval of new UWB standard multiple breakthroughs were realized in both commercial and military communication, which resulted in great interest in UWB system design and implementation in both academic and industry areas.

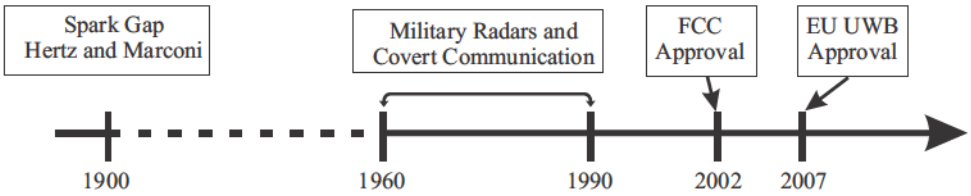

Fig. 1.1: A history of UWB developments in the USA and the EU [Nek11].

Under the UWB standards, UWB signals are defined as any signal that occupies more than 500 MHz in the band between 3.1 and 10.6 GHz or a relative bandwidth of larger than 20% and whose PSD[1] meets a given mask designed to introduce no interference to already deployed services, such as GPS[2], WPAN[3] and WLAN[4][KMO+06]. These existing narrowband systems will detect the UWB signal as noise, which can increase the system noise floor and negatively affect the performance of the system; therefore, the use of

[1]Power Spectral Density
[2]Global Positioning System
[3]Wireless Personal Area Network
[4]Wireless Local Area Network

UWB frequency spectrum is regulated very restrictively which places high requirements on UWB systems in terms of efficiency, sensitivity and increasing range. If the entire 7.5 GHz bandwidth is optimally utilized, the maximum power allowed to a transmitter is approximately 0.5 mW which is very low compared to the available power used in narrowband NB communication systems and will be very close to the noise floor and thus UWB technology can co-exist with the current (NB) technologies. On the other hand working close to noise level will offer good LPI[5] and LPD[6] which enables transmission of signal in a highly secured condition against intentional detection. The enormous allowed bandwidth of the system meant that UWB could potentially offer data rates of the order of Gbps[7]. Another advantage of having such wide range of frequency is that the signal would be able to penetrate through walls [OHI04].

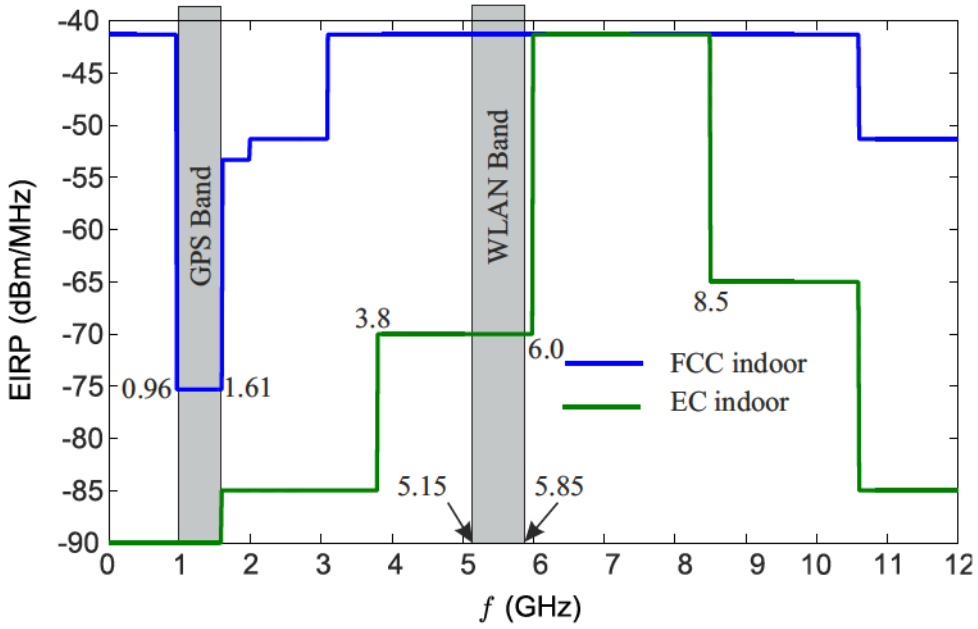

Fig. 1.2: FCC and EC UWB mask.

1.2 State of the Art

UWB systems can make use of the huge frequency band from 3.1 to 10.6 GHz in the USA and Asia and at least 6 to 8.5 GHz in the EU. These regulations as well as earlier interest in UWB have resulted in the UWB technology being regarded as one of the most promising wireless technologies. The technology promises to revolutionize very high data rate transmission over 2Gb/s for applications such as high-speed internet access, streaming content download (for example, video on demand, high-speed high-definition television (HDTV), home theater), real-time streaming, and wireless data bus for cable replacement [KZ10]. In recent years, more interest has been put into UWB technology worldwide from both industrial and academic research. However there are still challengers in making this technology live up to its full potential. The current signal processing systems on the market tend to utilize both analog and digital techniques depending on the

[5]Low Probability of Interception
[6]Low Probability of Detection
[7]Gigabytes per Second

required characteristics and functionality of the designed application. In many practical applications, the trend of techniques is clear and is going digital; however in many other applications there is still lack of clarity about which technique is best fit for each specific application. Digital signal processing (DSP) have some advantages, such as flexibility, reliability, repeatability and adaptively. Unfortunately, despite all of these advantages, one still cannot completely move to a pure DSP, but perhaps this will be possible in the near future, and until then we may have to continue using mixed-signal processing. Finite impulse response (FIR) filter principle is widely used in DSP for the realization of filter response with prescribed frequency behavior, only relatively few efforts have been made to produce a broadband analog FIR filter circuit for the microwave frequency range. In [NS11] an analog FIR filter is designed for the frequency range from 1.5 GHz to 2 GHz and even (to the author's knowledge) there is no MIC-technology analog FIR filter cover the UWB frequency band.

Tunability and adaptability for radio frequency (RF) and microwave circuits are highly desirable not only do they enhance the functionality and performance but they also reduce the circuit size, power consumption and cost. High performance RF tunable/adaptive filter are needed in reconfigurable system for efficient utilization of the available frequency spectrum, channel equalization, interference reduction, multipath reduction, or combinations of these processes [ZM07][CR90][Fu09]. Compared to fixed filters, a tunable filter promises greater functionality, better channel selectivity, reduced size and lower weight since the same hardware can be used at multiple bands [NGM+05]. However, the use of analog tunable filters in microwave frequency systems is still limited as some tunable analog filters are available but they still cover a narrow tuning bandwidth and most of them suffer from bulky size and relatively high insertion loss. Furthermore, they present only single type of filter art. For example, one cannot tune a LPF to be a HPF [Hit14][ZM07].

In many UWB applications, the signal's equivalent isotropically radiated power (EIRP) must conform to the regulation defined by the Federal Communication Commission (FCC). As a result, the closer the signal PSD conforms to the area under the FCC's PSD mask the more power the signal is able to transmit. This can be realized using pulse shaping (or pulse forming). Most research contributions on pulse shaper optimization and pulse design propose new theories or methods from the mathematical viewpoint without practical circuit implementation [TJ06] such as creating an optimal pulse through DSP implementation of a digital FIR filter which requires an immense computational effort [Pan09]. Analog technology proposals based on practical implementation techniques for pulse shaping suffer from large system dimension and/or only a single shape pulse is generated [RB08]. In [RB08], a well-designed adaptive arbitrary pulse shaper is presented, however it suffers from large size and cannot be used in UWB systems, as it does not fulfill the UWB spectrum mask requirements.

The conventional concepts of narrowband beamforming based on adjusting the phase shift of each antenna elements or in wideband beamforming by replacing the phase shifter by a true time delay are not able to provide a frequency invariant radiation pattern for the whole UWB frequency band. A common approach is to use the digital FIR filter for beamforming, however, digital beamforming still seems to be improper for microwave applications in the GHz-range due to an extremely high required sampling rate [Fou00] [NS11][Tex12][KMO+06][AG05].

1.3 Objectives of the Thesis

Most modern signal processing systems use a combination of analog and digital techniques in order to accomplish the desired function and take advantage of the best of both the analog and the digital world. Choosing the right technique might not always be clear and will depend on the expected functionality of the application [ABH+11]. As stated earlier digital signal processing (DSP) introduces multiple improvements including flexibility, reliability, repeatability, and adaptively. While these are great improvements over the analog signal processing technique, these improvements are not currently sufficient to adopt pure DSP techniques. Pure DSP might be possible in the future, in the meantime a use of mixed-signal processing will persist. The main disadvantage, beside power consumption and high cost, is the missing of ADC[8] with a high sampling rate; in order to satisfy the Nyquist criterion, one need a sampling frequency, $F_s \geq 2f_{max}$. Working in the UWB frequency band with $f_{max} = 10.6\,\text{GHz}$, which means F_s of at least $21\,\text{GHz}$; such an extremely high sample rate places great demand on ADC and is currently not feasible in low-cost applications. The 2012 state of the art supported RF-Sampling with $1.8\,\text{GHz}$ Nyquist bandwidth, which means $f_{max} \leq 1.8\,\text{GHz}$, and analog frequency down-conversion becomes a must, which increases system cost, size, and power. As a result, in this thesis the digital FIR will be realized in the analog form as an alternative. An analog FIR filter can offer benefits over a digital FIR filter in applications that require high-speed, low-power, and moderate degree of linearity. There are also situations in which an analog signal is desired at both input and output of the system. The use of analog FIR filter may be more efficient in terms of speed, power and circuit size than using an A/D followed by digital FIR filter and a D/A [NEHH+06][Tex12][KMO+06].
In recent years, there has been a considerable interest in the UWB technology and its applications in radar, communication systems, medical, etc. This opens the need for different UWB components, such as the UWB beamformer, pulse shaper, and adaptive filter.
In this thesis, a principle design of an analog FIR filter working over the complete UWB frequency band is developed. The processing architecture used by digital FIR filters will be used as the basis for the design. Furthermore, the implementation was done using the modified traveling wave concept presented in [Nei08]. While this concept has been proven for the frequency range from $1.5\,\text{GHz}$ to $2\,\text{GHz}$, there are many challenges in exploiting this concept for the complete UWB frequency band, in particular due to the parasitic effects of active and passive SMD components, and as a result a new topology was created replacing the traveling wave concept with the active node concept.

This thesis proposes the first realization of an analog MIC[9] technology FIR filter for the UWB frequency band, which opens the door for many application fields, for example, adaptive analog filtering, pulse shaping circuits and analog beamforming.

1.4 Thesis Organization

This thesis covers the design and implementation of an analog FIR filter, Fig 1.3 shows the chapter structure of this thesis, which is organized into seven chapters as follows: Chapter

[8] Analog-to-Digital Converter
[9] Microwave Integrated Circuit

2 reviews the basics of UWB Radio along with discussing its advantages, applications and standards. In addition, basic theory and mathematical frame work of FIR filter is introduced, and the chapter ends with the reasoning for choosing analog FIR filter. Next, Chapter 3 introduces the practical realization of an analog FIR filter. Presenting in detail the FIR filter components and the measurement results of each component. Moreover, the triple line concept is presented and the new topology is analyzed. A fabricated single tap FIR filter is measured. In chapter 4, the concept of adaptive filter is introduced, starting from ideal analog FIR filter design. In addition, the measurement results of the fabricated FIR filter are taken as the basis when optimizing different types of adaptive filter (lowpass filter, bandpass filter, highpass filter and notch filter). Chapter 5 concentrates on the pulse shaping networks, where different circuits for pulse shaping are discussed and verified with a design example for each method. The FIR filter as pulse shaper is also introduced. Chapter 6 presents a brief theory of UWB antenna and in particular to phased array with wideband beamforming using FIR filters. Finally, chapter 7 concludes the findings of the entire thesis, followed by suggestions for future work.

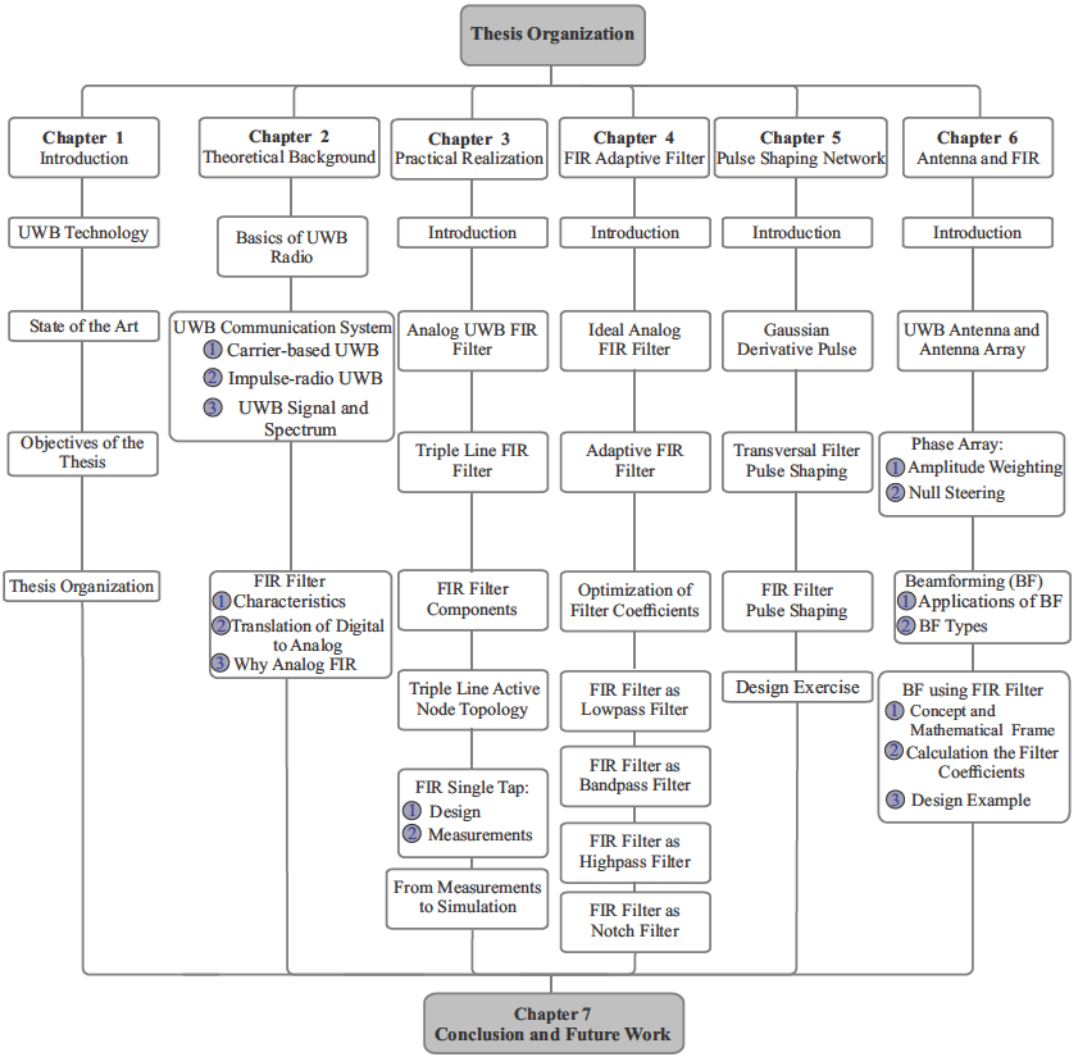

Fig. 1.3: Diagram of thesis organization.

CHAPTER 2

THEORETICAL BACKGROUND

As introduced in the previous chapter, the main focus of this thesis is to design an Analog FIR Filter for the UWB frequency band. In the following chapter an introduction to UWB technology will be presented, and the most important characteristics will be introduced. Furthermore, the theoretical background and a mathematical framework of FIR filters will be presented, starting from digital FIR filter components and translation of these components into analog, considering the advantages and disadvantages of FIR filters.

2.1 Basics of Ultra-Wide Bandwidth Radio

What makes UWB systems unique is their large instantaneous bandwidth where a few Giga Hertz, up to 7.5 GHz in the USA or 2.5 GHz in the EU are license-free operation for commercial systems. Although this spectrum overlays exiting users, its low power spectral density which is close to the noise level allows coexistence with existing narrowband radio systems and may cause very little interference. On the other side the UWB receiver should be protected against interference coming from such narrowband system. This kind of interference can either distort the pulse or saturate the RF front-end. Pulse shaping (see Chapter 5) provides a method for canceling narrowband interferes without distorting the UWB waveform. High data rates provided by UWB technology is also a typical feature of UWB technology and perhaps the most important aspect from a user's point of view. Replacing cables and going wireless and having high data rates will enable new applications and devices. This is now possible thanks to the large bandwidth provided by UWB. According to Shannon's theory in the case of a conventional narrowband system high data rate can be achieved by increasing signal power and the bandwidth. The channel capacity C can be calculated as follows:

$$C = B \ln(1 + S/N), \tag{2.1.1}$$

where B is the channel bandwidth in hertz, S is the signal power in watts, and N is the noise power in watts. Increasing the signal power will only logarithmically increase the channel capacity, but increasing bandwidth will increase it linearly, therefore, even at low power, high channel capacity can be achieved using UWB. Very short pulses allow high

temporal resolution which increases the possibility of high positioning accuracy compared to any other localization system operating at frequencies band below 10.6 GHz. Moreover, UWB systems can penetrate obstacles and thus operate under both LOS[1] and NLOS[2] conditions. This results in low fading margins, which provides robustness against multipath fading and is particularly attractive for indoor local area network (LAN) applications. UWB's low power spectral densities offer also good LPI and LPD which make it efficient for secure and military application [ACDB06][Ree05][GMK07][KMO+06][OHI04][CIW06]. The low power consumption of UWB based devices enable wireless connectivity for battery-operated portable devices where market considerations require that products be implemented in CMOS[3] technology in order to achieve low power, low cost, and very high data rates, besides integration with other devices [GRA03][INT07]. In general, the UWB transceiver is noticeably less complicated than that of a narrowband transceiver. This simplicity makes an all CMOS implementation of UWB transceivers possible, which lowers production costs [Ksh09].

2.2 UWB Communication System

UWB communication systems could be carrier-based or pulse-based communications:

2.2.1 Carrier-based UWB (CB-UWB)

In carrier-based UWB systems, usually the Orthogonal Frequency-Division Multiplexing, (OFDM) system is employed. E.g., the whole UWB spectrum is divided into 5 sub-band groups with 14 smaller non-overlapping sub-bands Fig 2.1. The bandwidth of a single sub-band is equal to 528 MHz.

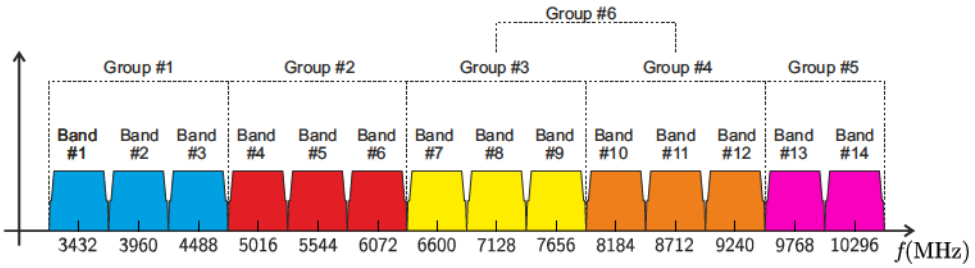

Fig. 2.1: UWB spectrum division into 14 sub-bands of 528 MHz each [Roh14].

An advantage of a multiband scheme is the ability to avoid sending signals in those frequency regions where a radio communication device is present. Disadvantages are the complexity in the transreceiver architecture which makes it not suitable for low cost and low power consumption devices [Sta07][Ksh09][RFSL04]

[1] Line of Sight
[2] Non Line of Sight
[3] Complementary Metal Oxide Semiconductor

2.2.2 Impulse-radio UWB IR-UWB

UWB systems have historically been based on impulse radio concepts. Impulse radio refers to the generation of a series of very short duration pulses, of the order of hundreds of picoseconds. Each pulse has a very wide spectrum which must adhere to the spectral mask requirements. Impulse radio has the significant advantage of being essentially a baseband technique [OHI04].

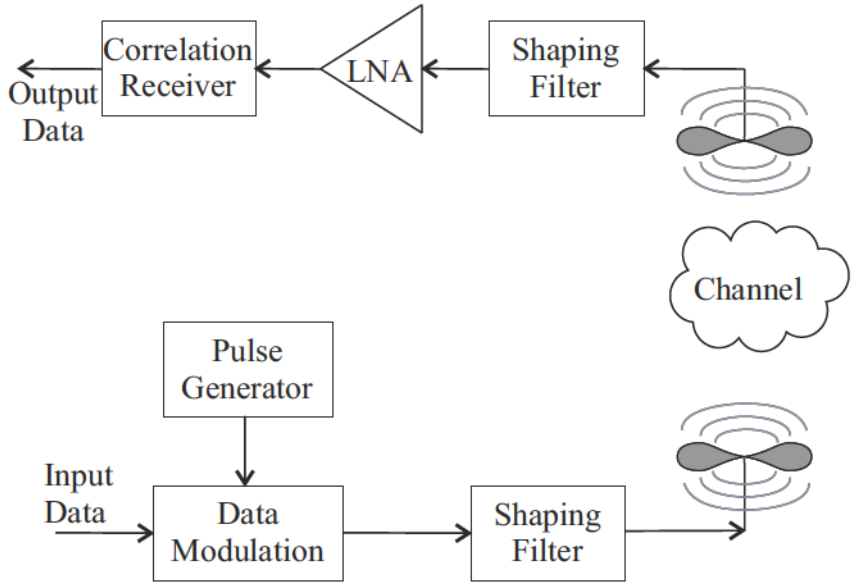

Fig. 2.2: An example of an IR-UWB based transceiver architecture.

As shown in Fig 2.2, the IR-UWB transceiver architecture is considerably less complicated than that of the narrowband transceiver, there is no need for power amplifier as the transmitted pulse level is low. Also because IR-UWB is carrierless, there is no need for mixers and local oscillators.

2.2.3 UWB Signal and Spectrum

As defined by the FCC, UWB signals are any signals having a bandwidth of greater than 500 MHz or a fractional bandwidth FBW[4] larger than 20%. The FBW can be defined as

$$FBW = \frac{BW}{f_c} = 2\frac{f_h - f_l}{f_h + f_l} \tag{2.2.1}$$

where f_c and BW are center frequency and bandwidth (defined at the -10 dB point of the spectrum) and f_h and f_l are the highest and lowest corner frequencies, respectively. A UWB signal can be any one of a variety of wideband signals, such as Gaussian, chirp, wavelet, or Hermite-based short-duration pulses. A summary of UWB pulse candidates is given in [AGG04]. The pulse needs to be narrow in order to benefit from the extremely

[4]Fractional Bandwidth

large available bandwidth. This section will concentrate in Gaussian pulses and its derivatives as it is the most common pulses used in the literature. Mathematically a Gaussian pulse power can be described as

$$p_0(t) = \frac{1}{\sqrt{2\pi\sigma^2}} e^{-(t-T_0)^2/(2\sigma^2)}, \tag{2.2.2}$$

where σ is the standard deviation of the Gaussian distribution and is related to pulse width T_p by $T_p = 2\pi\sigma$ and T_0 is the location in time for the midpoint of the pulse. The equivalent power spectrum density can be derived applying the Fourier transformation and is defined as

$$P_0(\omega) = e^{-\omega^2 \frac{\sigma^2}{2}} e^{-j\omega T_0}. \tag{2.2.3}$$

Based on Eq. 2.2.3, its n-th derivative can be determined from

$$p_n(t) = A_n \frac{\partial^n}{\partial t^n} e^{-(t-T_0)^2/(2\sigma^2)} \qquad \text{with} \qquad n \in \mathbb{N}_0, \tag{2.2.4}$$

where A_n is a constant and describes the pulse amplitude. The Fourier transform of the n-th order derivative pulse is

$$P_n(\omega) = A_n (j\omega)^n e^{-\omega^2 \frac{\sigma^2}{2}} e^{-j\omega T_0} \tag{2.2.5}$$

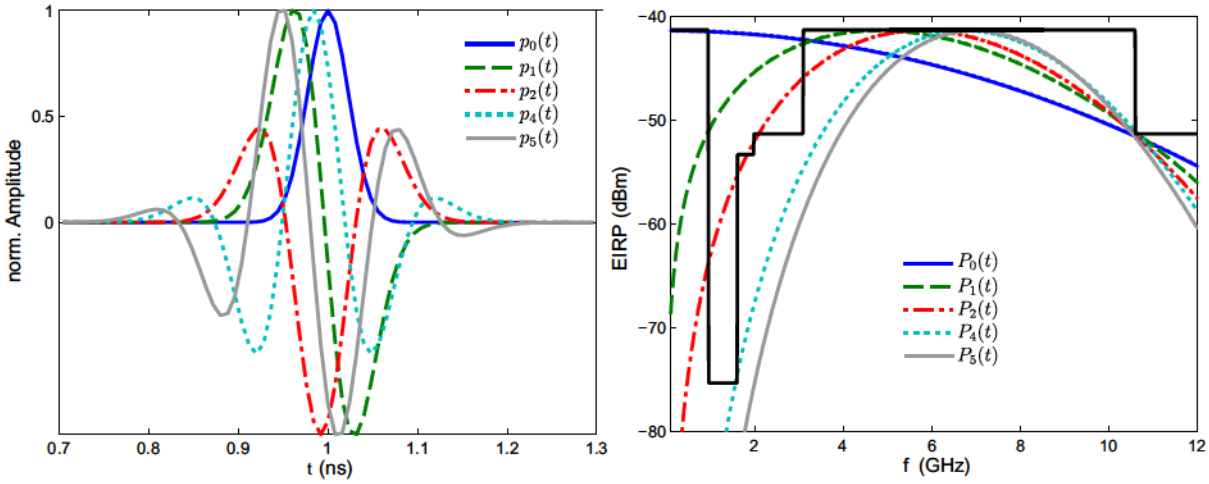

(a) (b)

Fig. 2.3: (a) Time domain Gaussian pulse and its derivative (b) The equivalent power spectrum density with respect to the FCC power mask.

Since the transmitted UWB signal is usually a baseband signal which directly generates the EM[5] wave, the basic pulse should not have a DC component. As a result, higher order derivatives are needed to allow effective radiation; this requirements is not necessary in carrier systems. Fig 2.3a shows the time domain waveform of a basic Gaussian pulse and its higher derivatives, while Fig 2.3b shows the frequency spectrum. The second derivative

[5]Electromagnetic

of the Gaussian pulse, known as the Gaussian monocycle, is often employed in impulse radio. Gaussian n^{th} derivatives are related to foregoing derivatives by:

$$p_n(t) = -\frac{n-1}{\sigma^2} p_{n-2}(t) - \frac{t}{\sigma^2} p_{n-1}(t) \quad \text{where} \quad n \geq 2 \tag{2.2.6}$$

where n is derivation order. As the order of the derivative increases, the number of zero crossings in time also increases; more zero crossings in the same pulse width correspond to a higher center frequency of a Gaussian pulse. To sum up, higher derivatives of the Gaussian pulse will move the center frequency higher and will reduce the bandwidth. By choosing the order of derivative and suitable pulse width one can find a pulse that complies with the FCC EIRP[6] mask. As shown in Fig 2.3b, one can observe that a 4^{th}-derivative Gaussian pulse slightly exceeds the FCC EIRP mask; while the 5^{th}-derivative Gaussian pulse complies with FCC EIRP mask, however is inefficient in using the FCC power mask.Chapter 5 will discuss in detail the generation and optimization of pulses which can efficiently use the allowed spectrum, and also discuss the effect of the antenna on the radiated pulse [AGG04][Nei08][SOH+03].

In order to transmit information using UWB pulses the digital information should be added to the analog pulse by means of modulation. In UWB systems there are several basic methods of modulation they will be mentioned briefly here and for more details refer to chapter 5 of [GMK07]. Four modulation schemes have been proposed for UWB systems. The first three are based on shape techniques and the forth is based on time techniques:

- On-Off Keying (OOK)
- Pulse Amplitude Modulation (PAM)
- Binary Phase Shift Keying (BPSK)
- Pulse Position Modulation (PPM)

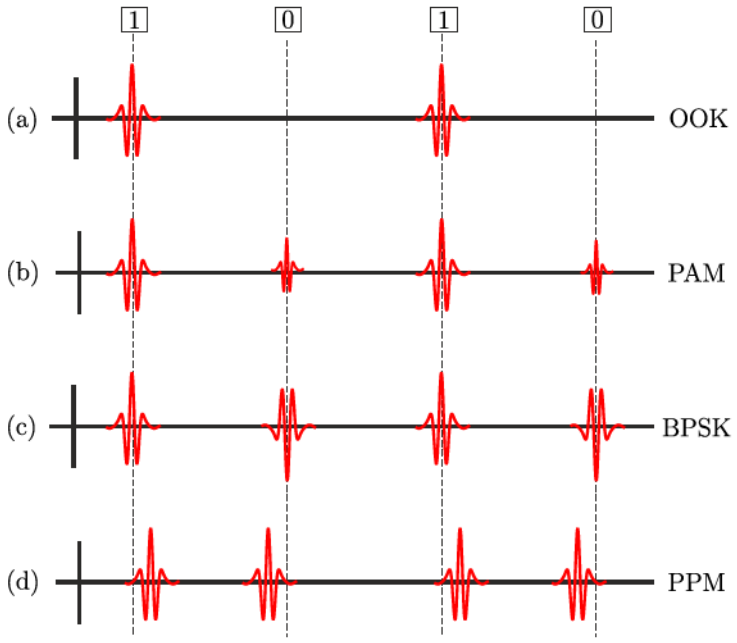

Fig. 2.4: Comparison of (a) OOK, (b) PAM, (c) BPSK, and (d) PPM [Pat03].

[6]Equivalent Isotropic Radiated Power

2.3 Finite Impulse Response Filter (FIR)

There are two fundamental types of digital filters: finite impulse response (FIR) and infinite impulse response (IIR). The FIR filter principle is widely used in digital signal processing, for the realization of filter responses with prescribed frequency behavior. Only relatively few efforts have been made to produce a broadband analog FIR filter circuit for the microwave frequency range. In [NS11] an analog FIR filter is designed for 20% fractional bandwidth from 1.5 GHz to 2 GHz but (to the author knowledge) there is no MIC-technology analog FIR filter covering the whole UWB frequency band. Unfortunately, the direct transposition of low-frequency design principles to the UWB frequency range is impeded by the lack of appropriate broadband, high-gain devices to realize operational amplifiers [Rau85]. In this section a theoretical background and a mathematical framework of FIR filters will be presented, starting from digital FIR filter components and translating them into analog, and considering the advantages and disadvantages of FIR filters.

2.3.1 FIR filter

The basic structure of a FIR filter is simply a tapped delay line and a combining line in which the delayed weighted signals from each tap are summed to generate the filter output; a block diagram of the filter is shown in Fig 2.5. At this point it should be mentioned that this diagram is valid for both the digital and the analog FIR filter structure. By adjusting the filter coefficients a_m one can almost realize any filter response with prescribed frequency behavior. Chapter 3 will discuss in detail the microwave analog FIR filter and its components.

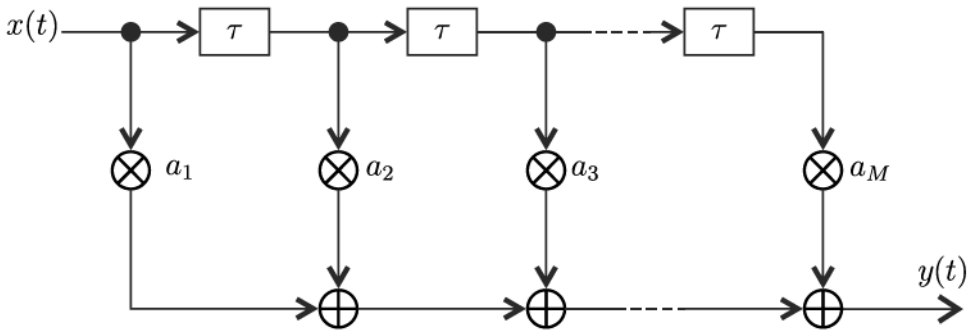

Fig. 2.5: Principle block diagram of a FIR filter.

The FIR filter can be represented mathematically in time domain as follows

$$\begin{aligned} y(t) &= a_1\, x(t) + a_2\, x(t-\tau) + a_3\, x(t-2\tau) + \ldots + a_M\, x\left(t-(M-1)\tau\right) \\ &= \sum_{m=1}^{M} a_m\, x\left(t-(m-1)\tau\right) \\ &= x(t) * \sum_{m=1}^{M} a_m\, \delta\left(t-(m-1)\tau\right). \end{aligned} \tag{2.3.1}$$

where the input signal $x(t)$ is weighted by weighting coefficients a_m and delayed by constant delay sections τ. The delayed and weighted versions of the input signal are summed together to create the filter output $y(t)$. The weighting coefficients are real (positive and negative) and can take a value

$$-1 \leq a_m \leq 1 \tag{2.3.2}$$

The incremental time delay τ is generally constant and is chosen as a function of the highest frequency f_h in the spectrum.

$$\tau = \frac{1}{2f_\mathrm{h}} \tag{2.3.3}$$

Converting Eq. 2.3.1 into the frequency-domain, yields the frequency response of the filter

$$H_\mathrm{FIR}(f) = \frac{Y(f)}{X(f)} = \sum_{m=1}^{M} a_m \, e^{-j2\pi f(m-1)\tau}. \tag{2.3.4}$$

In order to calculate the frequency response of a FIR filter, the number of taps and filter coefficients need to be estimated; normally this process is called filter design. The calculation of these coefficients will be introduced in section 6.6.2.

2.3.2 FIR Filter Characteristics

FIR filters possess certain desirable properties which make them attractive for both digital and analog applications. As the name indicates, the filter has a finite impulse response. Moreover, known as a non-recursive filter as has no feedback it is inherently stable. The filter is also said to be causal as the output is only dependent on the current and past inputs. One of the most important advantages, is that it can be designed with exactly linear phase: This can be done using symmetric or antisymmetric filter coefficients about the center of the filter. If the filter has an odd number of coefficients then the center coefficient will be the only coefficient without corresponding identical value. This linear phase results in a constant group delay with no amplitude distortion. In some applications the linear phase is not required. As a result, the symmetry of the filter coefficients is not important which can increase the degree of freedom during the design process since all filter coefficients are freely assignable. However FIR filters have some drawbacks: The most important are that it generally needs a much higher filter order than IIR filters to achieve a given filter response. Also, certain responses are not practical to implement with FIR filters. [Che02][RMP75][Fre94].

2.3.3 Translation of Digital to Analog FIR Filter

Digital filters can provide the same frequency characteristics as analog filters; a digital FIR filter is usually implemented by using a series of delay units, multiplier units, and adders as shown in Fig 2.6.

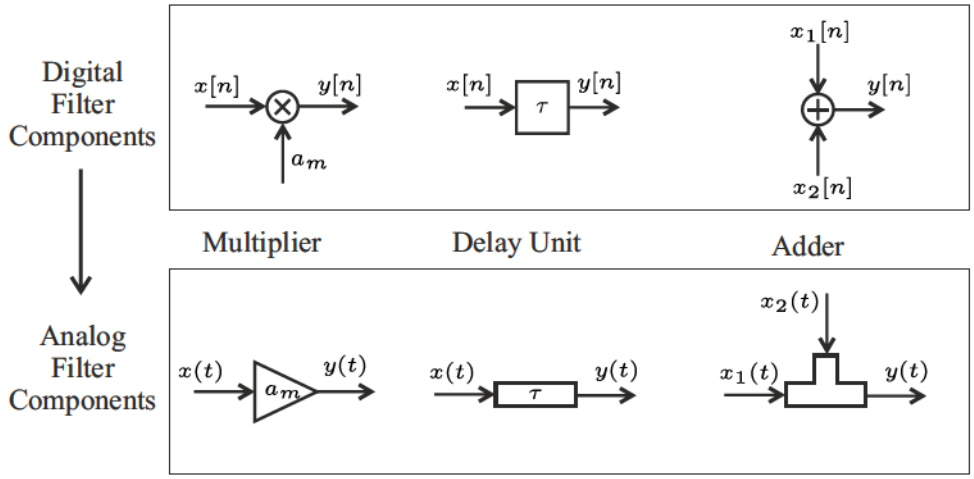

Fig. 2.6: Translation of digital filter components to analog filter components.

Fig 2.6 shows a way to translate digital filter components to analog microwave frequency components. In analog circuits, a multiplier can be realized in different ways: Firstly, as a passive component which include resistive splitters, Wilkinson dividers and combiners and secondly, using active devices which include a variable gain amplifier or voltage controlled amplifier. Moreover, a delay unit becomes a fixed length of microstrip transmission line. A discussion about implementation of delay units at microwave frequencies will be introduced in details in Chapter 3. Finally, adders can be realized by power combiners, with a simple T-junction of transmission line as the most simple case.

2.3.4 Why Analog FIR Filter

A review of techniques used for signal processing systems indicates that both analog and digital techniques are being used in various applications. This is the result of the inability of either technique to provide a complete solution that can meet the functional requirements for signal processing systems in various applications. While DSP continue to have the upper hand when it comes to flexibility, reliability, repeatability and adaptivity, some of the disadvantages of pure DSP like high levels of power consumption are delaying the full adoption of pure DSP. The main disadvantage, beside power consumption and high cost, is the missing of ADCs with a high sampling rate; in order to satisfy the Nyquist criterion, one need a sampling frequency, $F_s \geq 2f_{max}$. Considering the UWB frequency band with $f_{max} = 10.6\,\text{GHz}$, which means F_s of at least $21\,\text{GHz}$; such an extremely high sample rate places great demand on the ADC and is currently not feasible in low cost applications of, e.g., mobile communication. The 2012 state of the art in Software Defined Radio supported RF-Sampling with $1.8\,\text{GHz}$ Nyquist bandwidth, which means $f_{max} \leq 1.8\,\text{GHz}$, and analog frequency down-conversion become a must, which increases system cost, size, and power. As a result, an alternative, in this work is chosen to realize the digital FIR in the analog form. An analog FIR filter can offer benefits over a digital FIR filter in applications that require high-speed, low-power, and moderate degree of linearity. There are also situations in which an analog signal is desired at both input and output of the system, where the use of an analog FIR filter may be more efficient in terms of speed, power and circuit size than using an A/D converter followed by a digital FIR filter and a D/A converter [NEHH+06][Tex12][KMO+06].

CHAPTER 3

PRACTICAL REALIZATION

3.1 Introduction

Digital FIR filters are widely used in digital signal processing for the realization of filter responses with prescribed frequency behavior. The implementation of such filters can be done using standard digital hardware elements, unit delay, a multiplier, and an adder. This chapter will introduce the principle design of the analog FIR filter Fig 3.1. In order to implement it in microwave frequency range, the modified traveling wave concept will be used [Nei08] where part of the input signal is coupled in the weighting stage and the rest travel forward. The forward signal will be delayed by time delay τ and coupled again to the next weighting stage and so on until arriving to the end, where the transmission lines are terminated by match load to prevent the back reflection of signal. If there are enough filter taps, the signal arriving at the end will be weak, and as a result, the reflected signal will not affect the traveling forward signal as much. The output of every weighting stage will be coupled to the output transmission line and sum up together like this it will built the output signal $y(t)$. The other end of this output transmission line is terminated by a matched load. The principle looks similar (but not identical) to the design of traveling wave amplifiers; one main difference is the output signal contributions are not in-phase.

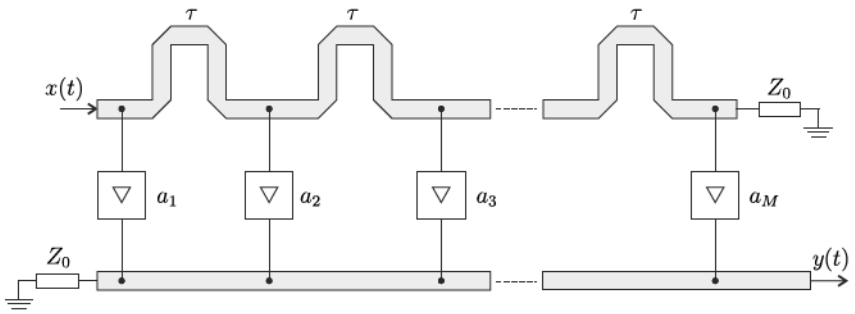

Fig. 3.1: Principle design of analog FIR filter

In this section, the microwave analog FIR filter and its component will be described in detail. Starting with the weighting stage (as shown in Fig 3.2 , where it consists mainly

of the active phase splitter, followed by the variable amplifier, and ending with the power combiner. The phase splitter will provide two output signals equal in amplitude, and have 180° out of phase. This is done by using an FET transistor where the output can be taken either from the source (in phase with the input signal) or from the drain (180° out of phase). An advantage of using an FET amplifier as a phase splitter is not having a heavy loading of the traveling wave signal, as the input impedance of a conventional FET transistor is high enough. As a result, a small part of the signal will be coupled with the weighting stage, and the rest can travel forward to the next weighting stage. There will be no need for gain block to compensate the heavy coupling of the forwarded traveling signal. The weighting stage was built using a variable gain amplifier, which will implement the filter coefficient. This can also be done digitally by using a digital control unit, which automatically translates the required filter coefficient by applying different bias conditions to the variable voltage amplifier.

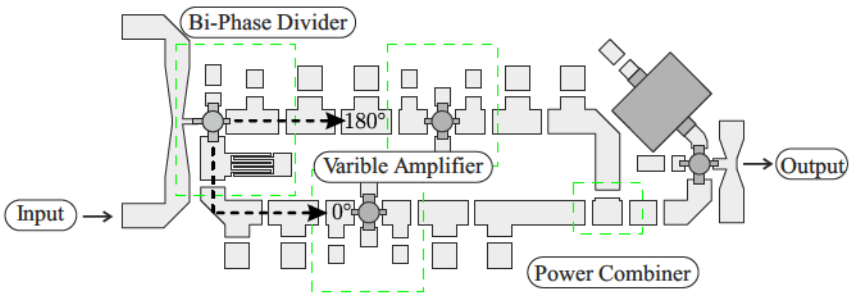

Fig. 3.2: Single weighting unit [Nei08]

Since only one path (either the in-phase or out-of-phase) should be conducting at a time, the variable amplifier will also act as a switch according to which one is active (applied DC bias). This means this branch is ON while the one without DC bias will be OFF. As the core design of the FIR filter is to be adaptive, and the filter coefficients should change its signs easily, there is need to have both branches excited and later on one will decide which one will be active. As a result, there needs to have a power combiner that will act not as a real combiner of multiple inputs, since only one input signal available. As mentioned before, only one branch will be active, dependent on the sign of the filter coefficient where it will have the value $-1 \leq a_m \leq 1$.
Before explaining in detail each component in the FIR filter, some basic information used in this thesis will be introduced, such as the calibration method and the type of transmission line used to fabricate the FIR filter.

3.1.1 Grounded CoPlanar WaveGuide (GCPWG)

The Grounded CoPlanar WaveGuide (GCPWG) is also referred to by some reference books as the Conductor Backed Coplanar Wave Guide (CBCPW). Conventional microstrip line (MSL) has a signal conductor at the top of the dielectric substrate and a ground plane at the bottom of the substrate. In the case of GCPWG, the signal conductor is replaced with a ground-signal-ground conductor as shown in Fig 3.3. The upper and bottom grounds are tied to each other by means of vias. Some drawbacks appear when the MSL is used at a higher frequency; for example, dispersion appears by MSL as changing of characteristic impedance of line over frequency, and the significant radiated

loss. Another drawback of MSL is the line width being wider, which means attaching the coaxial line will be harder, and therefore the MSL needs to be tapered and matched properly to the coaxial line. In terms of long transmission line losses, MSL still has lower insertion losses compared to GCPWG.

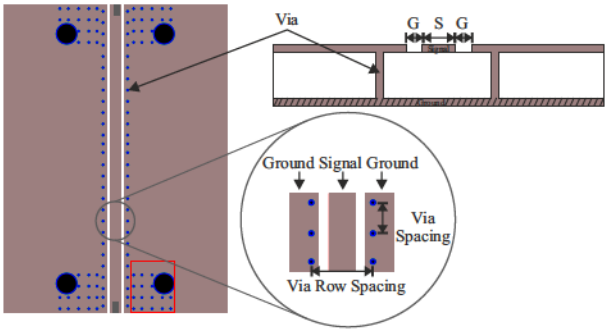

Fig. 3.3: Top view (a) and cross section of the CBCPW (b)

GCPWG addresses these drawbacks, as impedance is more stable over frequency. When the ground vias are properly implemented, there is a great reduction in radiated loss. And with GCPWG, where the geometry is largely arbitrary, there is the ability to choose line and ground widths that better match a coax line [Ros07]. Via spacing and via row spacing size is affects the useful bandwidth of the GCPWG, where vias will act as an electric wall. As a rule of thumb, the via spacing should be less than $\lambda/4$ at the highest frequency; for via row spacing, the closer the spacing between rows, the higher the cutoff frequency. With the help of lineCalc tools in ADS[1], one can calculate the signal width (center conductor (S)) and Gap (spacing (G)) between the center conductor and ground plane.

3.1.2 TRL Calibration

Starting to analyze and test every FIR component alone before combining them all together, the performance of the device under test (DUT) alone without the effect of extra transmission lines and connectors is important. One can then predict how the DUT will behave in the final complete FIR circuits. The network analyzer must be calibrated to cancel out this effect. The TRL (Thru, Reflect, Line) calibration method has some advantages compared to other calibration; for example, it is much simpler to realize a complete set of such standards. The TRL calibration, like other calibration methods, introduces a 12-term error correction vector for each frequency point [Agi12]. To calculate these terms, one needs to measure some standards which are: Short or open (Reflect), through line (Thru) which can be zero length or non-zero, and delay line (Line) which has electrical length longer than the (Thru). At each frequency, the phase difference between the (Thru) and the (Line) should be greater than 20° and less than 160°. This means that a single (Line) standard is only usable over an 8:1 frequency range; an extra delay line would be needed if the calibration frequency bandwidth is greater than 8:1. In this case, for the whole UWB frequency band, it is enough to use a single line. The fabricated standards are shown in Fig 3.4 . It is important that this standard is identical, and the only allowable difference between two lines is the extra electrical length. Precisely specifying the

[1] Advanced Design System

insertion losses of (Thru) or (Line) will not improve calibration accuracy. This standard has been fabricated and attached to board edge SMA connectors. Calculation and direct procedure of implementing TRL in Agilent network analyzer is mentioned in [Agi12].

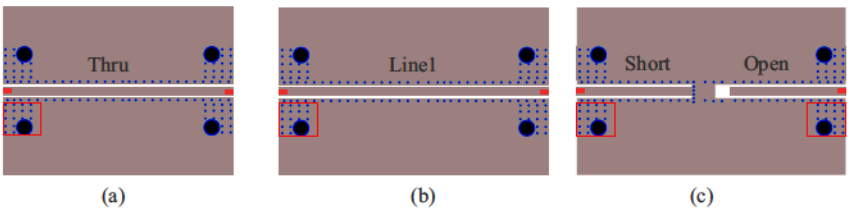

Fig. 3.4: TRL calibration standards used in all measurement at this work

3.2 Analog UWB FIR Filter

In recent years, there has been considerable interest in the UWB technology and its applications in radar and communication systems. This opens the need for different UWB components, such as the UWB beamformer, pulse shaper, and adaptive filter. In the following sections, the challenge faced in order to finally achieve an analog UWB FIR filter will be discussed in detail, which can solve some of the needs mentioned above.

3.2.1 FIR Filter Components

In this section, the analog FIR filter will be divided into two main components.

3.2.1.1 Bi-phase divider

Since the filter coefficient will ideally be between -1 and 1, there will be need for a bi-phase weighting stage. In the next section, different types of structure that have the ability to both invert the input signal, or divide it into two outputs equal in amplitude and having a 180° phase shift will be investigated.

3.2.1.1.1 FET Transistor as Bi-Phase Divider A bi-phase divider can be realized using the well-known feature of the FET transistor to provide two outputs equal in amplitude and having 180° degree out of phase. In [Nei08] the single FET shown in Fig 3.5(a) was used as bi-phase divider. At this frequency, from 0.76 to 2.6 GHz, the imbalance amplitude and phase were acceptable. Using the same structure was not possible for the whole UWB frequency band, not even by adding additional transistors to get more degrees of freedom in the design parameter and better control the phase and amplitude imbalance. Unfortunately the result did not match the design requirement as shown in Fig. 3.6. The amplitude and phase imbalance is far away from the tolerance interval. One source of this error could be the parasitic capacitance of the FET transistor at higher frequency.

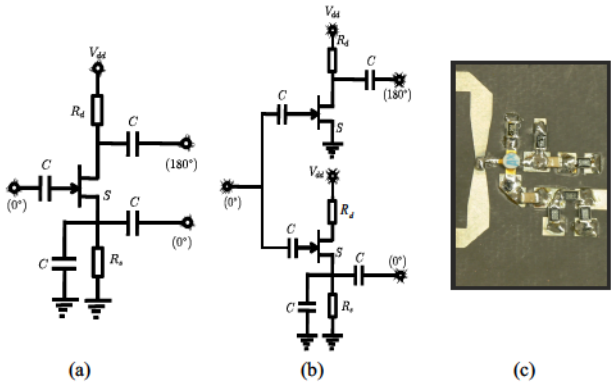

Fig. 3.5: Circuit design of FET transistor as bi-phase divider

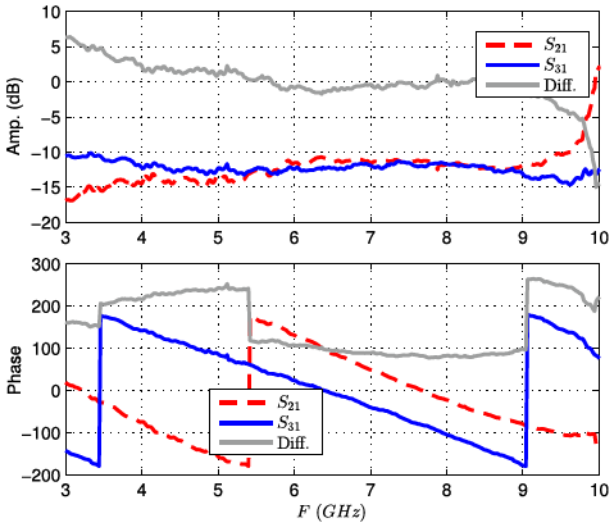

Fig. 3.6: Amplitude and phase imbalance

3.2.1.1.2 Ring Diode Mixer as Bi-phase Divider The built in center tap transformer inside the ring diode mixer with the help of the diode ring can provide bi-phase output according to which pair of diodes is biased. By using Radio Frequency (RF) and Local Oscillator (LO) as input or output signal and applying DC control to the Intermediate Frequency (IF), according to the sign of the DC, two diodes will be switched ON and the other two will be switched OFF as shown in 3.7(b). When applying a positive DC one will get diodes D2 and D4 ON which means output will be in phase, the 180° out of phase can be achieved by applying negative DC where diodes D1 and D3 will be ON and the output will be reversed which achieved 180° out of phase. Changing the diode forward voltage will give different insertion level. The disadvantage of using a ring diode mixer as bi-phase divider is its sensitivity to input power. The input power level should be high enough to ensure that the diode conduction is strong enough to achieve low noise and allow large signals to be converted without excessive spurious nonlinearity [Mix09]. The measurements were done with different input power levels. The measurements showed high dependency on the input power as the input power changed see Fig. 3.9. The variation of insertion losses and insertion phase is high and makes the use of the ring diode mixer as bi-phase divider impractical, while the phase imbalance is around ±15° in the whole UWB band as shown in measurement results in Fig. 3.8 and typical minimum insertion losses (conversion loss) are about 6 dB.

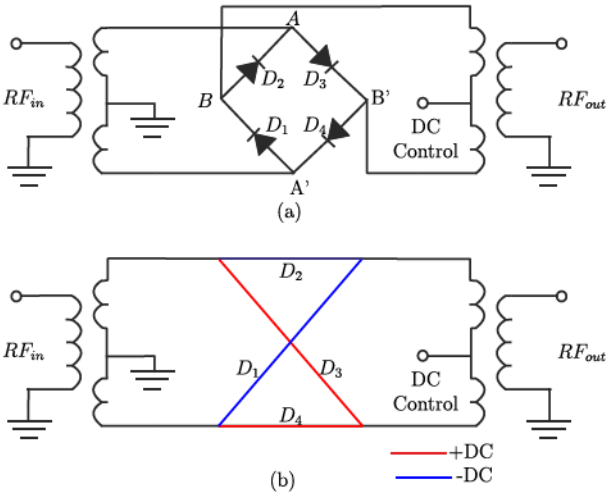

Fig. 3.7: (a) Ring diode mixer circuit (b) In-phase and Out-phase output according to DC sign

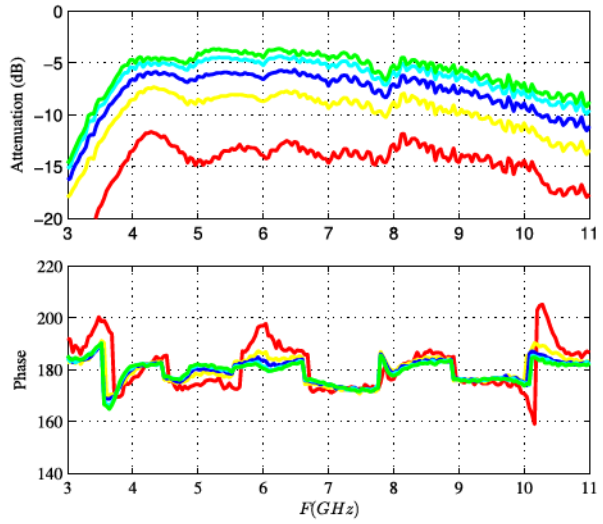

Fig. 3.8: (a) Insertion losses (b) Phase imbalance when applying different DC setting

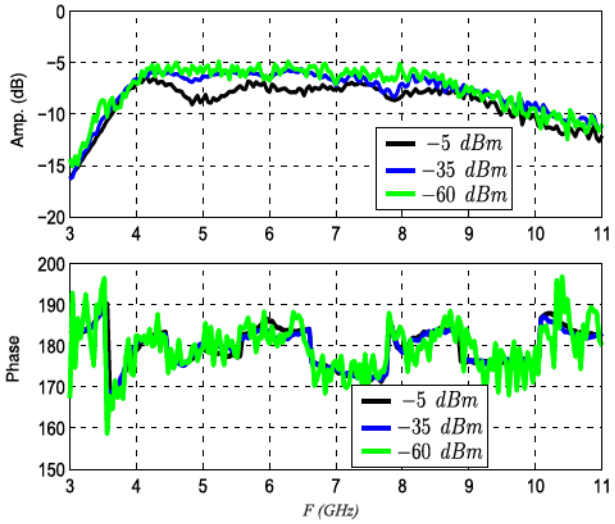

Fig. 3.9: (a) Insertion Losses (b) Phase Imbalance at different input power setting

3.2.1.1.3 Passive Bi-phase Divider In this section a compact passive bi-phase power divider with low insertion losses will be introduced. In order to convert the input port from microstrip line to slot line and again to microstrip line one needs a wideband transition [BA07]. This transition is formed by two complementary structures. First, the microstrip line is terminated with a capacitive circular disk, and second, a slot line is terminated with an inductive circular slot. The slot and the microstrip line (A-A') are electromagnetically coupled, this coupling will provide two outputs equal in amplitude and with a phase shift of 180°, this can be explained as if one look to the E field distribution on right and left side of the slot they have opposite direction which will be keep when it is coupled again to the microstrip line. The simulation where done using commercial available 3D EM field solver software called EMPIRE XCcel [Ims12] where very good agreement between simulation and measurement are achieved, the measurement results show low amplitude imbalance around $\pm 0.5\,\mathrm{dB}$ beside low insertion losses and $\pm 1°$ phase imbalance as shown in Fig. 3.11. As it was not possible to use the single FET transistor or ring mixer as bi-phase divider and it is decided to use the passive bi-phase divider some modification should apply to the principle presented in Fig. 3.1, as it will be explained in next section, keeping the same concept of traveling wave topology.

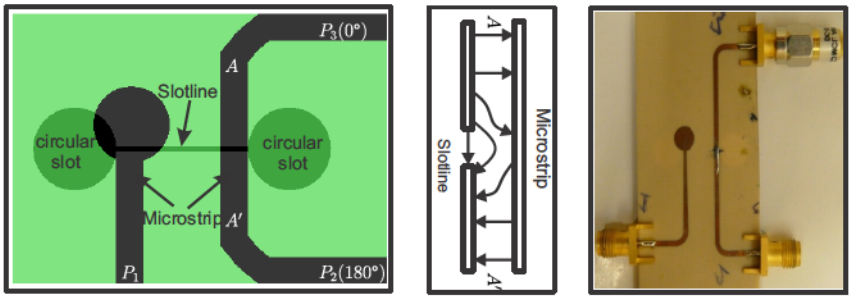

Fig. 3.10: Bi-Phase power divider

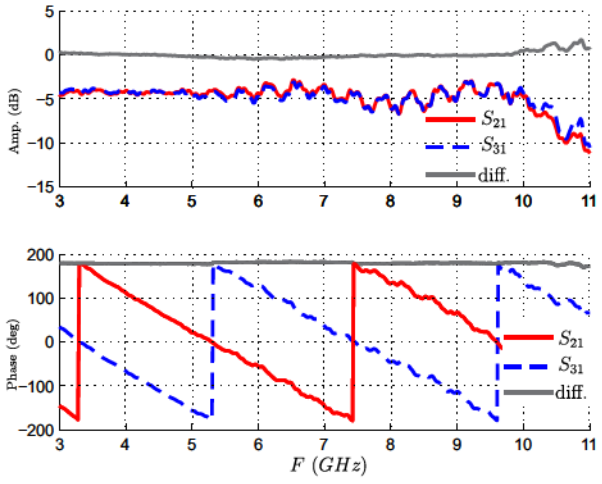

Fig. 3.11: Bi-Phase power divider amplitude and phase imbalance

3.3 Triple Line Analog UWB FIR Filter

The main change in this modified design is using the passive bi-phase divider, which creates two output transmission lines carrying the same signal amplitude, but having

180° phase shift. Keeping the same concept of having a traveling wave signal coupled by a weighting stage, in this case only one weighting stage conducting at a time (according to the sign of the filter coefficient, either positive or negative). In other words, the filter tap is represented by two weighting stages one is for positive filter coefficient, and the other for negative coefficient. Only one weighting stage is active at a time, according to the sign of the filter coefficient; for example, if the filter coefficient is positive, this will activate the weighting stage which is coupled with the in-phase signal. The FIR filter now looks like a triple line structure, as it has two input transmission lines and only one single output transmission line.

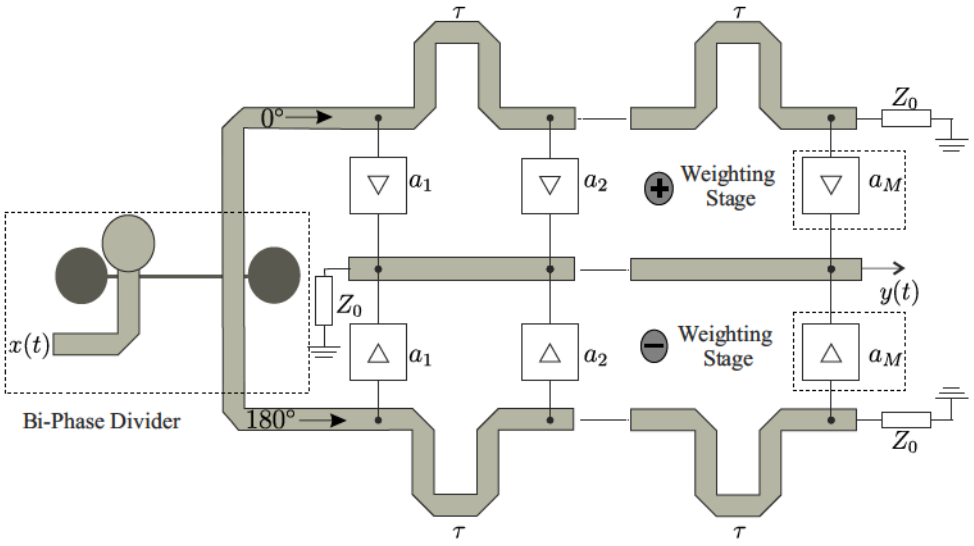

Fig. 3.12: Modified triple line analog UWB FIR filter

The new modified concept is shown in Fig. 3.12. In the next section, the main unit (weighting stage) to build this concept will be explained in detail.

3.3.1 Weighting Stage

Fig. 3.13 shows the weighting stage, which consists mainly of three parts:

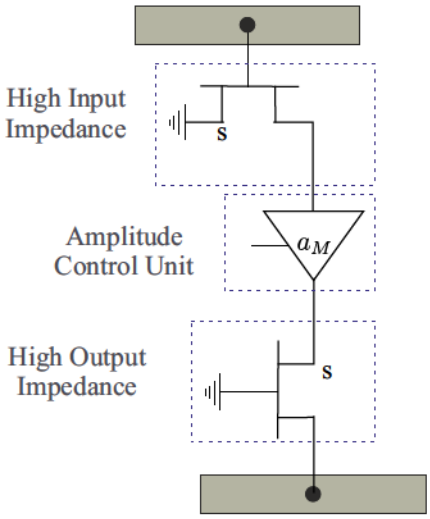

Fig. 3.13: Single weighting stage components

3.3.1.1 High Input Impedance

The input is built using the common source FET transistor (see Fig. 3.13). The gate/source terminal of FET will provide high input impedance, which is a very important requirement in order to realize the FIR filter using this concept. The forward traveling wave in input transmission line will not be overloaded by the weighting stage.

3.3.1.2 Amplitude Control Unit

In this case, the amplitude control unit, which will implement the FIR filter coefficients, will have the real value between 0 and 1. This can be done using a VVA[2]. The filter coefficients will be normalized to the highest gain which can be achieved by the VVA. The VVA should have constant gain in the whole UWB band, and a small group delay and good input output matching. The HMC34161C3B from Hittite was selected as the VVA; Fig. 3.14 shows the layout for testing the VVA and the measurement result is shown in Fig. 3.15, which provides almost constant amplitude and a proximately linear phase shift [ASA+09].This phase shift, dependent on the Filter coefficient, should be taken into account when one optimizing the whole FIR Filter performance.

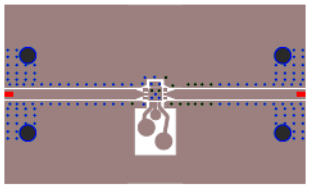

Fig. 3.14: Variable Voltage Attenuator (VVA) layout

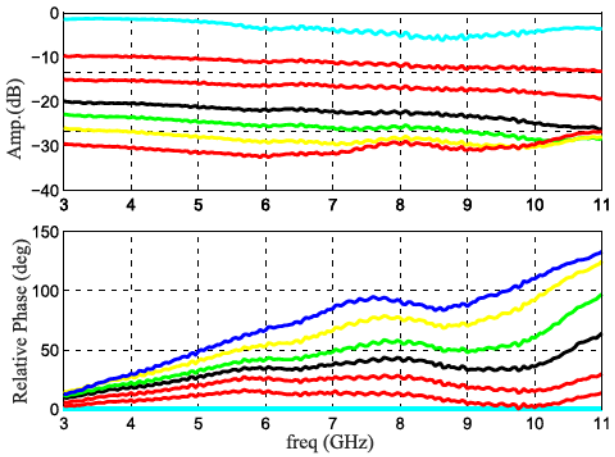

Fig. 3.15: Variable amplitude attenuation and relative phase

3.3.1.3 High Output Impedance

The output is built using the common gate FET transistor as it provides the highest output impedance possibility among all the FET amplifier structures (see Fig. 3.13). As it

[2]Variable Voltage Amplifier

was in the input transmission line, this is important for the implementation of FIR filter in order not to overload the output transmission line. Fig. 3.17 shows a full manufactured first order triple line analog UWB FIR filter, where all the FIR components are shown: bi-phase divider, input stage, weighting stage, and output stage. Unsurprisingly, the measurement result was not satisfying, as the performance of the SMD transistor could be optimized only to a narrow frequency band, but not for the whole UWB frequency band. This frequency, dependent on the input impedance of the transistor, will heavy overloaded the traveling wave in transmission line. The signal, after passing one single FIR tap beside it, will be highly attenuated; it will have a frequency dependent performance, meaning the amplitude will likely have a roll down performance with increasing frequency and high variation in amplitude. In order to compensate the heavy frequency dependence (Fig. 3.16) of a realistic SMD FET impedance, it becomes necessary to add amplifier and isolator stages to the FIR filter circuit (shown in Fig. 3.17).
As a consequence, the original design based on high-impedance input/output stages coupled to input/output transmission lines has to be given up, and replaced by a cascade of a resistive power dividers and power combiners with compensating gain stages.

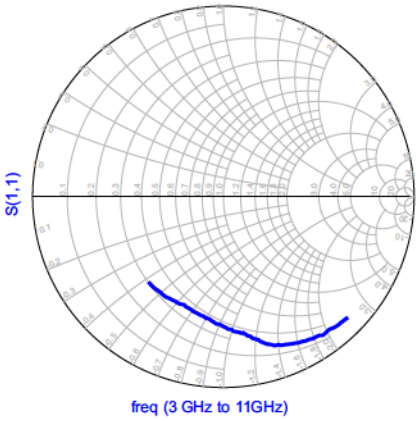

Fig. 3.16: Measured S_{11} of low noise HEMT transistor

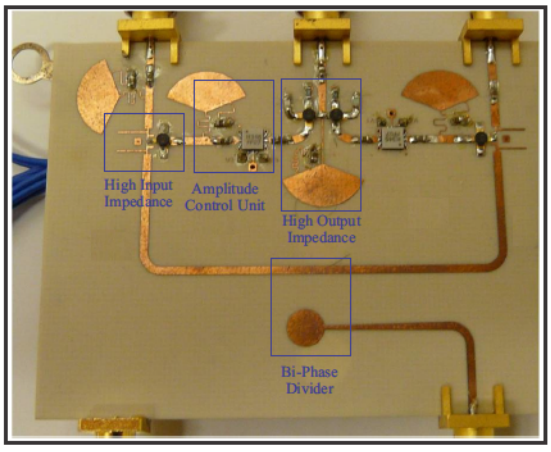

Fig. 3.17: Manufactured single tap triple line analog UWB FIR filter

The implantation of the UWB FIR filter with traveling wave concept using MIC technology is thus not possible. If the concept is implemented using the MMIC[3] technology, one

[3]Monolithic Microwave Integrated Circuit

could reduce the parasitic effect of active and passive SMD component, as well as transmission lines, since all these components will be integrated in the chip. One can therefore cover the UWB frequency band. One can also use the advantage of MMIC over MIC in design flexibility, broadband performance, reproducibility, reliability, low cost, and small size.

3.4 Triple Line Active Node Topology

The new topology will replace the traveling wave concept with a node concept where the input signal passes through a bi-phase divider. Instead of the travelling wave concept, cascading splitter nodes including the time delay are introduced. The second output of the splitter node will pass through the digital control unit (weighting stage) which simply is a variable voltage amplifier and will apply the filter coefficient. The combiner node will sum all output from splitter nodes and build a single output. Like in the previous concept, only one path ON at a time, according to the sign of the filter coefficients. The new proposed concept is depicted in Fig. 3.18, where a second order FIR filter is shown. In the next section, all components of the new proposed filter will be explained in details.

3.4.1 Active Node Concept Components

The Active Node consists of four parts:

1. Bi-Phase Passive Power Divider
2. Splitter Node
3. Digital Controlled Attenuator
4. Combiner Node

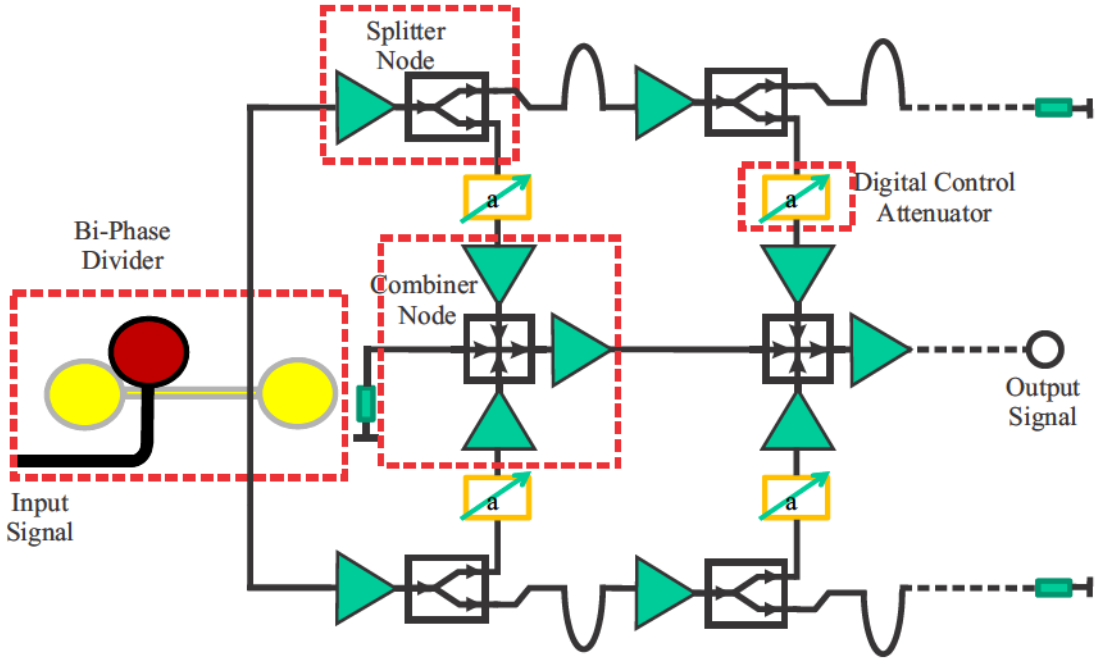

Fig. 3.18: New implementation of UWB FIR filter

3.4.1.1 Bi-Phase Divider

The bi-phase divider is has been explained in the previous section.

3.4.1.1.1 Splitter Node The input signal will be split into two equal signals, where the node consists mainly from:

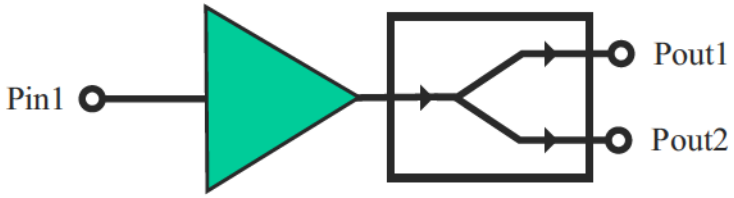

Fig. 3.19: Splitter node components

Gain Block As this gain block is the main unit in the FIR filter and will be used in every node, it should provide a flat gain over the whole frequency band, wideband input-output matching, good isolation between different filter taps, constant group delay, and (as for all amplifiers) a low noise performance. After investigating different types of broadband gain blocks, a commercially-available monolithic amplifier was selected, from the manufacturer Avago, VMMK-2503 [Ava12]. This gain block has a low noise figure and is easy to use, since it requires only positive DC voltage for bias. Also, matching impedance is not required, since it is internally matched to 50Ω; the only disadvantage is its gain roll-down (negative gain slope) by increasing frequency. To solve this, an extra gain roll-off stage is added, which is, in fact, an absorbing high-pass filter with positive gain slope. This will compensate the roll-down of amplifier gain and provide flat and constant gain. The concept circuit (the layout and manufactured example are presented in Fig. 3.20). One extra challenge using this gain block is that it has an advanced package which is not designed for hand soldering, but thanks to our workshop, they can solder it. When the gain block is damaged, re-soldering a new one is not possible. One needs to manufacture a completely new PCB.

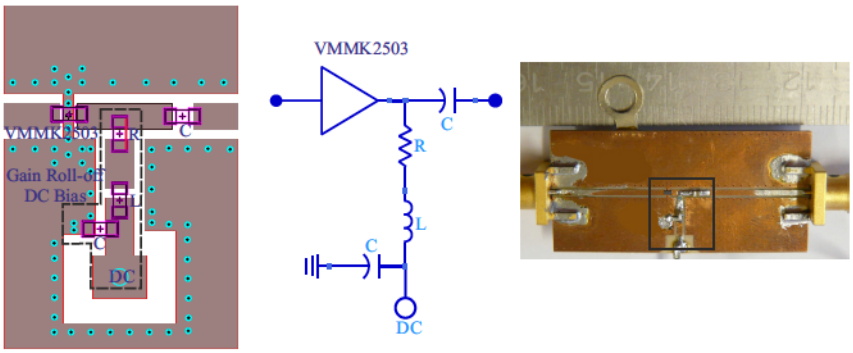

Fig. 3.20: UWB amplifier gain block circuit concept layout, schematic and manufactured device

The measurements in Fig. 3.21 result show a good input-output matching, better than 10 dB in the whole UWB frequency band, with a flat gain of 12 ± 0.5 dB and a small group delay (linear phase) of less than 0.2 ns. UWB gain block is unlike a common narrowband

gain block; it does not operate in a steady mode, but rather in short pulses. In order to see the influence of the UWB gain block at UWB short pulse, a 3rd order Gaussian pulse was selected to be the input of our gain block (as shown in Fig. 3.22). The output simulation results are given in Fig. 3.23, where it shows a little bit of distortion in the pulse. This happens as group delay is not constant at the whole frequency band, and this normally produces frequency dispersion as different frequencies propagate at different speeds. That is a reason why part of energy is moved to the second half of the pulse, as shown in the red curve of Fig. 3.23 (a). As the gain is really flat and almost frequency independent, there is no widening in the pulse, so both input and output pulses have the same pulse width.

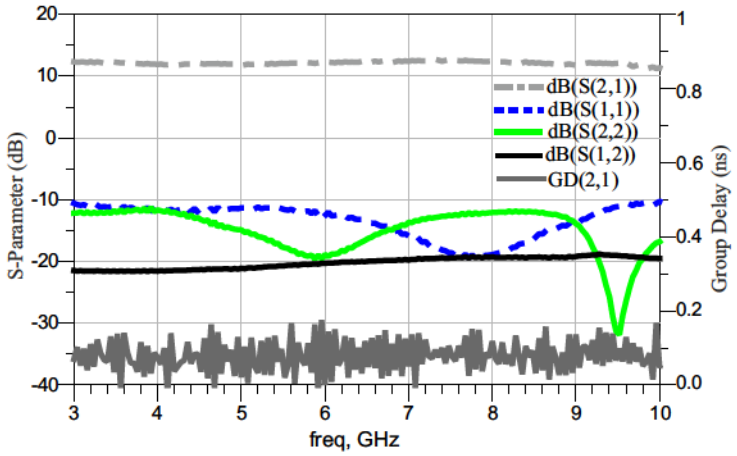

Fig. 3.21: S-Parameter and group delay of manufactured UWB amplifier

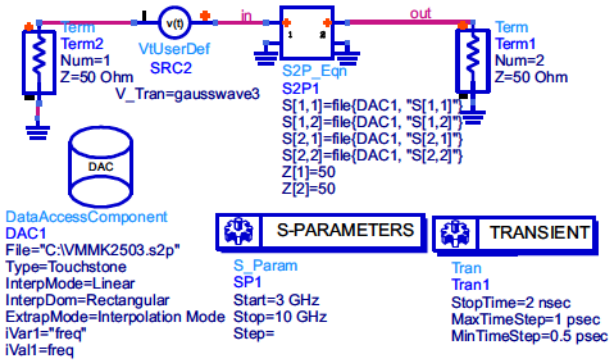

Fig. 3.22: Setup for pulse distortion test caused by UWB gain block

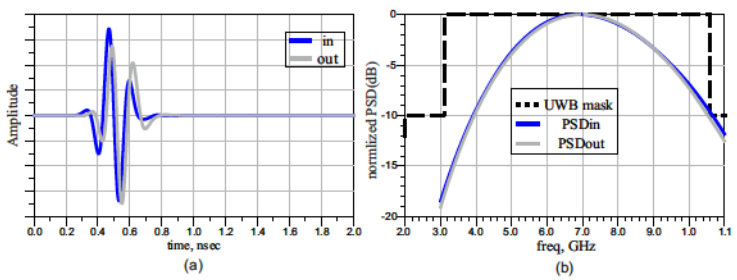

Fig. 3.23: Voltage and PSD of 5^{th} derivative Gaussian before and after

Resistive Power Divider A resistive power divider was selected based on [mic12]. Its resistive divider size will be very small since it contains only lumped elements, and it is almost frequency-independent performance provides a very good isolation between different split ports. This is important in our node concept. Another advantage to using this type of divider is its ability to adjust the insertion losses between input and output ports; with this divider, a gain block was used to compensate the losses from the divider and back to 0 dB insertion. This type of divider has higher insertion losses when it is compared with a delta or star resistive divider, as it has more resistances. This loss, however, can be compensated by gain block. SMD 0402 resistors were used to build this divider, since it has a lower parasitic effect compared to other SMD resistive sizes. Fig. 3.24 illustrated the circuit model, layout and symbol for this divider. The structure was tried to be as symmetrical as possible, and soldered the SMD resistors as close to each other as possible to reduce amplitude and phase imbalance error between the split ports.

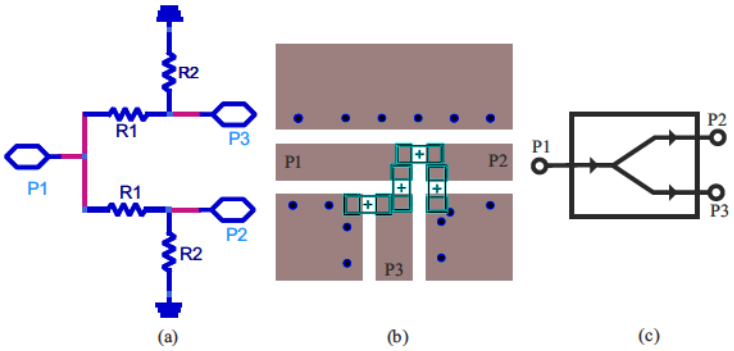

Fig. 3.24: Resistive power divider (A) Schematic (B) Layout (C) Symbol

The measurement results of the resistive power divider (shown in Fig. 3.25) show a very good input and output matching, with an insertion loss of approximately −10 dB and an isolation of better than −20 dB.

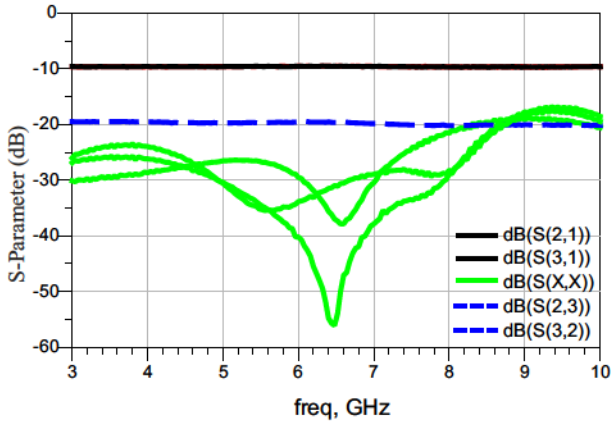

Fig. 3.25: S-Parameter of the resistive power divider

3.4.1.1.2 Delay Line The delay line is a structure which provides specific time delay to the input signal. These lines can be accomplished in many different ways; the most natural way is to use a transmission line, like microstrip, stripline, CPW, or GCPW. Some delay lines can be built using fiber optics, or on-chip as lumped LC network.

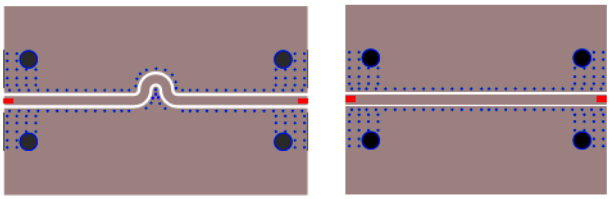

Fig. 3.26: Delay line using CPWG and reference line

The delay line was built using GCPWG technology (as can be seen in in the layout in Fig. 3.26); the approximate length is $\lambda/2$ at the highest frequency, in this case 10 GHz will be around 8 mm with RO4003 material, where $\varepsilon_r = 3.55$ and it has a delay of 50 ps. The GCPWG was bent in order to have compact size, although the length of the delay line at this high frequency will be not so large. The phase and S-parameter measurements are shown in Fig. 3.27. Two lines are generated, one as reference and the other with the extra delay line, and a linear phase shift between reference and line can be seen, very low insertion losses, and very good input output matching.

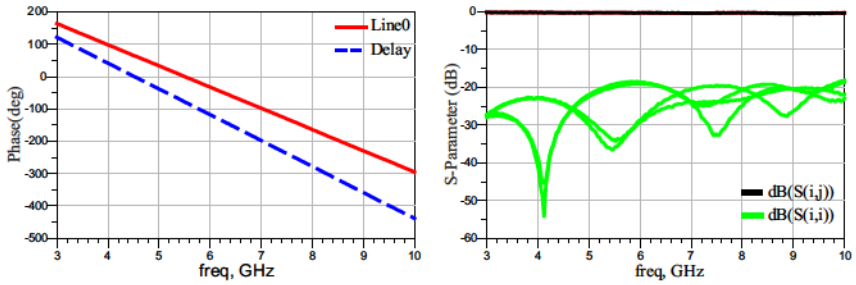

Fig. 3.27: Delay line measurement S-Parameter

For verification, the measured S-parameter is used to calculate the time domain impulse response, using Impulse Writer in ADS software. The two transmission lines have a difference in length of about 8 mm; the impulse response of those two lines is shown in Fig. 3.28.

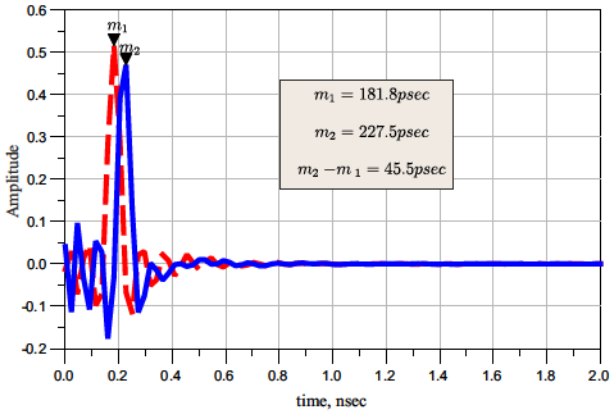

Fig. 3.28: Time impulse response of two different transmission lines

In reverse method using equations, the difference in length can be calculated using the time delay difference of the two transmission lines.

$$\Delta l = \Delta t \cdot v \qquad \text{with} \qquad v = c/\sqrt{\varepsilon_{eff}}, \tag{3.4.1}$$

Where Δl is difference in length between two transmission lines, Δt is the difference in time domain impulse responses, c is the speed of light, v is the phase velocity in the substrate, and ε_{eff} is effective permittivity of the substrate. In this case, using RO4003, it has a permittivity of 3.55, thickness of 0.508 mm, copper cladding of 17 μm and the $\varepsilon_{eff} = 2.79$ (calculated using lineCalc in ADS software [Agi10]). The calculated Δl is 8.1 mm which agrees well with the predesigned value.

3.4.1.1.3 Combiner Node The Combiner Node is the last part of the node concept, consisting mainly of the following:

Gain Block Gain Block has been previously explained, in section 3.4.1.1.1.

Resistive Power Combiner The Resistive Power Combiner is similar to the resistive power splitter, but combine different input signals, in this case three inputs to a single output (3:1). The resistive power divider was modified by adding another port, and optimized the series and parallel resistance to have certain insertion losses with maximum possible isolation. The schematic design, layout ready for manufacturing and symbol are shown in Fig. 3.29. The resistance values of R1 and R2 can be optimized to achieve the required insertion losses.

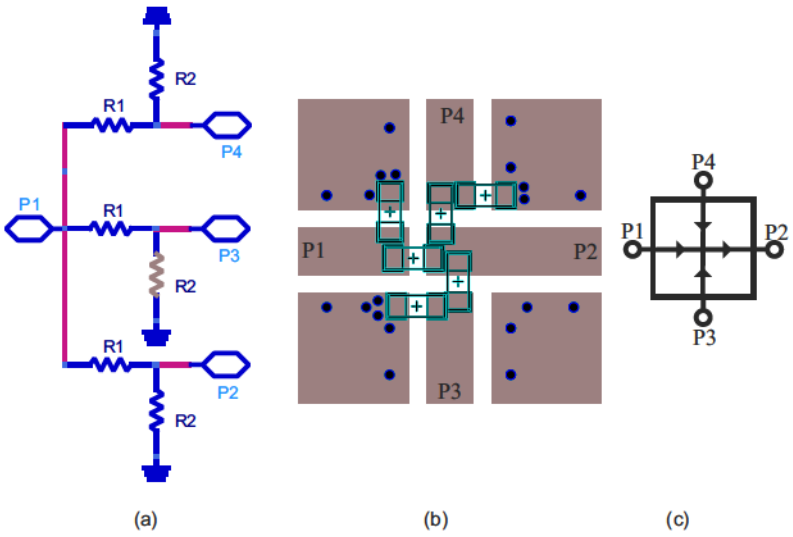

Fig. 3.29: Resistive power combiner (a) Schematic (b) Layout (c) Symbol

In this example, $R1 = 120\,\Omega$ and $R2 = 100\,\Omega$ to achieve 12 dB insertion losses (as shown in measurement results in Fig. 3.30), with isolation around 23 dB, input and output matching better than 15 dB, and also 0402 SMD resistor where used. The resistor positions were optimized to produce symmetry in the structure, and as a result a reduce amplitude and phase imbalance error in the combined signal was achieved.

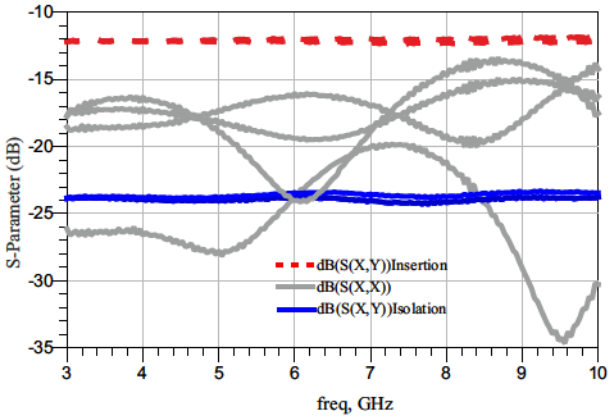

Fig. 3.30: Combiner measurements S-Parameter

Pi Attenuator In order to achieve 0 dB insertion after the split node or combiner node, there is need to use an attenuator and a gain block. The gain block has constant gain, and the variable attenuator also improves isolation between different stages, as the reflected signal will be twice attenuated. Fig. 3.31 shows the schematic, layout and symbol of such Pi Attenuator. The 0402 SMD resistors was used to reduce parasitic effects; the measurement results of the 1 dB attenuator in Fig. 3.32, show a flat frequency, independent insertion losses, and a very good input and output matching.

Attenuation	**In (dB)**	R_1	R_2
1	∞	Open	Open
0.9	-20	56	220
0.8	-13.98	68	100
0.7	-10.46	100	82
0.6	-7.96	120	56
0.5	-6.02	150	39
0.4	-4.44	180	22
0.3	-3.10	270	18
0.2	-1.94	560	12
0.1	-0.92	1200	5
0.0	0	Open	Short

Table 3.1: Pi attenuator resistors

Table 3.1 provides resistor values for Pi Resistor Attenuator. The values have been calculated for a 50 Ω system.

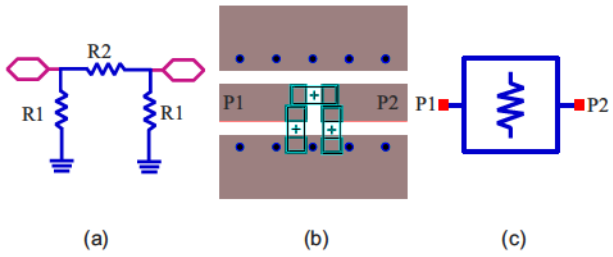

Fig. 3.31: Pi Attenuator

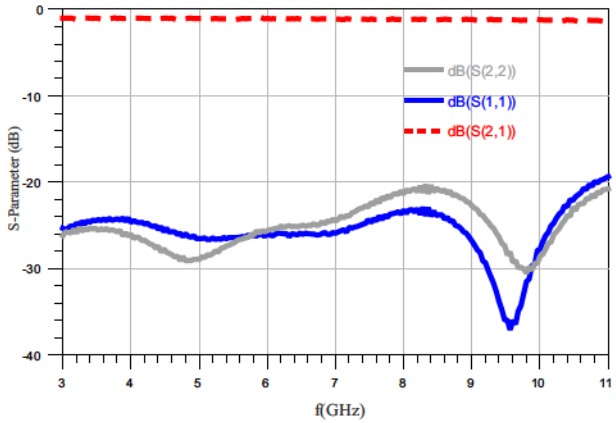

Fig. 3.32: S-Parameter of 1dB Pi attenuator

3.5 FIR Single Tap

After measuring every single FIR component alone (splitter node, weighting stage, delay line, and combiner node), they are combined together (without the delay line) and manufactured; a single FIR Tap is shown in Fig. 3.33. The single tap looks like a triple lines filter, with two lines for inputs and one single line for output. The divided out-of-phase signal will be applied to P1 and P2, and according to the sign of the filter coefficient, only a single path will be active and the other one will have no DC bias applied (meaning it will be open).

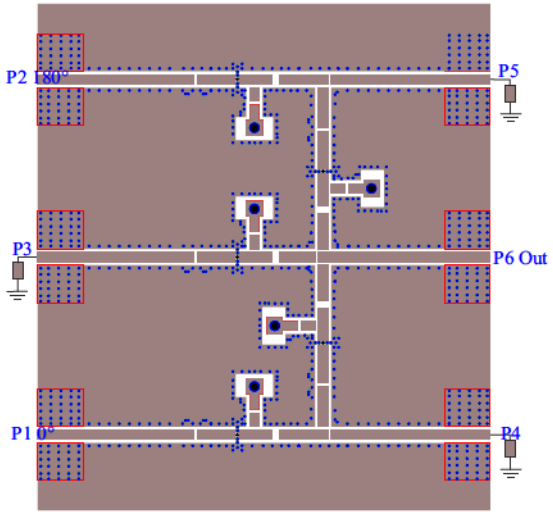

Fig. 3.33: Final FIR single tap layout

For simplicity and prototype design, a Pi-Attenuator was used as weighting stage instead of using a variable voltage amplifier. The experimental single tap FIR filter is shown in Fig. 3.34; its equivalent circuit is shown at the right side, delay lines were not inserted here. All the SMD components are of size 0402 to reduce the parasitic effect, and transmission lines were built in GCPWG technology.

3.5.1 FIR Single Tap Measurements

The measurements were done after TRL calibration; the desired measurement ports were connected to the Agilent network analyzer 8510, and the remaining ports were terminated by a broadband matching load MCL ANNE-50+ from Mini-Circuits. Insertion losses of around 0 dB(desired goal) was achieved in case the input signal will travel to the next filter tap. For example, P1P4, P2P5, and P3P6 (forward transmission) and a flat transmission close to 0 dB from the input filter tap to its output (P2P6 or P1P6); in this case the filter coefficient was assumed to be =+1 to P2P6 path, and P1P6 is turned OFF.

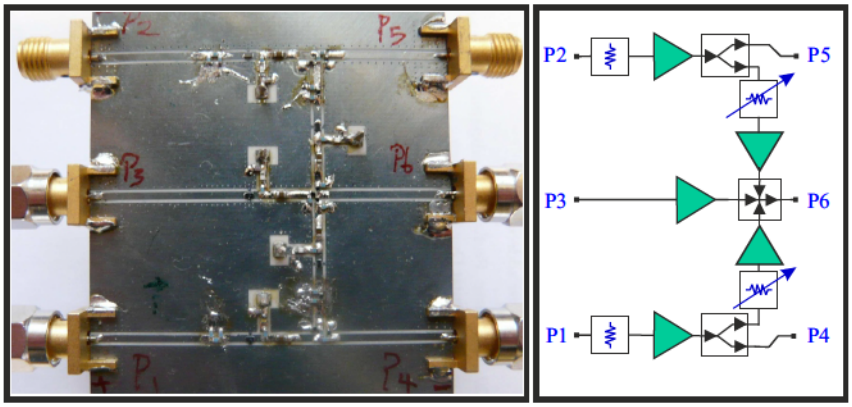

Fig. 3.34: Prototype single tap FIR filter

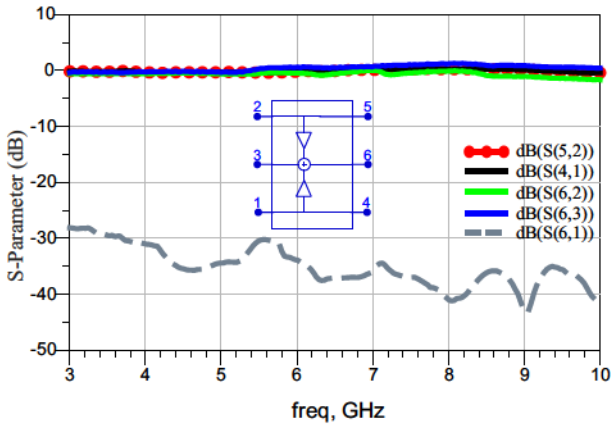

Fig. 3.35: S-Parameter measurements of single FIR tap (Transmission S_{xy})

As mentioned before, only one path is active at a time, so either P2P6 or P1P6 will be active. Fig. 3.36 shows the measurement results when a filter coefficient equal to 1 was applied. As shown all the transmission are close to 0 dB except the path P1P6 which is turned off and have insertion losses larger than 30 dB. For more details, the symbol for

the FIR tap is also inserted in this figure. Fig. 3.35, shows the input and output matching for all ports; the matching is larger than 10 dB.

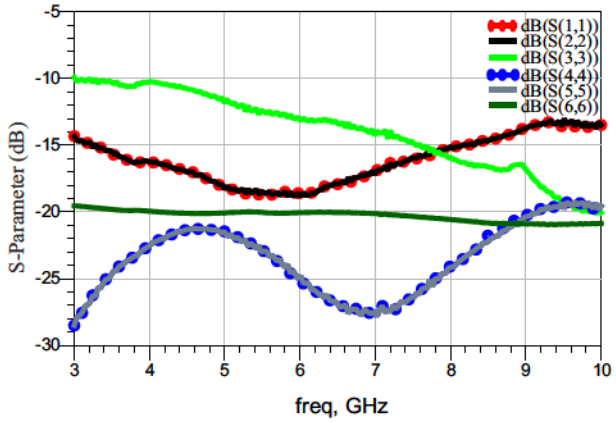

Fig. 3.36: S-Parameter measurements of single FIR tap (Transmission S_{xx})

The group delay in case of forward transmission between different filter taps and ON transmission from input to output is shown in Fig. 3.37. The delay (6,2) has a higher group delay than the forward transmission delay (4,1) or delay (5,2). This small difference came from the longer signal path, and this difference in group delay will be taken into account in the final optimization of the FIR filter coefficient.

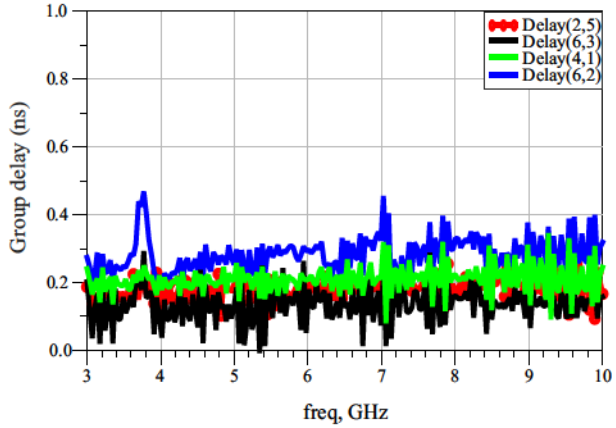

Fig. 3.37: S-Parameter measurements of single FIR tap (transmission S_{xx})

Fig. 3.38 shows the Input-Output transmission under different filter coefficient values. The measurements were done at different attenuation levels using variable pi-attenuator, then normalized to the lower insertion losses to be the maximum filter coefficient, which is ($a_0 = \pm 1$). Then the remaining measurements were normalized to have values between ± 1 to 0. The P2P6 path was OFF the whole time, which means only positive filter coefficients are implemented; the insertion level of P2P6 when it is OFF is always lower than -30 dB.

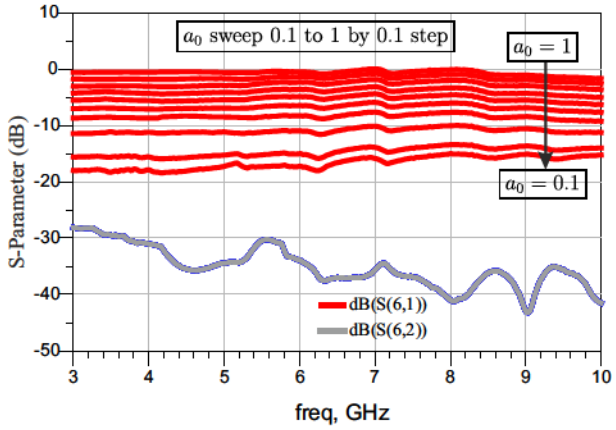

Fig. 3.38: Transmission S_{xy} over frequency (different filter coefficient)

3.5.2 From Measurements to Simulation

In the previous section, the measurement results of a single FIR tap were presented, proving the possibility of building a single FIR filter tap in MIC technology. Generally, a FIR filter will consist out of more than a single tap; this proof of concept will prevent the manufacturing of N number of filter taps. Consequently, the cost will be reduced. For this reason, in the next section the ADS software will be used to create the S-parameter model of a single FIR tap. By doing this, one can generate different orders FIR filter, in order to study, analysis, and investigate the analog UWB FIR filter with a greater degree of freedom. In the following chapters, the ability of using an analog FIR filter for different applications will be shown.

3.5.2.1 Generating ADS Model for Measurement Data

After doing measurements for every setup condition, taking advantage of some symmetry in the structure, a single file from different five measurements is generated. The available network analyzer is able to measure only 2 ports, and the other ports should be terminated by a broadband 50 Ω load. Using the setup (in Fig. 3.39), the newly generated touch stone file format will have six ports. For every filter coefficient, such a single file was generated. These touch stone files are then combined, with the help of the Data File Tool in ADS, to generate a single file having all the measurement data, including all the S-parameter for filter coefficients from -1 to 1 with step 0.1.

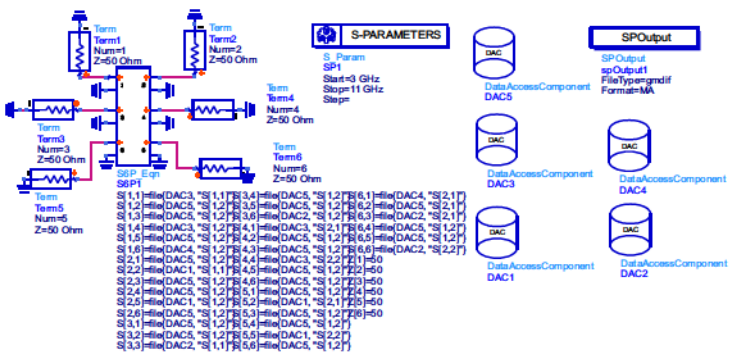

Fig. 3.39: Convert 5 measurement files to single file

This single file will act as a model file for the FIR filter by setting the filter coefficient as a variable inside it, and then assigning an S-parameter set for every filter coefficient; interpolation can be used for filter coefficients in between these fixed values to create a new S-parameter set. An extra transmission line is added, having the electrical length of $\lambda/2$ at specific frequencies at output ports $P4$ and $P5$. This transmission line will represent the delay τ in the FIR filter. In a conventional FIR filter, τ is constant, but it also can be inserted as a variable (by changing the specific frequency where $\lambda/2$ is calculated) inside the FIR tap model, one can increase the degree of freedom while optimizing the FIR filter coefficient.

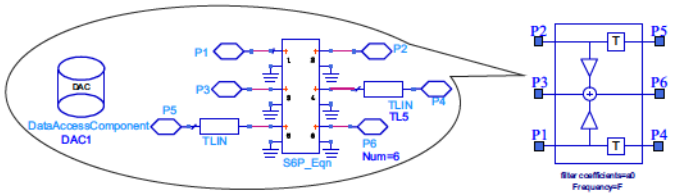

Fig. 3.40: Symbol will be used later on for FIR tap

The symbol in upper side of Fig. 3.40 will be used later on as symbol for a FIR Single Tap, which means if one use n of them an nth order FIR filter is generated (as shown in Fig. 3.41).

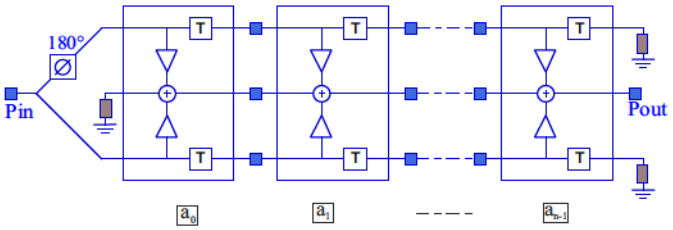

Fig. 3.41: Circuit model for n^{th} order FIR filter

The input signal Pin is divided into two output signals, and one path is phase shifted by 180° degrees. The forward signal path of the last filter tap will be terminated by a 50Ω broadband load, to prevent any reflection. The same will be done by port $P3$ in the first tap. The high isolation provided by the combiner node is a result of both gain block and resistive combiner.

3.5.3 Advantages of Using the Node Concept

1. Only a single precision bi-phase divider is needed.
2. Good isolation between filter taps and inside taps components.
3. The compensation gain allows for increasing the filter taps number without considering the level of signal.
4. Easy to change the sign of filter coefficient.
5. Symmetric structures with out-of-phase product could help in cancellation of parasitic effect.

CHAPTER 4

FIR ADAPTIVE FILTER

4.1 Introduction

Although there are many different kinds of filters, one can describe them using a few common characteristics. The frequency response of a lowpass filter will be used to describe these characteristics [Ram01], as shown in Fig 4.1. "passband" describes the range of frequencies over which the incoming signal will pass; the magnitude in the pass band of the filter output should be flat. Far outside this frequency band will be the stopband, where the signal will be highly attenuated. In between the passband and stopband is the transition band. The smaller the transition band, the better the performance of the filter. The ideal filter has a unity gain and no distortion in the passband, which means no ripple $\delta_p = 0$, infinite attenuation in the stopband, and no transition band in between. Cut-off-frequency f_c is the frequency at which the magnitude of the filter output is 3dB lower than the input magnitude. Table 4.1 summarize the main filter characteristics. Ripple in the passband δ_p is defined as the tolerance amount from the unity gain. The other filter specification is the attenuation amount A_s(in dB) of the stopband with respect to the passband as in Equation 4.1.1, where A_{in} and A_{out} are input and output amplitude, respectively:

$$A_s = 20 \cdot \log_{10}\left(\frac{A_{out}}{A_{in}}\right) \tag{4.1.1}$$

The filter order is also an important parameter in characterizing a filter, where higher order tend to provide better filter properties, but needs more stages or reactive elements.

4.1.1 Filter Types

Based on the overall shape of the filter response, one can categorize the filter into four different types. In Fig. 4.2 the effects of those filter types can be seen on a swept frequency input signal [Ram01].

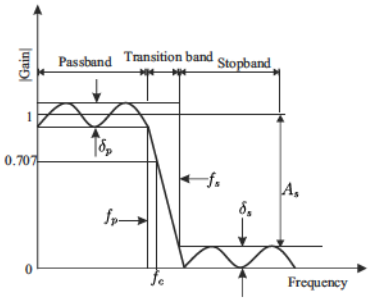

Fig. 4.1: Low pass filter frequency response parameters

Characteristic	**Description**
Passband (A_p)	Unity gain 0dB (ideal)
Stopband (A_s)	Attenuation region -8 dB (ideal)
Transition Band (f_{tr}=f_p-f_{st})	Region between passband and stopband
Ripple (δ_p , δ_s)	Amount of deviation from nominal value
Filter Order (N)	Number of stages or reactive elements the higher the order the closer to ideal filter response
Cut-off frequency (f_c)	Frequency where passband and stopband begin and end

Table 4.1: Filter characteristics and description

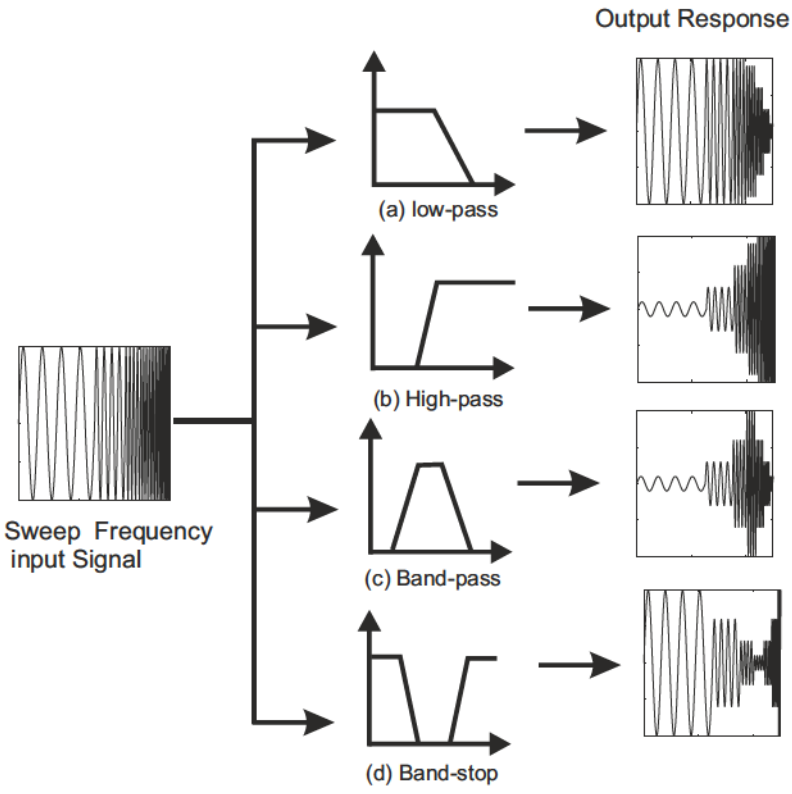

Fig. 4.2: Filter effects on a sweep frequency signal input signal

4.1.1.1 Lowpass Filter LPF:

As the name says, it passes the lower frequency's signal until the cutoff frequency, while attenuating the high frequency's signal. Fig. 4.1, shows the frequency response of such filter type.

4.1.1.2 Highpass Filters HPF

This filter will pass the high-frequency's signal while attenuating the DC and the low-frequency's signal, as shown in Fig. 4.3.

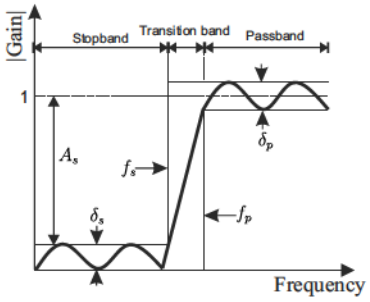

Fig. 4.3: HPF frequency response and its parameters

4.1.1.3 Bandpass Filters BPF:

As shown in Fig. 4.4, BPF pass only signals between two given frequencies, attenuating lower and higher signals. The pass band lies between two frequencies, f_L and f_H. Signals between DC and f_L are attenuated, as are signals from f_H to infinity. The pass band of these filters is often characterized as having a bandwidth that is symmetric around a center frequency.

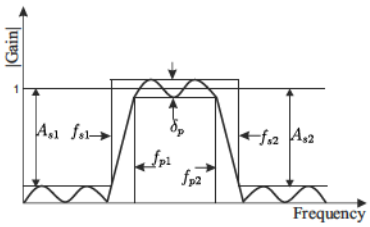

Fig. 4.4: BPF frequency response and its parameters

4.1.1.4 Bandstop Filters BSF:

Signal blocking occurs between two given frequencies, f_L and f_H. The pass band is split into a low side (DC to f_L) and a high side (f_H to ∞), as shown in Fig. 4.5. For this reason, it is often simpler to specify a bandstop filter by the width and center frequency of its stop band. BSF are also called notch filters, especially when the stop band is narrow.

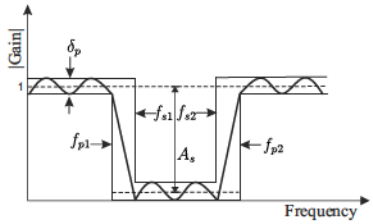

Fig. 4.5: BSF frequency response and its parameters

4.1.2 Group Delay

Group delay (GD) is a criterion which evaluates phase nonlinearity, the transfer function of a filter can be described as

$$H(j\omega) = |H(j\omega)| .e^{j\theta(\omega)} \tag{4.1.2}$$

Where $\theta(\omega)$ is the insertion phase component and the group delay $\tau(\omega)$ can be defined as

$$\tau(\omega) = -\frac{\partial\theta(\omega)}{\partial\omega} \tag{4.1.3}$$

Linear phase variation with frequency implies a constant GD and no phase distortion, which preserves the integrity of a pulse through a system. Having a linear phase means a constant GD, so the incoming wave will be delayed by the same time for all frequency components across the passband. But in reality, the GD of a filter is not constant and therefore different frequency components of the incoming wave in the filter will be delayed differently; as a result, this will distort the time domain response. To avoid this distortion, one should keep the GD inside the passband flat. GD of filter is function of many factors for example filter type, filter order and filter bandwidth. The GD of different filter types are plotted in Fig. 4.6 with the help of the ADS filter design guide tools (ADS). Different filter types were designed keeping the filter order and filter bandwidth the same. As it can be seen from this figure, the maximally flat filter provides the lowest GD comparing with chebyshev and Elliptic filters.

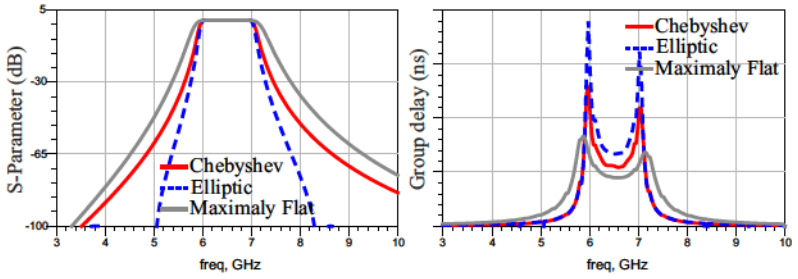

Fig. 4.6: S-Parameter and GD at Different Filter Types

One parameter that also can influence the GD is the filter order, as is clear from Fig. 4.7. Increasing filter order will increase the GD, so one should find a tradeoff between filter requirements and GD.

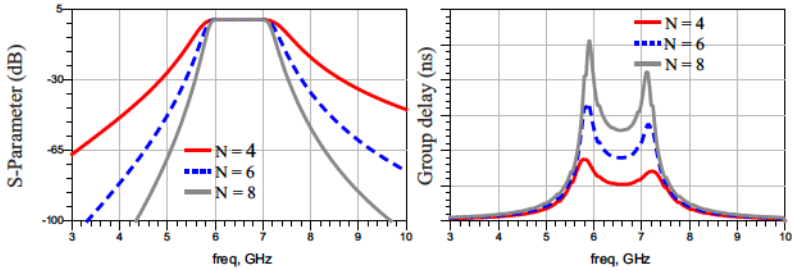

Fig. 4.7: S-Parameter and GD at different filter order

Finally, bandwidth also affects GD; increasing the bandwidth will reduce the GD. As a result, bandwidth is inversely proportional to GD.

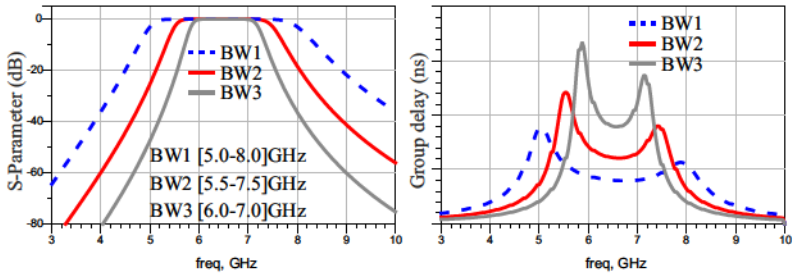

Fig. 4.8: S-Parameter and GD at same filter order and at different bandwidth

4.2 Ideal Analog FIR Filter

4.2.1 Ideal Analog FIR Filter Implemented in ADS Circuit Simulator

Starting with ideal FIR filter design using the circuit simulator (ADS). The filter consists of ideal power splitters and combiners. Between each filter tap at the input side, there is a delay line which normally takes a delay τ equivalent to an electrical length of 180° at the center frequency. Every filter tap also has a component which realized the filter coefficient; in the simulation, the S-parameter equation (S2P_Eqn) of ADS was used which defines the S-parameter matrix as it can be seen in Fig. 5.10. One advantage of such a component is its ability to define the input and output matching via S_{11} and S_{22}. The input transmission line is terminated by 50 Ω resistance.

The implementation of such analog ideal FIR or transversal filter in ADS will help us to understand the non-ideal characteristics of a real implementation of the analog FIR filter. For example the phase and amplitude variation due to frequency dependency of the filter coefficient, insertion phase of components and non-ideal power dividers and combiners. In order to calculate the filter coefficient, the Signal Processing Toolbox (Filter Design & Analysis Tool) in Matlab was used. A screenshot of this tool is shown in Fig. 4.10. Although this tool is designed for digital FIR or IIR filters, one can use it to generate filter coefficient and implement it in the ideal analog FIR filter modeled in ADS, as in the following.

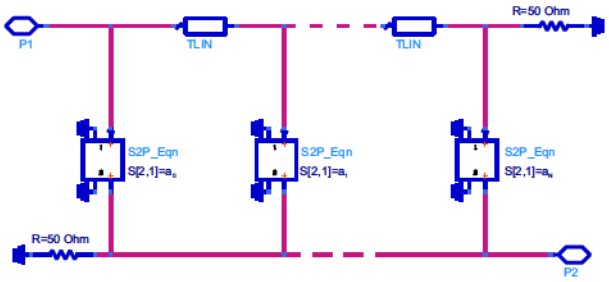

Fig. 4.9: Ideal FIR filter implementation using ADS

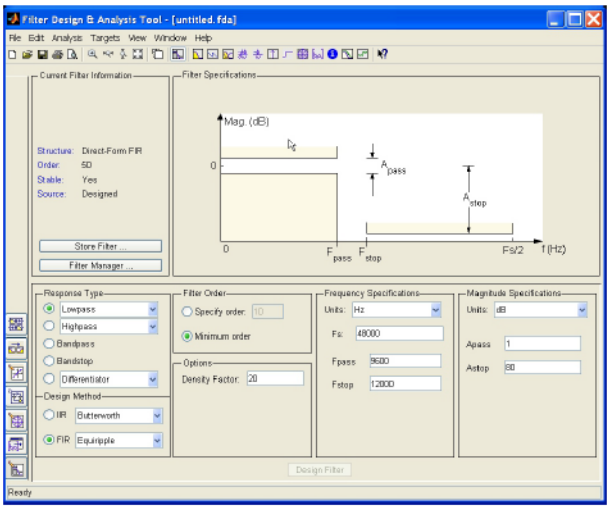

Fig. 4.10: Screenshot of filter design and analysis tool in Matlab for filter design

In the next section, an example of exporting digital FIR coefficients generated by Matlab into an ADS model of an ideal FIR filter will be illustrated . One interesting note in FIR design is that one can easily convert a LPF response into HPF response by inverting the sign of filter coefficients under some conditions. Under the condition, that the filter order (N) is odd, and the filter coefficients are symmetrical $a_n = a_{(N-n)}$. Equation 4.2.1 shows how to calculate the new coefficient to design complementary HPF from LPF.

$$\begin{aligned} a_{n(HPF)} &= -a_{n(LPF)} \\ a_{((N+1)/2)(HPF)} &= 1 - a_{((N+1)/2)(LPF)} \end{aligned} \tag{4.2.1}$$

Table 4.2 show an example of a LPF design at 6 GHz. The filter coefficients were calculated using filter design and Analysis Tool in Matlab, and then applied to the Ideal FIR design using ADS. The equation above was used to calculate the HPF filter coefficients with complementary properties which means passband frequency will become stopband and vice versa. Fig. 4.11 shows the attenuation of a LPF and its complementary HPF. Filter Coefficients were taken from Table 4.2, thus proving that by a simple modification (inverted sign) of the filter coefficients, one can easily turn LPF into HPF filters.

a_n	LPF	HPF
a_0	-0.039	0.039
a_1	0.065	-0.065
a_2	-0.012	0.012
a_3	-0.127	0.127
a_4	0.280	-0.280
a_5	0.653	0.347
a_6	0.280	-0.280
a_7	-0.127	0.127
a_8	-0.012	0.012
a_9	0.065	-0.065
a_{10}	-0.039	0.039

Table 4.2: Filter coefficients for LPF and conversion to HPF;$N = 11$

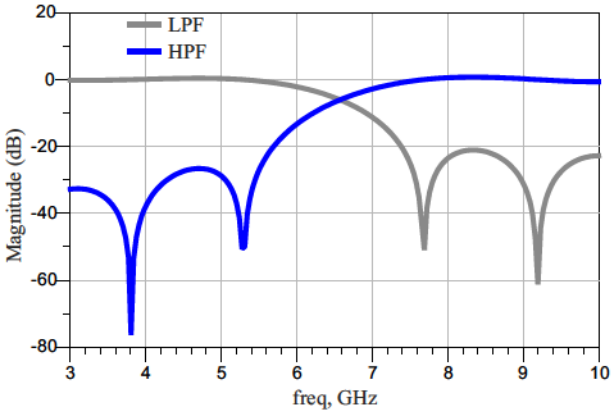

Fig. 4.11: Attenuation of both LPF and its complementary HPF. Ideal FIR tap filter versus measured one

4.2.2 Ideal FIR Tap Filter versus Measured One

In this section, the performance of an ideal FIR filter tap with the real measured one will be compared; while concentrating the comparison on amplitude and phase performance. An ideal tap will have a transmission coefficient with frequency independent amplitude. On the other hand, the measured amplitude one has frequency dependency on both input-output (applying a filter coefficient) and between input and next tap (transmission to next filter tap). For the phase, there will also be an insertion phase between input and output. This insertion phase is linear with frequency; this will be the same for the signal traveling from tap to tap (it will also have an insertion phase). Another extra phase will be inserted when different filter coefficients is applied, as it also has a frequency dependent phase.

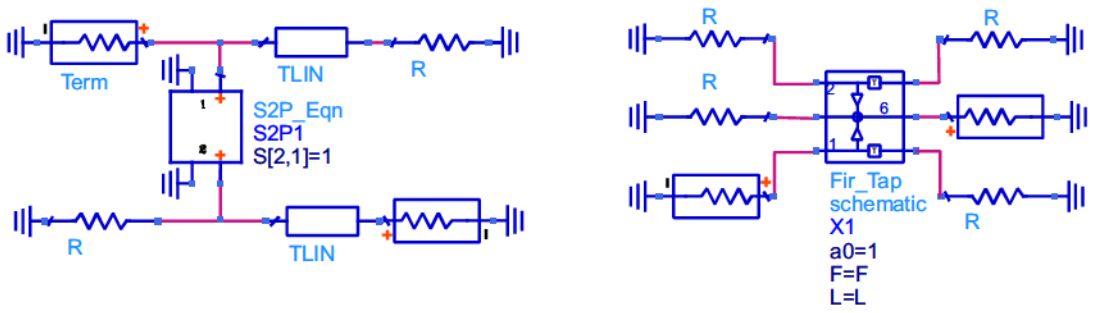

(a) Ideal Filter Tap

(b) Measured Filter Tap

Fig. 4.12: Comparison between ideal tap and measured FIR tap where filter coefficient $a_0 = 1$ and L is electrical delay.

Fig. 4.12 shows the setup for the comparison between ideal FIR filter tap and measured one, while Fig. 4.13 shows the amplitude and phase deviation of the transmission coefficient of measured FIR tap compared to the ideal one. In this the filter coefficient was $a = 1$. With respect to amplitude ripple, the measured values still are acceptable for a frequency range up to 9 GHz less than 1dB amplitude ripple. The insertion phase exhibits a linear variation which indicates that the tap effectively was a transmission line of about 2λ at 10 GHz. When the realistic filter tap is used in an FIR filter with many taps, its non-ideal properties repeat in the design and this will prevent us from using the already existing algorithms for calculating the filter coefficient, as was done in a previous section for ideal FIR filter. In this case, one can use suitable optimization tools to achieve a desired response by compensation of such amplitude imbalance effects and phase insertion, as will be seen in the following sections.

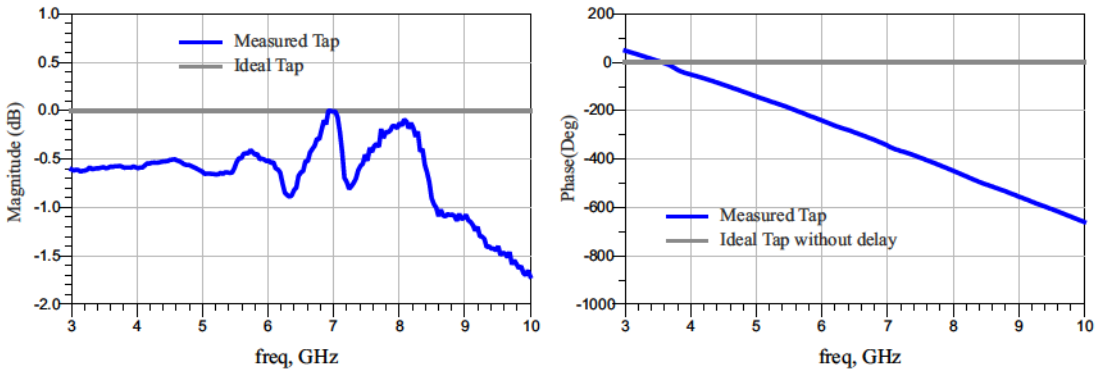

Fig. 4.13: Amplitude and phase of the transmission coefficient of the ideal FIR tap and measured one.

Note that the amplitude ripple will affect the ripple level inside the passband; where, for most applications, outside this band it is not as critical as it is inside the passband.

4.3 Adaptive FIR Filter

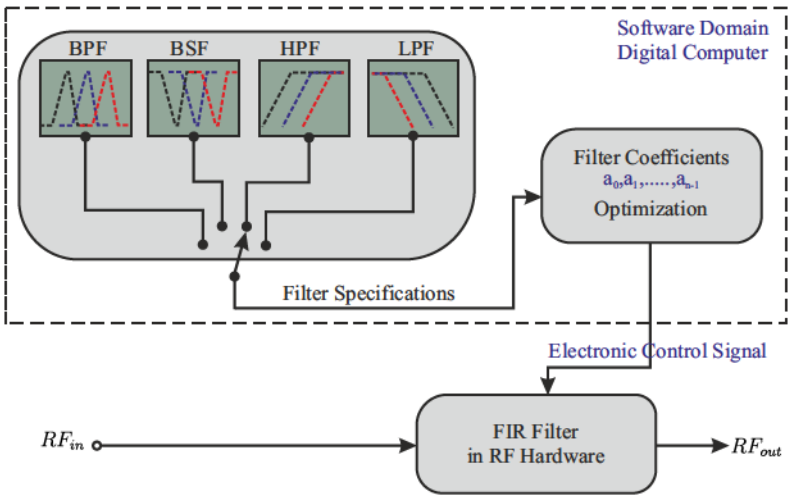

Fig. 4.14: Universal tunable analog FIR filter concept.

In conventional filter design, the design is for specific frequency bands and it is hard to modify it to use under different frequency bands. Even the type of filter cannot be modified; for example, one cannot easily modify a PBF to be a BSF. The big advantage of a tunable FIR Filter is that one can adaptively adjust the filter parameters and cut off frequency by only changing the filter coefficients. As shown in Fig. 4.14, this tuning of filter coefficients can be done digitally by using a computer. The next sections, will show how to generate any type of filter using a FIR filter. Not only produce different filter types, but also tunable cut off frequencies. The design flowchart is shown in Fig. 4.15. When the goal is to design an adaptive FIR filter, one enter the desired filter specification, then as a starting point and select the FIR filter order N, optimize the filter coefficients, and test. If the goal is achieved, then done, or else increase N and optimize the coefficient again until the goal is reached.

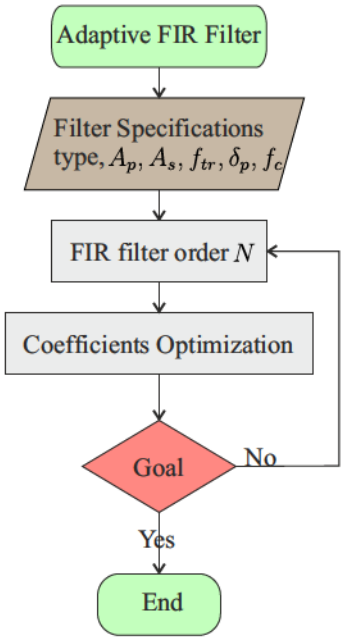

Fig. 4.15: Flowchart for design of the adaptive FIR filter.

4.4 Optimization of Filter Coefficients

The main challenge in this section is how to optimize the filter coefficients to satisfy a desired goal. As mentioned in previous sections, the already known algorithms used to design digital FIR filter cannot be used, as they assume ideal FIR filter taps and cannot compensate for the amplitude ripple and insertion phase of real measured filter taps. For this reason, a new optimization algorithm will be generated, which takes into account these non-ideal characteristics, and run the optimizer to achieve our desired goals. Our set of parameters to be modified or optimized will be only the filter coefficients; in some cases one can also include the delay lines as variable in the optimization algorithm. The optimization uses the optimization tool in ADS software [Agi10]. This tool provides multiple optimizers for different design problems, but all of these types are based on minimizing the error function EF, which measures the difference between the computed and desires response. The smaller the values of the error function, the more closely the response coincides.

$$EF = \sum_{allGoals} W_i \cdot |simulation_i - goal_i|^P \tag{4.4.1}$$

EF first determines the difference between the simulation (simulation_i), where simulation represent the transmission and/or reflection coefficient of a N order FIR filter and the ($goal_i$) representing a predefined desired response. For all goals ($allGoals$), this difference is usually called residual. Each residual is then raised to a power P. In the case of Random optimization and Gradient optimization (which is used here), $P = 2$, so both optimizers use the least square EF, and the result is multiplied by a weighting factor, W_i. The final EF value is determined as the sum of all these terms. The weighting factors may have different values from one goal to another, and they are used to emphasize some optimization goals versus others by making their contribution to the error function more significant. In the optimization process, one started with a Random Optimizer which achieved faster convergence to the goals, and which randomly selects a value for a variable and calculates the EF. This will be done for so many iterations until an improvement is made, then the variables will be updated to the current value. Later on, if the optimization converges, one change to a Gradient Optimizer to improve the final result. A Gradient Optimizer calculates the gradients of the EF with respect to each variable, and moves the variables in the direction of steepest decent of the EF. It keeps doing this until it reaches an error boundary ($EF = EF_{max}$). One drawback of this optimization method is that one can land up at a local minimum, but a much better solution might exist with completely different values for one or more of the variables. In order to avoid such cases, the start value of the variables were changed and the optimizer started again. As a result a lower EF in many cases was achieved and in some cases reached the desired goal ($EF = 0$). During the optimization, was noticed that starting the variable with the initial value equal to zero for all filter coefficients gives better optimization results. In this case the initial values for filter coefficients are in the middle of the variable range -1 and +1.

4.5 FIR Filter as Lowpass Filter

Using the adaptive FIR filter, one can approximate any desired filter response. In this section, a lowpass filter will be designed. This will include the filter specifications as

goals, and then optimize the filter coefficients and the filter order. The goals, as shown in Fig. 4.16, are the ripple inside the passband (δ_p), not to be greater than a constant (in this case, it was selected as 3dB), and the attenuation in the stopband (As) to be at least lower than a threshold value (in this example, it was selected as -13 dB). Different parameters can be also inserted as goals, for example GD, ripple in the stopband, maximum FIR filter order, etc. The evaluation bandwidth for the passband was selected to be from 3 to 10 GHz, and the FIR filter order was $N = 11$ initially. The result in Fig. 4.17 shows that the goals, like maximum ripple in passband and minimum attenuation in stopband are achieved with very good return losses in the whole frequency band. In Fig. 4.18, one sees a linear phase with frequency. The reverse transmission, or isolation, S_{12} has a very low value, which will provide a good isolation for the reflected signal, if this LPF is combined with other stages (for example, an antenna array beamforming).

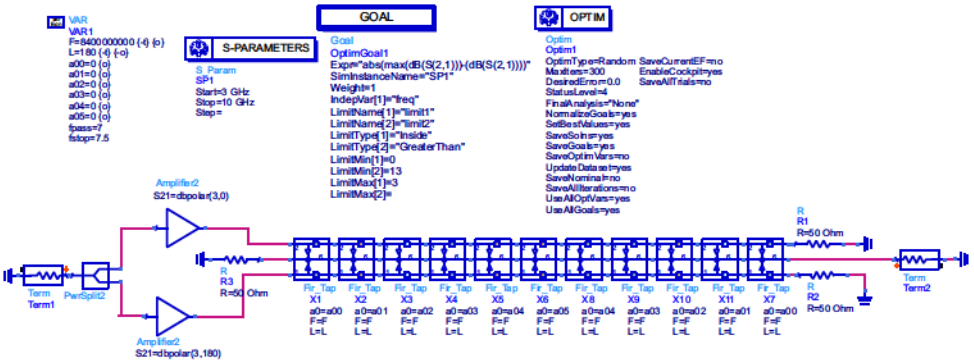

Fig. 4.16: Schematic of LPF FIR filter $N = 11$, where goals are defined as limit1 and limit2.

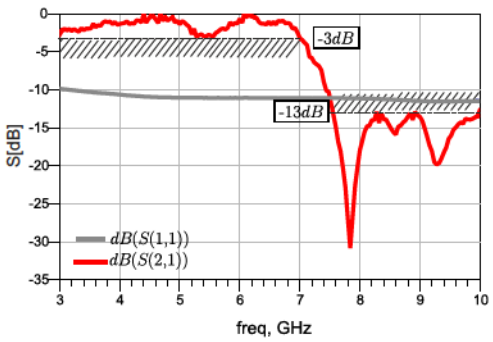

Fig. 4.17: Transmission and reflection coefficients of a LPF FIR filter $N = 11$.

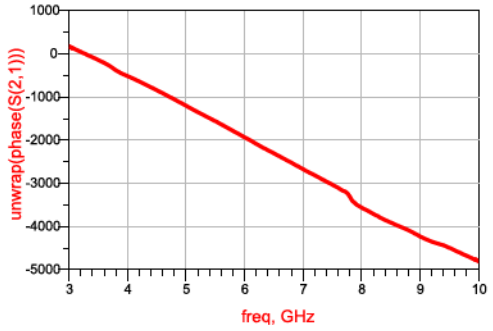

Fig. 4.18: Insertion phase of a LPF FIR filter $N = 11$.

The next step is to reduce the filter order to $N = 9$ with the same goals as for $N = 11$; the schematic looks like Fig. 4.16 with $N = 9$.

$a_n \backslash$ **Order**	5	6	7	9	11
a_0	-0.06	-0.12	-0.12	-0.08	-0.06
a_1	0.61	-0.59	-0.50	-0.16	-0.02
a_2	0.10	-0.54	-0.58	-0.16	0.01
a_3	0.50	0.56	0.60	-0.03	0.02
a_4	0.15	0.28	0.46	0.24	0.32
a_5		-0.17	-0.17	0.66	0.82
a_6			0.28	0.28	0.16
a_7				-0.49	-0.78
a_8				-0.13	0.00
a_9					0.15
a_{10}					-0.12
EF	0.111	0.024	0.018	0.0004	0.000

Table 4.3: Summarizes the filter coefficient and resultant residual for different filter order.

As it can be seen in Table 4.3, the EF increases by decreasing the filter order below $N = 11$. In Fig. 4.19, one see the performance of the LPF at different orders; as the filter order is increased, this will improve the filter roll-off slope. This means fast transition from the passband to the stopband, or rather, closer to the ideal LPF response. It also keeps the attenuation level in the stopband under the prescribed value; at filter order $N = 5$, it was impossible to keep A_s below the -13 dB value, but adding a new filter tap achieved this goal. This is seen by $N = 6$, but still the transition is slow. In the passband, all filter orders satisfy the minimum ripple requirement.

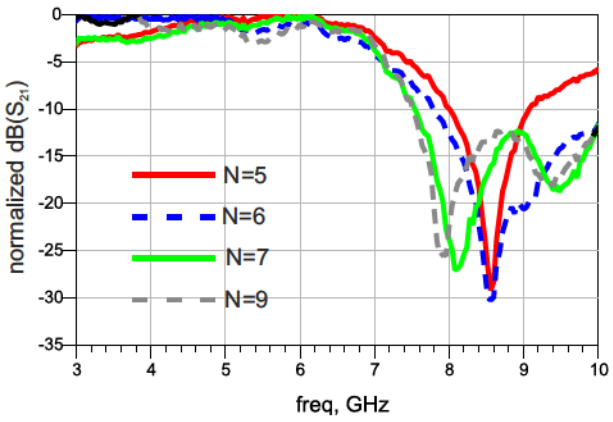

Fig. 4.19: LPF insertion loss for different FIR filter order.

The GD of the different order LPFs is shown in Fig. 4.20. Inside the passband, the GD is flat, around 1 ns. If the filter order is increased, the level of GD will increase; at filter order 9 the GD is around 2 ns.

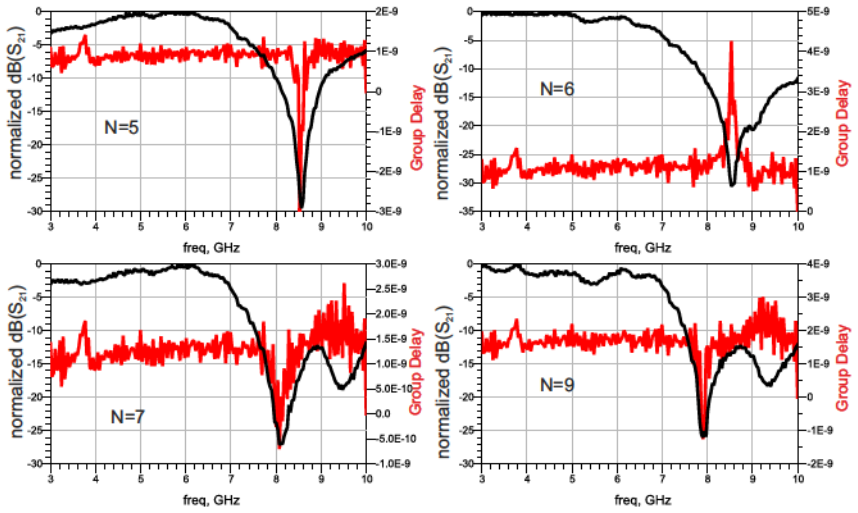

Fig. 4.20: GD (red) and insertion loss (black) of LPF FIR filter with different order.

As seen in Fig. 4.20, GD can have negative peaks as a result of positive phase slope at deep insertion loss minimum. Since the negative GD appears outside the passband and in combination with a steep decay in amplitude an input pulse will suffer some extra distortion but there will be no output pulse appearing earlier than the input pulse. For more comparison, the GD is plotted in Fig. 4.21 for different filter orders. As the filter order is increased the GD level inside the passband is increased; this is expected as the signal at input, will pass through more filter taps before it arrives at the output port of the filter, which causes more delay for the signal.

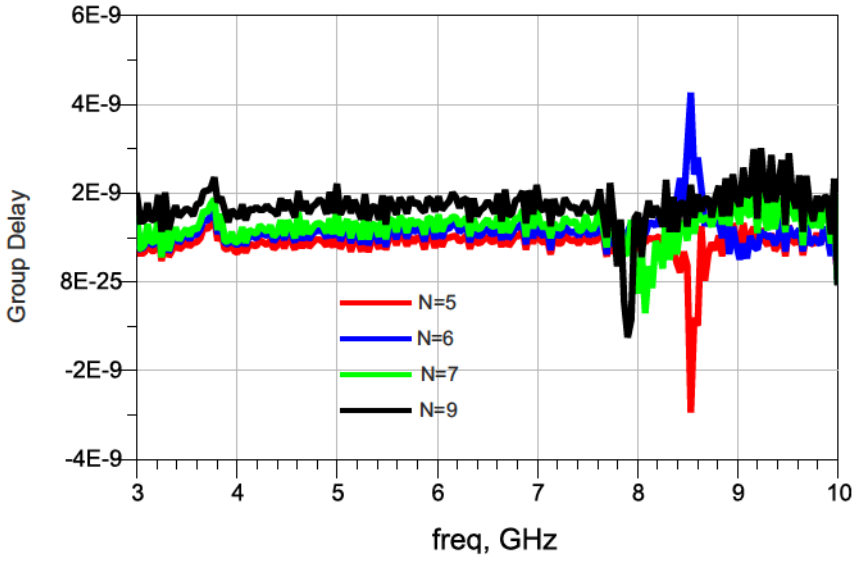

Fig. 4.21: GD at different filter order.

In Fig. 4.21, in the frequency band from 3 to 4 GHz,a small peak in the GD can be seen; this is an artifact produced from phase error in measurement, as mentioned in a previous chapter.

4.5.1 FIR as Tunable Lowpass Filter

To design a tunable or adaptive lowpass filter with tunable cut-off frequency f_c, the filter order was fixed to $N = 7$. The design schematic is shown in Fig. 4.22, where one can see the filter order and optimization goals.

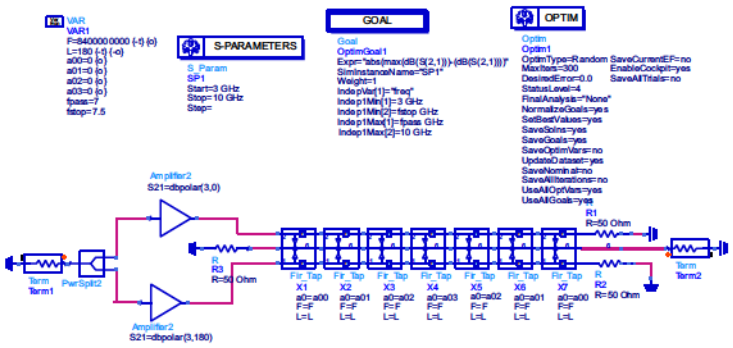

Fig. 4.22: Tunable LPF filter.

$a_n \setminus f_c(GHz)$	4	5	6	7	8
a_0	0.27	0.42	-0.12	-0.12	-0.25
a_1	0.05	0.29	-0.15	-0.50	-0.56
a_2	-0.54	-0.86	-0.78	-0.58	-0.11
a_3	-0.61	-0.91	-0.63	0.60	0.67
a_4	0.29	0.30	0.8	0.46	-0.24
a_5	0.94	-0.02	0.07	-0.17	-0.14
a_6	0.41	-0.78	-0.97	0.28	0.04
EF	0.037	0.024	0.089	0.042	0.020

Table 4.4: Filter coefficients for different cutoff frequencies.

The goal was varied according to the new cutoff frequency. The final result is shown in Fig. 4.23. Different cutoff frequencies between 4 and 8 GHz was selected; at all cut off frequencies, a very low EF close to zero was achieved, which means a low attenuation level in stopband and minimum ripple in passband. The filter coefficients under different cut-off frequencies are summarized in Table 4.4. These coefficients are plotted in Fig. 4.23, versus the cut-off frequency. One can see that filter coefficients of largest absolute amplitude are concentrated in the middle of the filter coefficient array and that all filters require positive and negative coefficients.

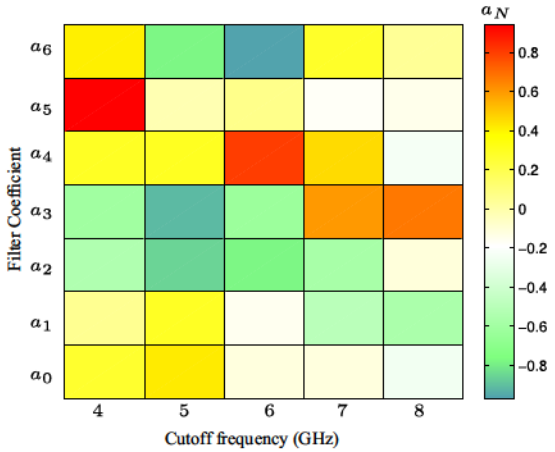

Fig. 4.23: Filter coefficients for different cutoff frequencies.

Fig. 4.24, proves that the FIR filter can be used as adaptive LPF. Only by changing the filter coefficients one can shift the cut-off frequency to any desired frequency in the complete UWB band.

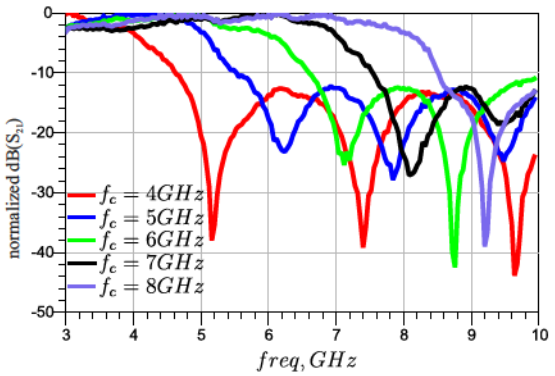

Fig. 4.24: Insertion loss of FIR filter for different cut-off frequencies.

Including the delay τ between filter taps as parameter in the optimization can increase the degree of freedom in the design of the tunable FIR filter, which can reduce the EF and bring us closer to the goal. in Fig. 4.25, the optimization is done with including τ as a variable in the optimization and an improvement at the upper frequency edge can be seen by choosing the delay line to be $\lambda/2$ at 9.9 GHz rather than 8.4 GHz

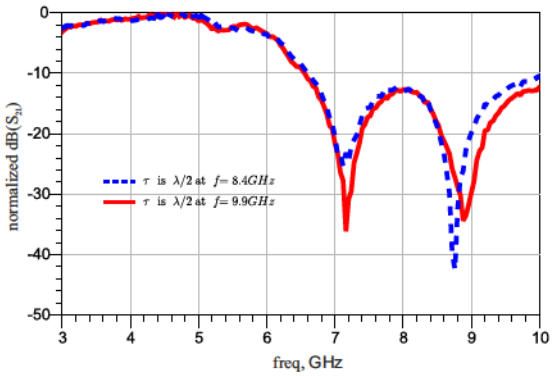

Fig. 4.25: LPF performance at different τ

4.5.2 Compactness Design of LPF Filter

In order to save weighting stages, as well as make the filter more compact and still satisfying the filter requirements, one can define a minimum threshold value and replace all filter coefficients within this threshold by zero. The weighting stages with zero weight is omitted, but the delay line for the next coefficients is kept, which have not zero value. In Table 4.5, filter coefficients $\{a_4, a_6, a_7, a_{10}\}$ in design A were replaced by zero in Design B. A special case appears here, where due to the coefficient $\{a_{10}\}$ equal to zero one can reduce even the filter order by deleting the delay line.

a_n	A	B
a_0	0.358	0.358
a_1	0.596	0.596
a_2	0.253	0.253
a_3	-0.116	-0.116
a_4	0.024	0
a_5	0.127	0.127
a_6	-0.035	0
a_7	-0.030	0
a_8	0.158	0.158
a_9	0.08	0.08
a_{10}	-0.003	0

Table 4.5: Zeros inserted for FIR coefficients with value close to zero.

Fig. 4.26 shows an ideal FIR filter design, the difference in performance when zeros inserted for the small coefficient values, and leaving the significant coefficients. If the filter performance after inserting zeros is affected, one can optimize the significant coefficients to achieve again the desired performance (has not been done in this case). This kind of redesign of filter coefficients will be necessary if, for example, {a8} is replaced with zero in the present case.

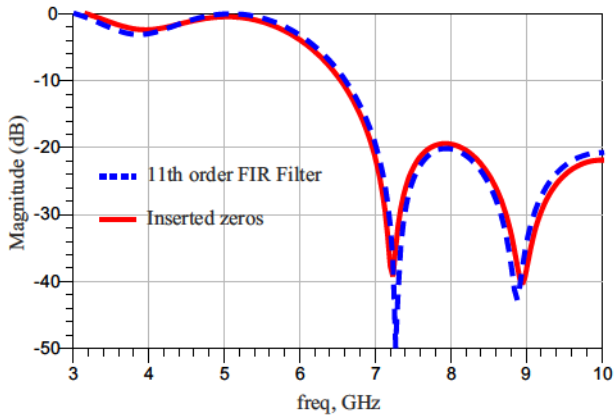

Fig. 4.26: Zero inserted for small filter coefficients, as shown in Table 4.5

4.6 FIR Filter as Bandpass Filter

The bandpass filter is one of the important filters in UWB systems. According to the Federal Communication Commission (FCC) [Fed02], UWB systems can operate in wide frequency bands from 3.1 to 10.6 GHz, as shown in Fig. 4.27. However, The European Commission (EC) [Eur07], in 2007, approved the use of UWB bands with 2.5 GHz bandwidth in the band from 6 to 8.5 GHz, as shown also in Fig. 4.27. Since the FCC rules cover the frequency band from 3.1 GHz to 10.6 GHz, and was published in 2002 (much earlier than the publication of the EC in 2007), most impulse based UWB devices mentioned in literature operate in the FCC band. In order to use such an existing device, an additional filter has to be included, which should shape the spectrum to fulfill the EC rules. This means restricting it to the 6-8.5 GHz EU frequency band, and the signal level below 6 GHz should be attenuated by 28.7dB, while above 8.5 GHz, the signal should be attenuated by 23.7 dB. Moreover, the need of a well-designed UWB band-pass filter arises in the UWB system; before the signal is transmitted into the space for communication, it must follow the regulations - a filter is a most effective device, for shaping the signal [LKM06]. Beside the conventional requirements for a well-designed filter, such as low insertion loss and high attenuation in the stopband, one needs the filter to shape the signal to fulfill the UWB mask (in either case, FCC or EC), and one also needs flat GD, which is especially important to an impulse radio system to keep the distortion of the short pulse to a minimum.

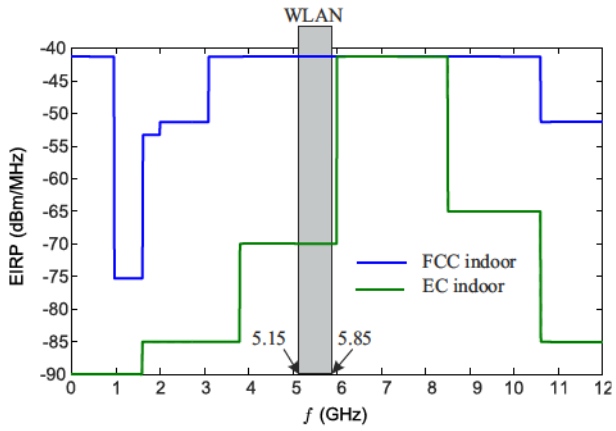

Fig. 4.27: FCC and EC UWB mask

4.6.1 UWB Bandpass Filter

In Fig. 4.28, a bandpass filter using the adaptive FIR filter approach is presented, taking into account the requirements of standard conventional bandpass filters, as well as the FCC and EC requirements.

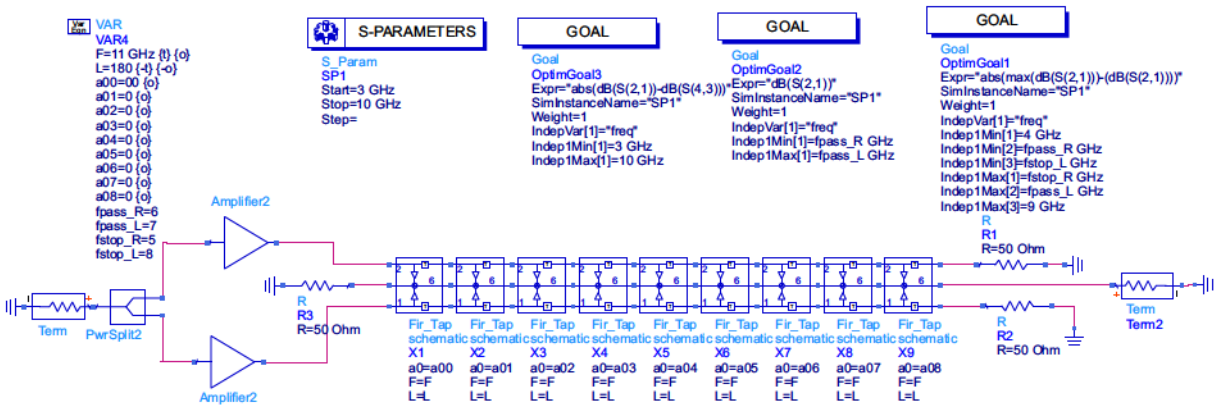

Fig. 4.28: Schematic design of FIR BPF for FCC and EC requirements

In the case of FCC requirements, the design is done to follow part of the FCC mask requirements, shown in Fig. 4.29, with little modification as the passband was redefined to be from 4 to 9 GHz as measurement data show useful properties only from 3 to 10 GHz. Circuit components change their behavior dramatically after the 10 GHz, especially the gain block where the gain drops very fast. For the lower frequency edge, 4 GHz was selected just to show the ability of providing a good attenuation level outside the assumed passband; in this case, better than -20 dB, while the ripple inside the passband was maximum 3 dB.

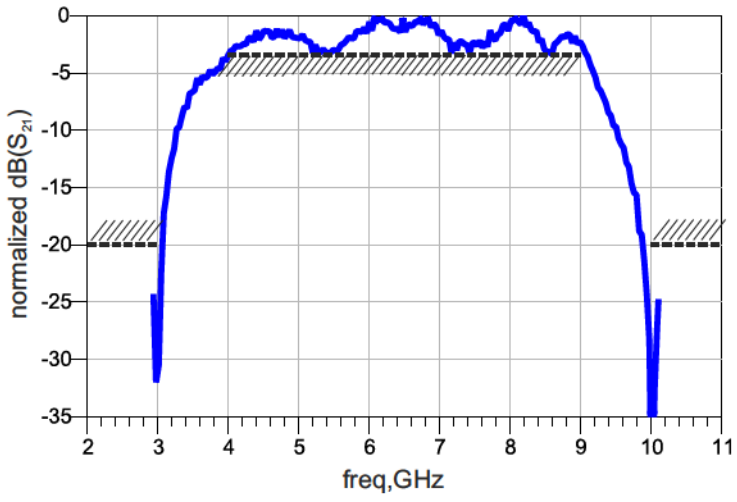

Fig. 4.29: Transmission coefficient of an UWB BPF with bandpass from 4 to 9 GHz

A small and flat GD lower than 2 ns over the whole frequency band was achieved, as shown in Fig. 4.30.

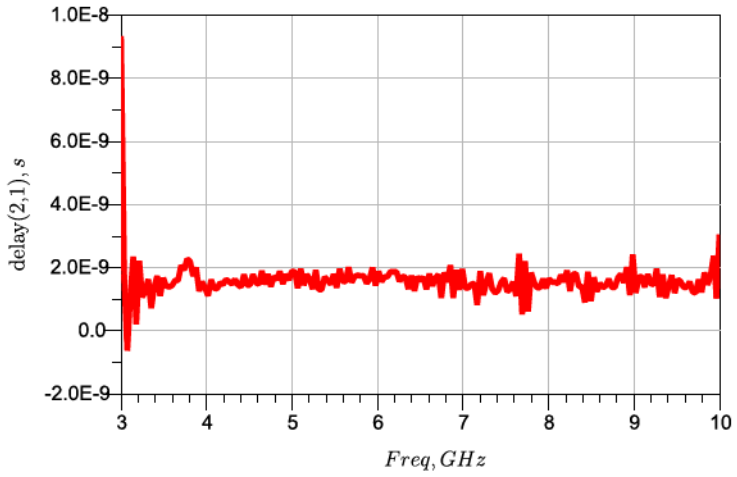

Fig. 4.30: GD of FIR bandpass filter

4.6.1.1 Tunable Bandpass Filter

In this section the FIR filter as tunable band pass filter will be introduced, which has many applications in the industry. As many countries have their own frequency bands definition, using a tunable BPF will allow RF systems to be easily integrated under different circumstances. An example of this is that the EC UWB only allows part of the FCC mask, so that a BPF may be used to adapt a system design for the EC mask in this case. Fig. 4.31 shows an adaptive BPF at different frequency bands.
Table 4.6 mentions the frequency band of the tunable BPF and the optimized filter coefficients of the designs. The parameter F (GHz) in this table refers to the frequency where the incremental delay of the FIR was calculated. The goals is achieved for all the frequency bands, with EF = 0.

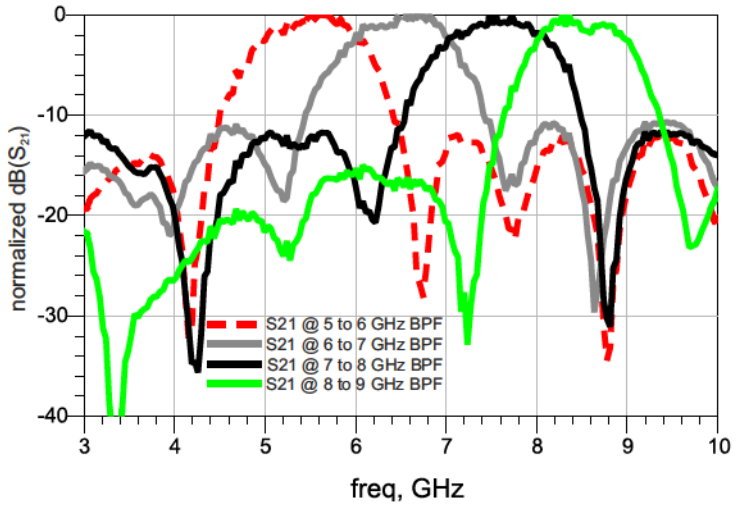

Fig. 4.31: Insertion loss for FIR filter of different passbands.

a_n	$5-6GHz$	$6-7GHz$	$7-8GHz$	$8-9GHz$
a_0	0.23	0.66	-0.38	-0.85
a_1	0.23	0.66	-0.38	-0.85
a_2	0.55	0.79	-0.19	0.41
a_3	-0.16	0.08	-0.16	0.77
a_4	0.65	0.22	-0.02	-0.39
a_5	-0.16	-0.45	-0.08	-0.99
a_6	0.75	0.20	0.08	0.10
a_7	-0.12	-0.19	-0.03	0.86
a_8	0.95	1	0.78	0.54
$F(GHz)$	5.78	6.73	9.09	5.66
EF	0	0	0	0

Table 4.6: FIR coefficient at different passband frequencies.

The GD and normalized response of the tunable FIR BPF are plotted in Fig. 4.32. As it can be seen in all plots, the GD inside the passband is flat.

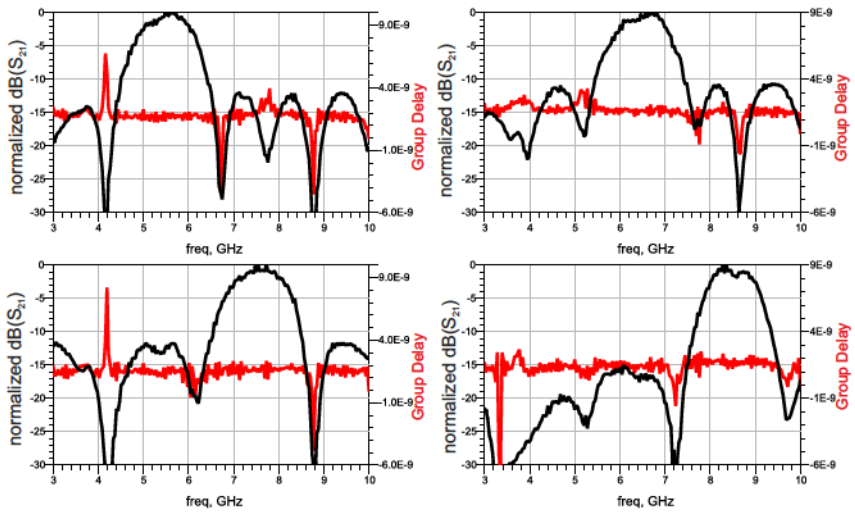

Fig. 4.32: Insertion loss and GD for FIR BPF designs.

4.6.1.2 Combined Bandpass Filter

Adding a compact section of a periodic band pass filter can improve the performance of the adaptive band pass filter. In this section, a supplementary section will be added, which consists mainly of two parallel transmission lines having the same characteristic impedance Z, with different electrical length, such as 90° and 450° at a center frequency

f_0. The structure will provide a periodic band pass filter centered at f_0 with bandwidth equal to $f_0/2$. More theory about the design can be found in [MR90]. Fig. 4.33 shows the performance of such parallel lines; the simulation used the ideal transmission lines model in ADS. When this section is cascaded with the adaptive BPF, one can improve the steepness of filter skirt edges by reducing the transient band, and also improve the attenuation in the stopband. If the supplementary section is well designed to cover the whole passband of the adaptive BPF, then the amplitude in the passband will not be attenuated.

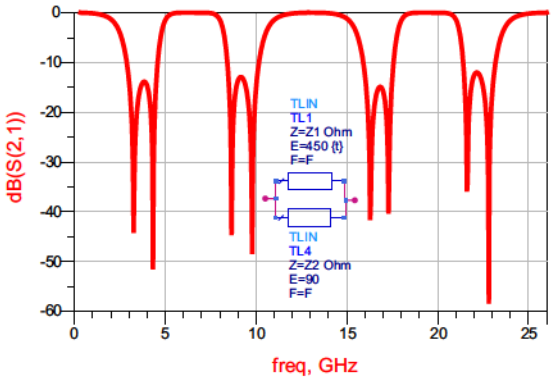

Fig. 4.33: Parallel transmission lines as periodic bandpass filter schematic design and insertion loss.

As shown in Fig. 4.34 an improvement in the steepness of the filter skirt is clear without affecting the transmission.

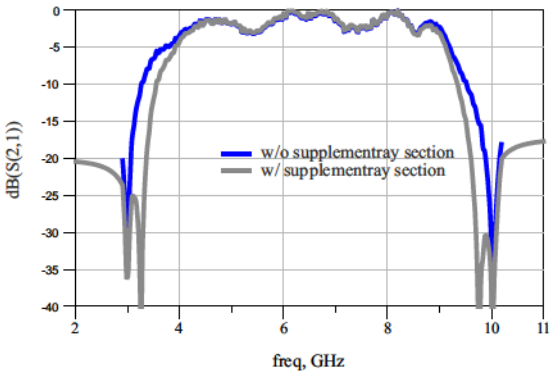

Fig. 4.34: BPF performance with and without supplementary section.

In order not to lose the adaptivity of such filter, one can use a digitally controlled variable transmission line.

4.7 FIR Filter as Highpass Filter

In the same way optimization was done to generate a HPF using an adaptive FIR filter; a 9^{th} filter order was chosen, as seen in Fig. 4.35.The final optimization results should fulfill some requirements for example (insertion losses in passband, attenuation in the stopband,

input and output reflection, and also high isolation), the final filter coefficients are summarized in Table 4.7, with filter coefficients for the HPF at different cut-off frequencies.

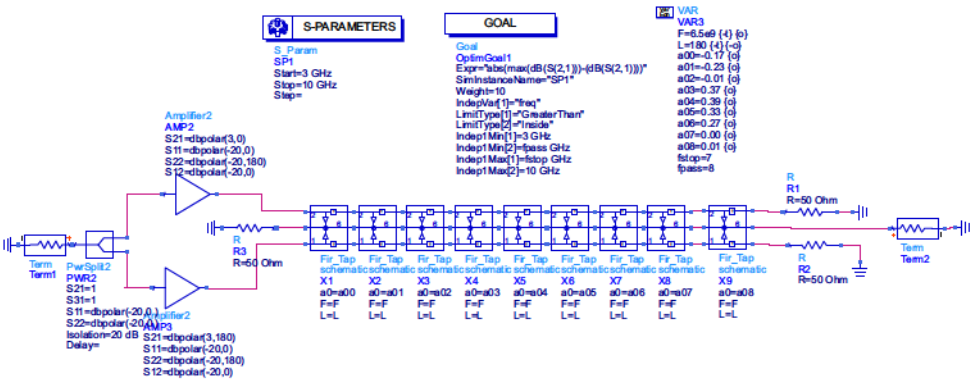

Fig. 4.35: Highpass filter design.

$a_n \backslash f_c(GHz)$	5	6	7	8
a_0	-0.11	-0.4	-.08	-0.13
a_1	0.04	-0.03	-0.09	-0.13
a_2	0.54	0.07	-0.08	0.01
a_3	-0.26	0.75	0.06	0.25
a_4	0.40	-0.97	0.26	0.19
a_5	0.47	0.11	-0.02	0.06
a_6	-0.15	-0.8	0.00	0.22
a_7	0.33	0.23	-0.05	0.12
a_8	0.3	0.61	-0.05	0.21
$F(GHz)$	8.84	8.5	6.47	6.55
EF	0	0	0	0

Table 4.7: Optimized coefficients for HPF at different Cut-off frequencies.

The normalized values of S_{21} are shown in Fig. 4.36. The resulting filter character perfectly matches the goals with $EF = 0$. The threshold value is defined for the insertion losses in the passband not to be larger than 3dB and attenuation in the stopband to be lower than 15 dB in the whole stopband. Besides, a very good input and output reflection (not illustrated in Fig. 4.36) and also a very good isolation S_{12} in the whole UWB frequency band is realized.

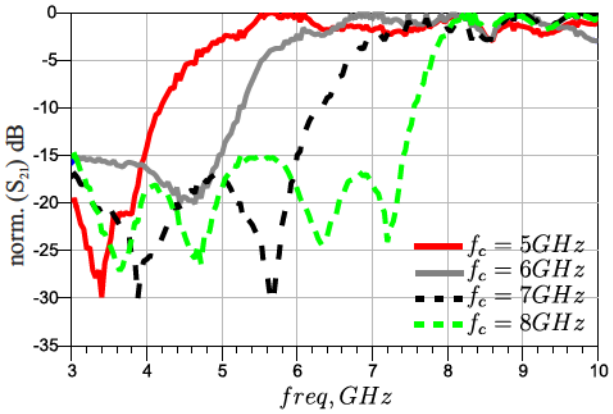

Fig. 4.36: Insertion loss of HPF at different Cut-off frequencies.

In Fig. 4.37 the filter order was changed while keeping the same cutoff frequency. As the filter order was increased, a sharper transition between the stopband and the passband was achieved. In this optimization, one tried to keep the absolute passband ripple under same value (here it was selected to be -2.2 dB) and the stopband attenuation under -20dB.

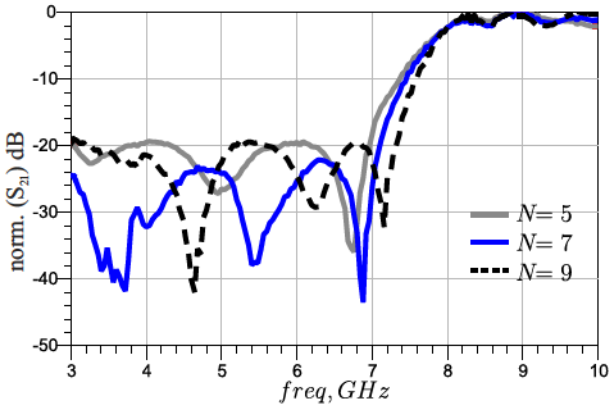

Fig. 4.37: Insertion Loss of HPF with different filter orders at same Cut-off frequency.

In Fig. 4.38, the GD level is increased as the filter order was increased, but still approx. constant inside the passband frequency of the HPF. The HPF was designed here to have cutoff frequency at 8 GHz.

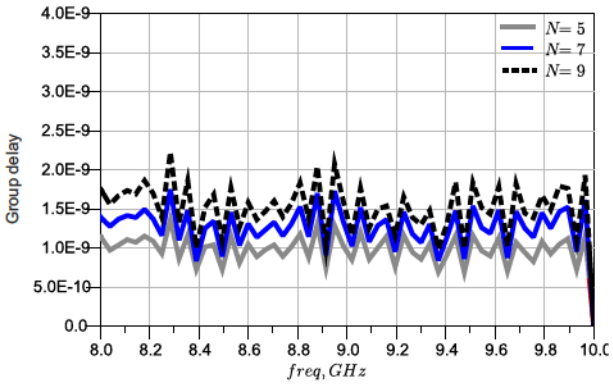

Fig. 4.38: GD of HPF at $f_c = 8GHz$ and different filter order FIR filter as notch filter

$a_n \backslash$ **Filter Order**	5	7	9
a_0	-0.49	-0.10	-0.17
a_1	-1	-0.14	-0.23
a_2	-1	-0.04	-0.01
a_3	-0.31	0.24	0.37
a_4	0.37	0.30	0.39
a_5		0.17	0.33
a_6		0.01	0.27
a_7			0.00
a_8			0.01
$F(GHz)$	5.21	5.93	6.5
EF	0	0	0

Table 4.8: Filter coefficients for HPF at $fc = 8\,\text{GHz}$ and different filter order.

4.8 FIR Filter as Notch Filter

In order to overcome the interference that can happen with already existing standards, such as IEEE802.11a wireless local area network (WLAN), and HIPERLAN/2 (which operate in the frequency interval $5-6\,\text{GHz}$), the rejection of such already used frequency bands becomes important. One can use notch techniques inside the antenna itself to achieve the rejection of the unwanted band [Pan09], but since this solution does not work for all antenna types, a more general solution is to use a notch filter in the UWB system. Adaptive FIR filters can generate this frequency notch, as well as compensate for some of the distortion which could occur from the antenna itself, and carry out pulse shaping to reform the generated pulse to fulfill some prerequirement. The simplest way to create a deep notch at a single frequency is to use a first order transversal filter. The transversal filter can be seen as a special case of FIR filter, but with the filter coefficients assumed equal to one $a_n = 1$. By dividing the signal into two paths and providing one path with a 180° phase shift exactly at the notch frequency, the signal transmission will be attenuated at this notch frequency due to destructive superposition. Fig. 4.39 shows the schematic and the simulation result of such setup.

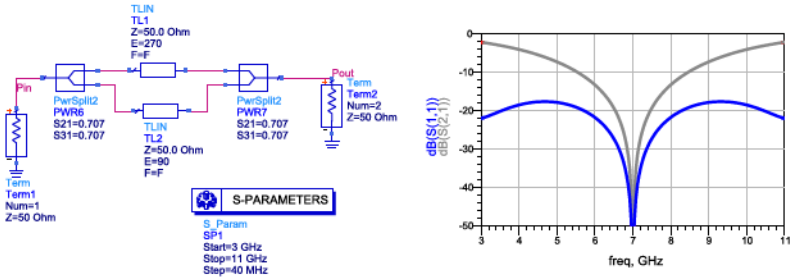

Fig. 4.39: Transversal notch filter.

4.8.1 Single Notch Frequency

A notch filter was designed using 4^{th} order FIR filter, as shown in Fig. 4.40. The table below shows the final optimization values which satisfied the requirements.

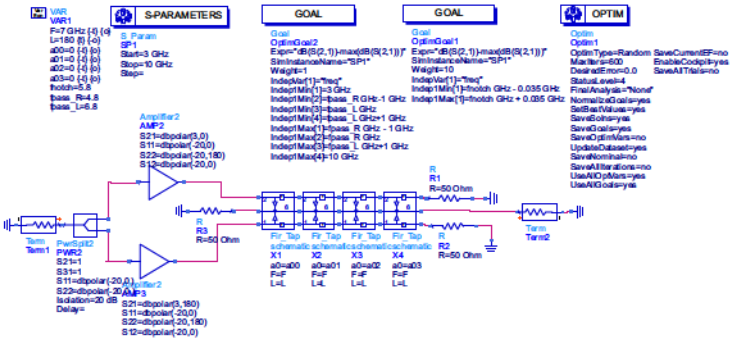

Fig. 4.40: Design and optimization of a notch filter at different frequencies.

$a_n \backslash f_n(GHz)$	5.5	6.5	7.5
a_0	-0.03	-0.14	-0.53
a_1	0.20	-0.23	0.38
a_2	0.37	0.65	-0.84
a_3	-0.63	-0.24	-0.32
$F(GHz)$	3	3.69	3.97
EF	0	0	0

Table 4.9: FIR filter coefficients for different notch frequencies.

The final result is shown in Fig. 4.41, as it can be seen inside the notch band a very good attenuation of more than 20dB, and outside the notch frequency (passband) the insertion loss is less than 3dB. By adjusting the filter coefficients, one can tune the notch frequency to any desired frequency.

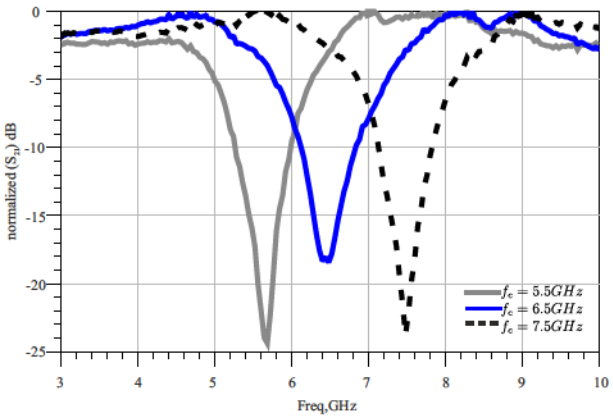

Fig. 4.41: Insertion loss of notch filter at different frequencies.

The GD of the designed filter is flat outside the notch band, as shown in Fig. 4.42.

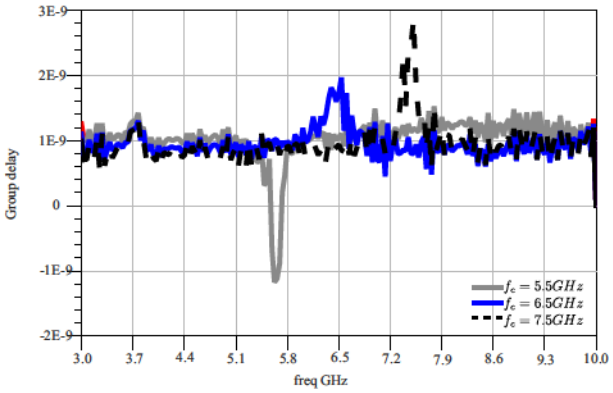

Fig. 4.42: GD of notch filter at different notch frequencies.

The next step uses the results from optimization at the notch frequency of 5.5 GHz and changes the electrical length, which is equivalent to the delay τ, which normally is $\lambda/2$ (180° phase shift) at a specific frequency. By just sweep this electrical length and observe the notch frequency while keeping the same filter coefficients. One notice a shift in the notch frequency as the electrical length was changed, and acceptable insertion loss in the passband Fig. 4.43.

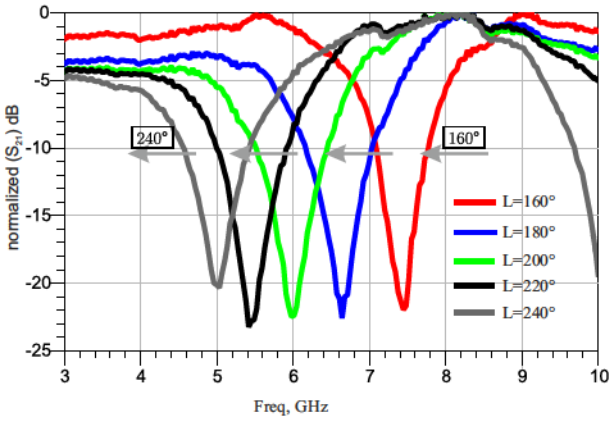

Fig. 4.43: Notch frequencies at different electrical length of delay sections with fixed filter coefficients.

$a_n \backslash f_n(GHz)$	6.5
a_0	0.08
a_1	0.58
a_2	0.83
a_3	-0.12
$F(GHz)$	3.5
L(Electrical Length)	180°
EF	0

Table 4.10: Filter coefficients for notch filter.

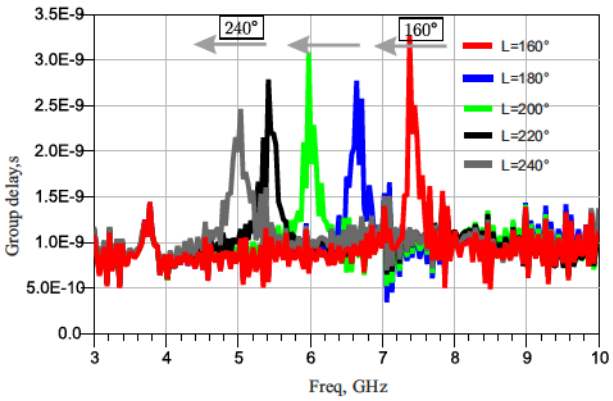

Fig. 4.44: GD at different electrical length of delay sections with fixed filter coefficients.

As is mentioned above, one problem of UWB system is a possible interference with relatively strong narrowband signals, like those in WLAN at 5.8 GHz; therefore a notch should be designed in the UWB system to reject this frequency. A notch filter is designed using the adaptive FIR filter. In order to see the effect of the passband ripple and stopband attenuation, two optimizations where done; Design (a) has a very low ripple in the passband, and design (b) has a very high attenuation in the stopband. Both optimizations have the same filter order $N = 4$. At the right of Fig. 4.45 shows the insertion loss for both designs. Inside the passband, although there are differences in the Insertion loss (IL), there is little effect in the GD, Fig. 4.45, right. However, in the stopband, the attenuation level (AL) is different; the transition is faster and sharper in design (b). One can see this effect in the GD where is the level inside the stopband is much higher for design (b) (around 10 ns). The GD behavior inside the notch band will be studied in detail in the next chapter, and the notch influence on a UWB signal will also be discussed in more detail, by studding the time domain response and spectrum using different types of Gaussian pulses. The variation of GD outside the notch band is very small, almost flat, and the level of GD less than 1ns.

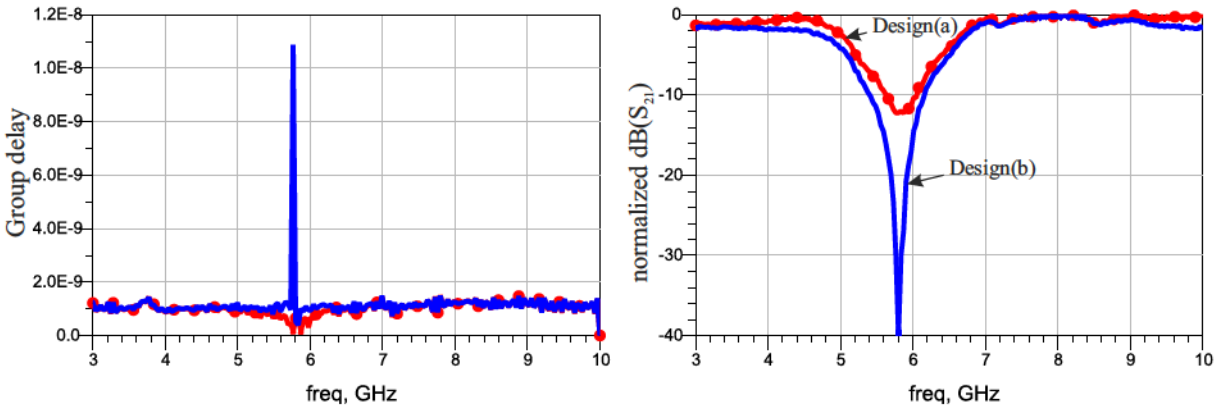

Fig. 4.45: GD and insertion loss of a notch filter for different design optimizations at the same frequency.

4.8.1.1 Dual Notch Filter

To check the ability of controlling more than one notch frequency, the design was made to have two notch frequencies (one at 5 GHz and the other at 8 GHz). The final filter coefficients produce a low IL inside the passband not larger than 3 dB, and a very good AL inside the two notch frequencies better than 25 dB, as can be seen at the right of Fig. 4.46. At the left, the GD is almost flat outside the notch band.

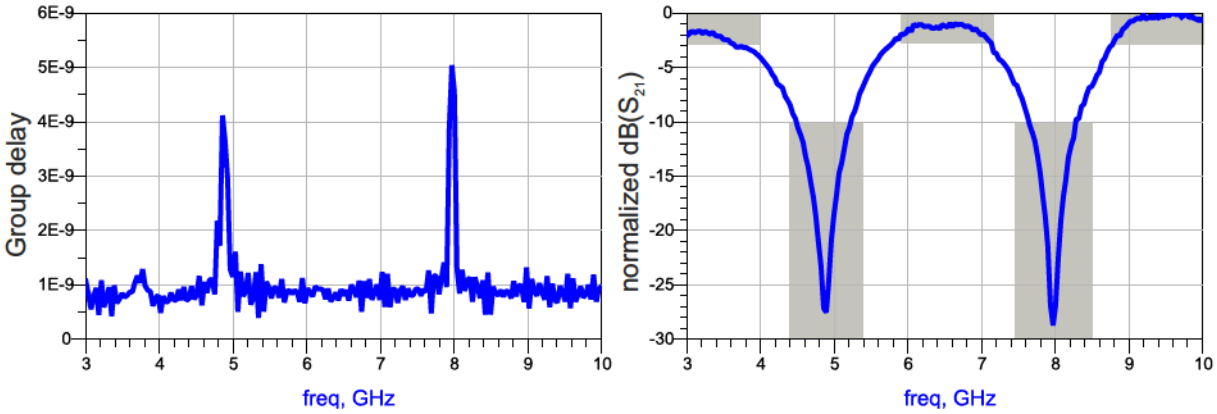

Fig. 4.46: Dual notch using adaptive FIR filter.

Inside the notch band, the variation of GD is high and dependent on how sharp the transition from the passband to the notch band is. As the attenuation inside the notch band is larger, the peak of GD increases in the notch band.

CHAPTER 5

PULSE SHAPING NETWORK

5.1 Introduction

In many UWB applications, the signal's equivalent isotropically radiated power (EIRP) must conform to the regulation defined by the Federal Communication Commission (FCC). As a result, the closer the signal PSD conforms to the area under the FCC's PSD mask the more power the signal is able to transmit. This can be realized using pulse shaping (or pulse forming). Most research contributions on pulse shaper optimization and pulse design propose new theory or methods from the mathematical viewpoint without practical circuit implementation [TJ06] such as, creating an optimal pulse through DSP implementation of a digital FIR filter which requires an immense computational effort [Pan09]. Analog technology proposals based with practical implementation techniques for pulse shaping suffer from large system dimension and/or only a single shape pulse is generated [RB08]. In [RB08], a well-designed adaptive arbitrary pulse shaper is presented, however it suffers from large size and cannot be used in UWB systems, as it does not fulfill the UWB spectrum mask requirements. Its large size is a result of using a parallel structure with separated delay lines for every weighting stage. Where the design presented at this work provides a distributed delay lines in series structure, which increase the possibility of constructing higher order filter and as a result better pulse shapers. In this chapter, different methods for achieving pulse shaping will be introduced. Using Gaussian pulse derivatives to generate a higher order Gaussian pulse, which fits closely to the FCC PSD mask. In section 5.3, the conventional transversal filter with different combinations and modified versions is introduced, to achieve pulse shaping. Lastly, a practical design of a pulse shaper using a FIR filter is presented. Starting with the ideal FIR design, and then end with the practical implementation. By using a FIR filter as a pulse shaper, one can generate nearly arbitrary pulse shape, which not only effectively uses the spectral mask, but also allows real-time adaption to different spectral masks. It can also be used for equalization and pulse optimization, to compensate for pulse distortion in the over-all UWB system.

5.2 Gaussian Derivative Pulse Shaping

In order to fulfill the requirement of the PSD for UWB wireless indoor system, while at the same time maximizing bandwidth, higher order Gaussian pulses may be used, as this increases the efficient use of the available spectrum by shifting the peak frequency and as a result changing the bandwidth of the pulse [DBG04]. Moreover, one can use a FIR filter as a differentiator of the Gaussian pulse.

5.2.1 First Derivative Gaussian Pulse

In this subsection, a simple implementation of Gaussian pulse differentiator based on the straightforward approximation $(\triangle t) \cdot f'(t) \approx f(t + \triangle t) - f(t)$ is introduced [TJ06]. The design concept is shown in Fig. 5.1(a) where the input signal $f(t)$ is divided, one goes through delay line (l) where signal is inverted and added again to the other signal with longer delay line $(l + \triangle l)$. The output is approximately proportional to the derivative of the input signal. One can use a coupled line as differentiator, by using the mutual capacitance that exists between two conductors in RC network [MSF07].

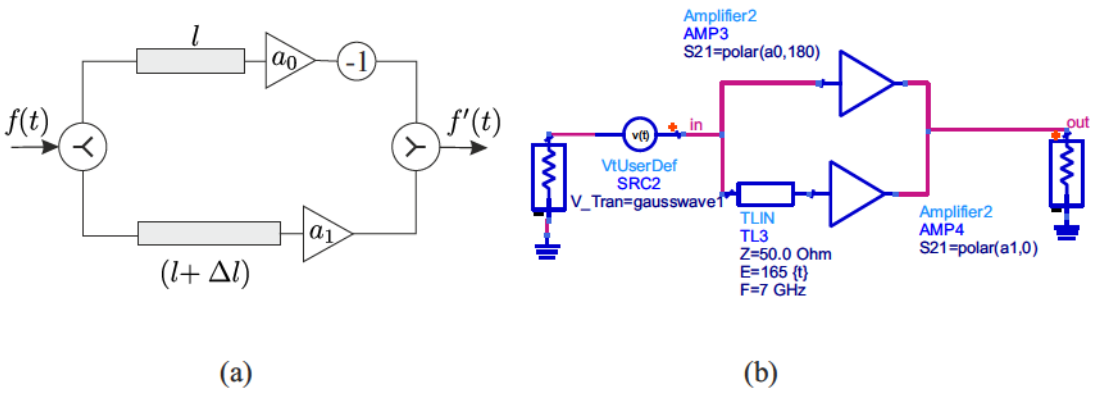

(a) (b)

Fig. 5.1: (a) Gaussian pulse derivative design concept, (b) Implementation of pulse derivative in ADS.

In Fig. 5.1(b), the ADS implementation of such a concept is shown using ideal components. The input signal is a first order Gaussian pulse, the signal is divided into two parts, one is inverted (180° phase shift) and weighted by coefficient a_0, and the other path of signal is delayed by an extra transmission line and weighted by a_1. This delay line was optimized to achieve the best approximation to the derivative of input pulse, where also the PSD fulfills the UWB mask. The design looks like a first order transversal filter with the restriction that one of the coefficients is positive and the other is negative. The extra length of the transmission line in one branch can be seen as delay line when it compared with a transversal filter, which will be studied in detail in the next section. The output signal will be approximately the derivative of the input signal. The simulation result is shown in Fig. 5.2, in both time and frequency domain. The input signal is a first derivative Gaussian pulse, and the output is a clean second derivative Gaussian pulse without distortion. For further comparison, the generated second derivative Gaussian pulse is compared with the ideal one, and the result is very good (as shown in 5.2(c) and (d). However, the PSD for the generated 2^{nd} Gaussian pulse does not fulfill the UWB mask at the edges. Such pulses will not be allowed to be used in UWB systems. In order to solve this problem in

the next section a higher order Gaussian derivative will be introduced which fulfills the UWB mask.

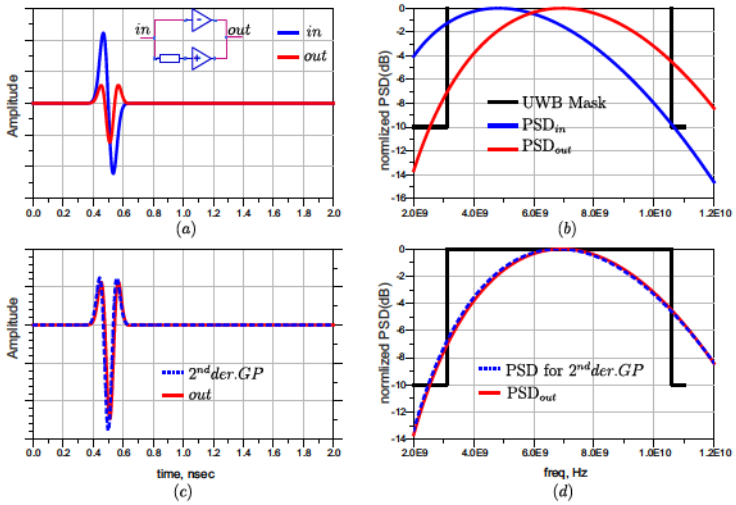

Fig. 5.2: Simulation Result of the Gaussian pulse differentiator: (a) Input and Output pulses, (b) PSD for Input and Output pulses, (c) Ideal 2^{nd} derivative Gaussian pulse and the generated one, (d) PSD for both in Part C.

5.2.2 Higher Order Gaussian Derivative

In Fig. 5.3(a), two differentiators were cascaded to produce the 2^{nd} derivative of an input signal. Where the input pulse was a 1^{st} derivative Gaussian pulse, the generated pulse looks like an ideal 3^{rd} derivative Gaussian pulse, with a small shift in time; this shift is produced by the extra transmission line when the differentiator was implemented. Both ideal and generated Gaussian 3^{rd} derivative fulfill the FCC mask requirements, except, at edge frequencies, the ideal 3^{rd} Gaussian derivative exceeds the limitation of the FCC mask. In the generated one, this can be solved by optimizing the parameter σ parameterized the effective width of the pulse) the optimized value was 35 ps. The input was first Gaussian derivative pulse which was fed to the differentiator,

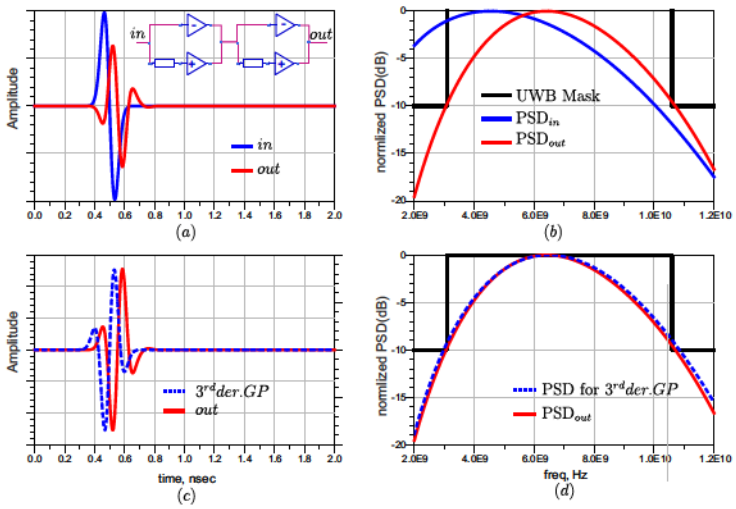

Fig. 5.3: Two cascaded pulse differentiators to generate the second derivative of an Input pulse.

In Fig. 5.4, an extra differentiator was added to produce a 3^{rd} derivative Gaussian pulse from an input Gaussian pulse. The generated pulse has the exact shape of the ideal 3^{rd} Gaussian pulse and better fulfills the FCC mask, especially at edge frequencies (as is shown in Fig. 5.4(d)).

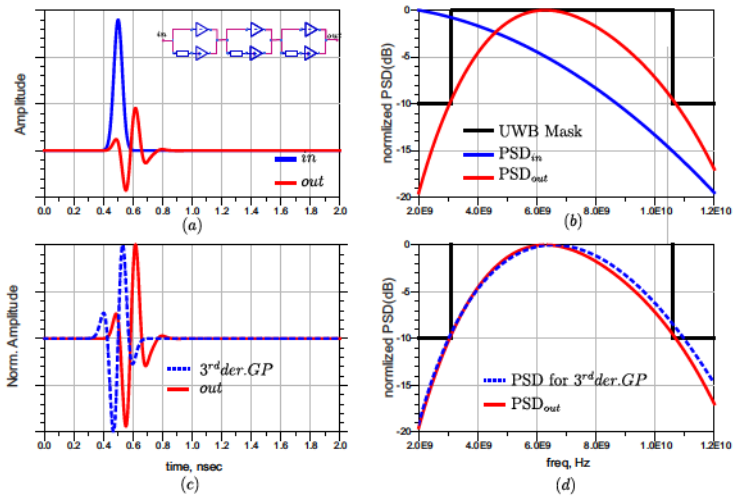

Fig. 5.4: Three cascaded pulse differatiators to generate the 3^{rd} derivative of an Input Gaussian pulse.

This Gaussian differentiator was implemented in ADS using ideal components, Implementations of such a design with non-ideal components will be not an easy task, especially when one need a broad band inverter to invert the divided signal. Also a broadband weighting amplifier is needed which should not distort the input signal, which means constant amplitude and constant group delay across whole frequency band. A broadband power divider and combiner will not be difficult to produce.

5.3 Transversal Filter Pulse Shaping

The standard transversal filter is shown in Fig. 5.5, which shows a single input. This signal is applied to the first weighting coefficient (a_0), and is delayed by τ_1 to be applied to the second weighting coefficient and so on. The weighted signals are combined to produce the output signal. So two parameter set are available to control this transversal filter: The weighting coefficients and the length of the delay lines. By the combination of these two parameter set one can produce four different types of transversal filters as follows:

1. Equal delays τ and equal weights (a).
2. Equal delays τ and unequal weights (a_i).
3. Unequal delays τ_i and equal weights (a).
4. Unequal delays τ_i and unequal weights (a_i).

These combinations increase the freedom in design, and can make pulse shaping easier, but in the case of unequal delays τ, adaptability of delay settings is very difficult. Changing the delay τ is difficult as a transmission line is used to represent this delay, and changing the length of this line is not possible after manufacturing unless one can replace this

transmission line by a variable delay line. While the conventional concept of transversal filters assume that the input signal is used to fed the weighting branches as well as the next delay section, in an analogue microwave realization the signal (power) has to be divided first before using in separate branches of the filter.

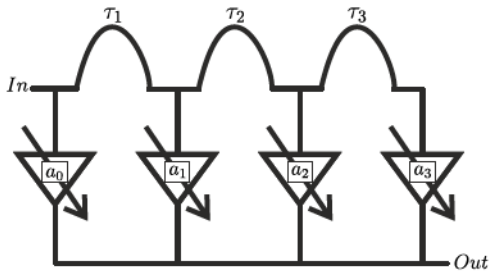

Fig. 5.5: Conventional transversal filter (series structure).

A modified version of the transversal filter is shown in Fig. 5.6, where the input signal is equally divided by the number of filter taps (in this example $N = 4$), so the divided signal can propagate in different parallel paths and is delayed and combined at the end. The advantage of using such parallel structures compared to the series one in Fig. 5.5 is that one can use a single power divider and combiner. However they have the disadvantage of using separated delay lines for each weighting stage, which means the average delay line length is larger than in the series arrangement. On the other hand it can be seen as advantage by increasing the degree of freedom for easy fulfilling the design goals.

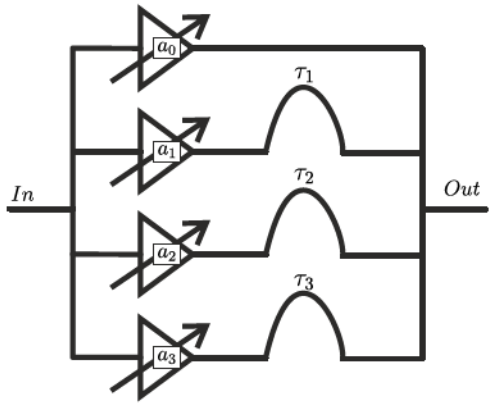

Fig. 5.6: Modified transversal filter (parallel structure).

The implementation of this filter in ADS is shown in Fig. 5.7 where ideal components were used. The power divider is followed by the weighting stages which are implemented by 2-port S-parameter equations, where the $S21$ is our filter coefficient represented in the schematic by (a_{0i}), where i takes the value from 0 to 3 (here the filter order is 4^{th}). The value of (a_{0i}) will be between 1 and -1 where the - sign was implemented by $180°$ phase shift. The delay was implemented by an ideal Time Delay with the delay t_i as optimized variable as shown in the schematic, Fig. 5.7. In this case the delay lines with t_0, t_1, t_2 and t_3 are not equal. The weighted and delayed signals are combined to provide the output of the modified transversal filter. An extra gain block was added after the power combiner to compensate the insertion losses of the power divider and combiner.

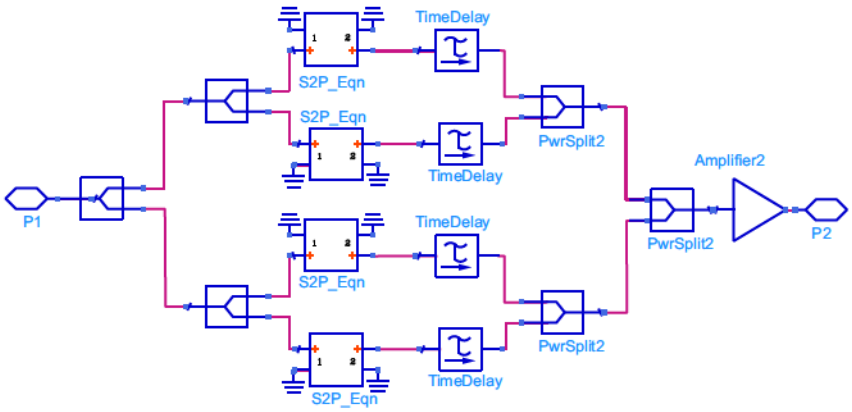

Fig. 5.7: Implementaion of transversal filter (parallel structure) in ADS with variable time delay t_i

The input signal for the modified Transversal filter was 1^{st} Gaussian derivative, as shown in Fig. 5.8 which did not fulfill the FCC concerning the PSD requirement. The output signal PSD from the optimized filter is plotted in the same figure (red curve) and looks similar to the 5^{th} Gaussian derivate (it crosses the time axis five times). The optimized pulse fulfills the FCC mask better but still exceeds the limit at lower and higher frequency edges, as it can be seen in part b of Fig. 5.8.

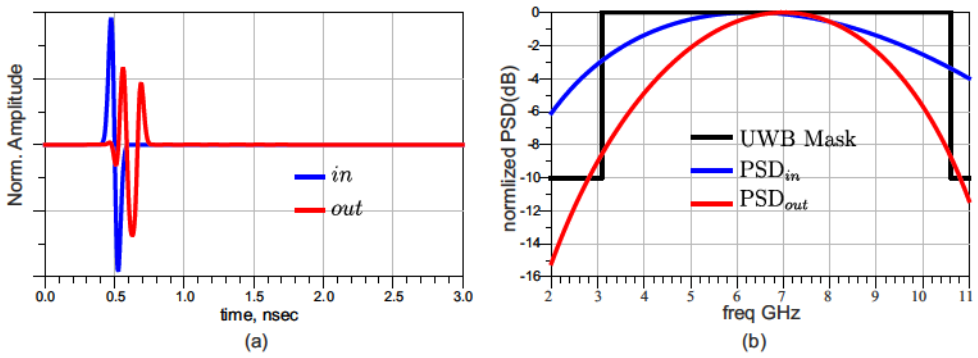

Fig. 5.8: Output pulse amplitude and PSD after applying the modified transversal filter.

To generate an optimized pulse shape which efficiently fulfills the EC requirement for PSD in the frequency band from 6 to 8.5 GHz, the input pulse was selected to be 5^{th} Gaussian derivative. Although it fills the EC mask more efficiently than the final optimized signal, outside the EC band the PSD level is higher than allowed. The filter was optimized with the final result shown in Fig. 5.9. The red curve represents the filtered signal, with a pulse width around 0.94 ns.

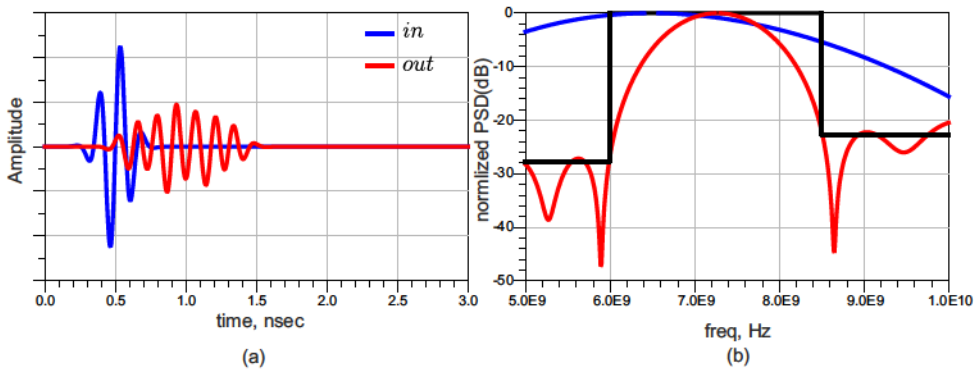

Fig. 5.9: An optimized pulse shape fulfils the EC requirement for PSD.

It might be easier to insert a BPF and form the input signal to fulfill the EC requirement by eliminating the undesired signal components outside the desired UWB frequency band. Inserting such filter besides making the circuit complicated will limit the application of such a device only a specific frequency band while many standards exist around the world with different frequency bands; at the end the structure will not be adaptive any more.

5.4 FIR Filter Pulse Shaping

5.4.1 Ideal FIR Filter

The ideal FIR filter consists of ideal power splitter, combiner and weighting circuits; in the simulation the S-parameter equation of ADS is used to define the S-parameter matrix as shown in Fig. 5.10. Inside each filter tap, there is a delay line with delay τ which normally takes a value equivalent to the electrical length of 180° at a specific frequency.

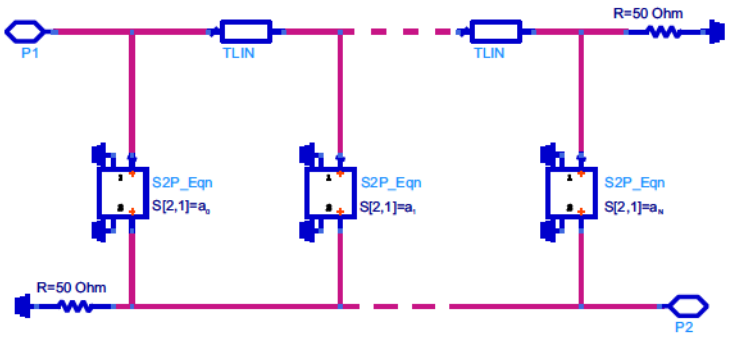

Fig. 5.10: Ideal FIR filter implementation Using ADS.

The filter coefficients is defined as parameters which can be optimized to achieve the desired goal. The input signal is a first derivative Gaussian pulse, which is created using a user defined voltage source in ADS (as shown in Fig. 5.11). The goal is to generate a new pulse satisfying the spectral mask emission requirements specified by the FCC. In Fig. 5.12, on the left side, the input pulse before applying the FIR pulse shaper, and on the right after applying the pulse shaper. The generated pulse is now wider in pulse width and has more zero crossings. This increase in zero crossings can explain the improvement which is achieved in the PSD, where the PSD of the 1^{st} derivative Gaussian

pulse, Fig. 5.13(a), at lower frequency does not fulfill the FCC regulation, while at higher frequencies there is a rapid decrease of power level resulting in an inefficient usage of the FCC mask. The filtered pulse fulfills the FCC mask, but does not optimally exploit the allowable bandwidth and power density so improvement can be tried by replacing the input by a 3^{rd} derivative as shown in Fig. 5.14, and run the optimization again.

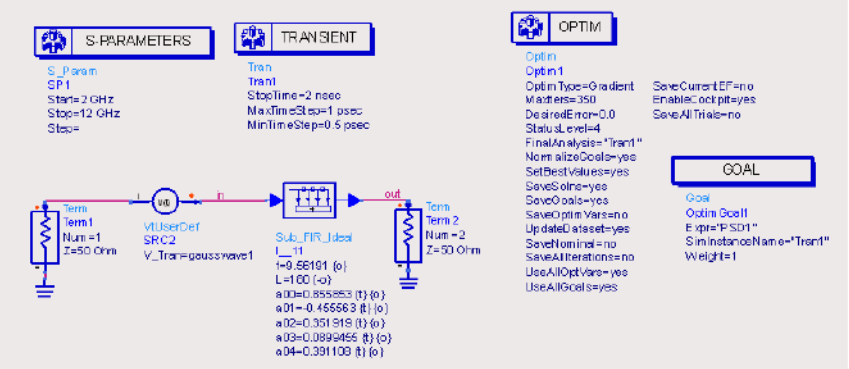

Fig. 5.11: Optimization of Ideal FIR filter in ADS.

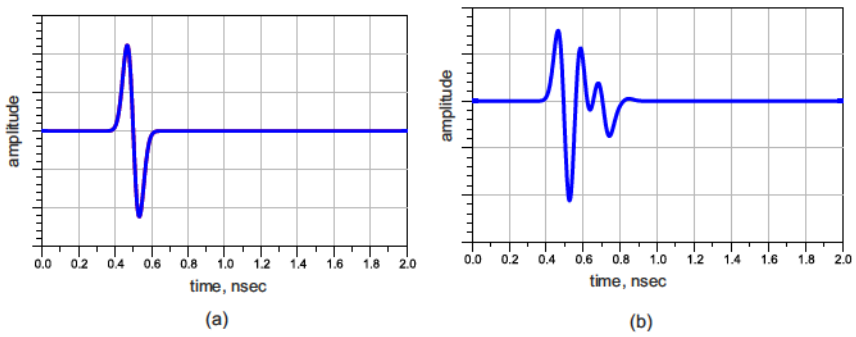

Fig. 5.12: (a) 1^{st} Derivative Gaussian pulse, (b) Generated pulse using FIR filter.

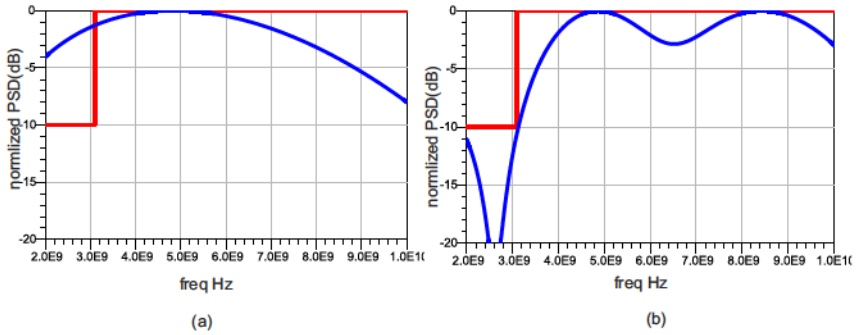

Fig. 5.13: (a) PSD of 1^{st} derivative Gaussian pulse, (b) PSD of generated pulse using FIR filter

As shown in Fig. 5.14(b), the filtered pulse is wider and has more zero crossings. The calculated PSD in Fig. 5.15, validates the improvement in the efficient usage of the FCC spectrum. while the FCC spectrum regulation is still fulfilled.

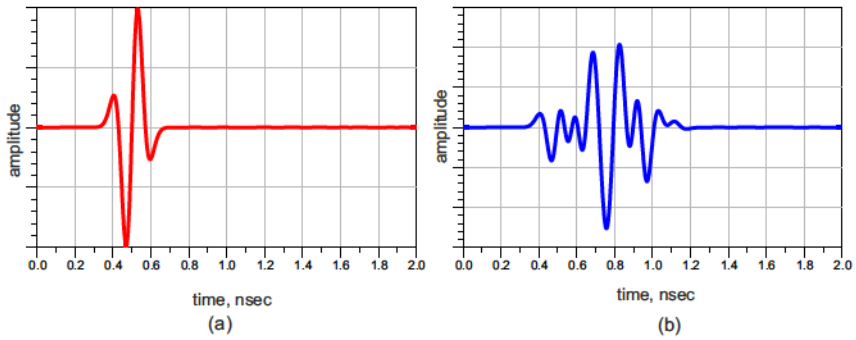

Fig. 5.14: (a) 3^{rd} Derivative Gaussian pulse, (b) Generated pulse using FIR filter.

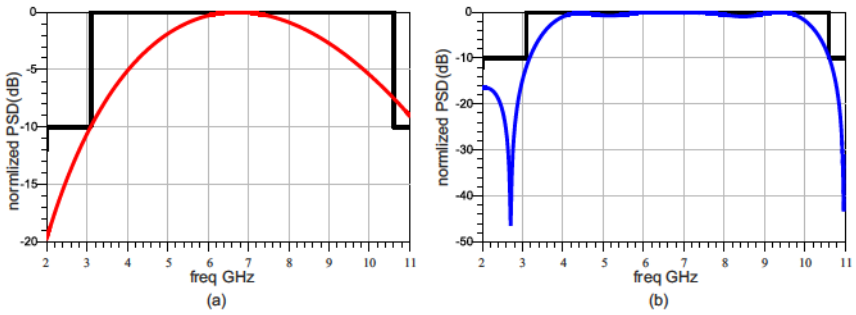

Fig. 5.15: (a) 3^{rd} Derivative Gaussian pulse, (b) Generated pulse using FIR filter.

For better comparison, Fig. 5.16 is inserted which shows how the improvement (red curve) is close to the FCC mask, compared to the input pulse (blue curve).

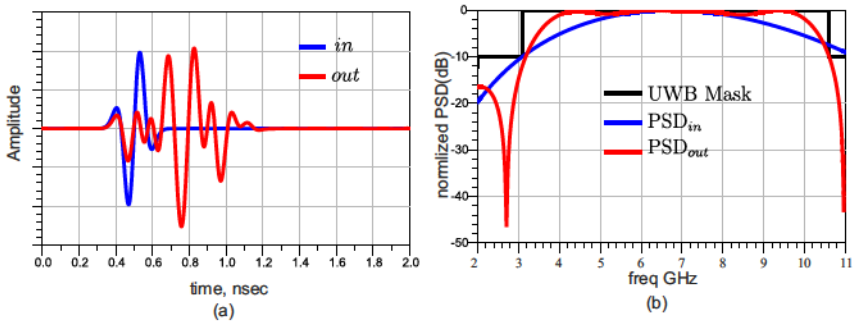

Fig. 5.16: Amplitude and PSD before and after using FIR pulse shaper.

Still, one disadvantage of this optimization is that the generated pulse has a higher pulse width, which can affect the performance of the application system. In the next section, two new goals in the optimization process will be inserted: One is the output pulse width and the other is the amplitude of the output signal compared to the amplitude of the input signal as shown in Fig. 5.17. The input pulse is a 3^{rd} derivative Gaussian pulse, and the goal is to have the best pulse shape that fits in the FCC mask, taking into account also that the pulse should not be wider than a predefined threshold, and the amplitude of output signal should not be smaller than a threshold value.

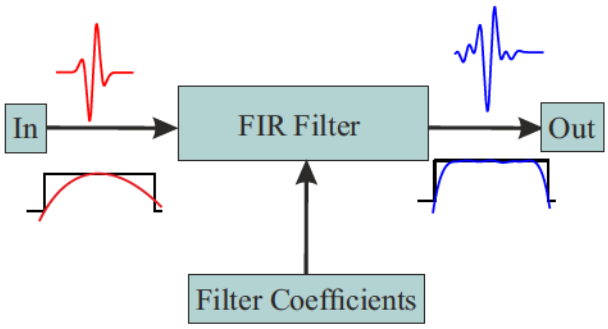

Fig. 5.17: Pulse shaping using FIR filter.

```
MeasEqn
Meas3
indices=find(abs(mag(out))>0.1*max(abs(out)))
firstpoint=indices[0]
Lastpoint=indices[sweep_size(indices)-1]
pulseWidth=time[Lastpoint]-time[firstpoint]
```

Fig. 5.18: Definition of pulse width under ADS.

In Fig. 5.18, the pulse width is defined at amplitude levels of 10% of the peak level. As is expected, there will be more than two points that will satisfy this condition, since there are more than two zero crossing points. An indices is inserted and select the first point and last point which fulfill this criterium, and calculated the time difference to be the pulse width, as defined in Fig. 5.19.

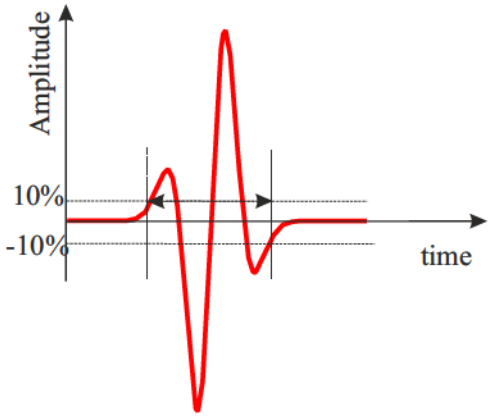

Fig. 5.19: Pulse width definition.

In Fig. 5.20(a), it can be seen a large improvement by decreasing the pulse width. One can also see some ringing, but its amplitude is lower than the 10% of the pulse peak. If this pulse width is compared with what in Fig. 5.16, one see a very good improvement with almost the same efficient use of FCC spectrum, as shown in Fig. 5.20(b). To sum it up, the pulse width was reduced, which should improve the achievable data rate. A measure of utilization efficiency of the input and output signal was calculated by integration of the logarithmic scale of the PSD and results are presented in Table 5.1. The area of integration is the area of the rectangular shape of the UWB band from 3.1 GHz to 10.6 GHz. This area is assumed to be 1 or 100%, while the integration of the PSD over the same UWB frequency band for both the input and output signal PSD results in lower

efficiency, as shown in Table 5.1. An improvement in the efficiency of more than 15% was achieved with the help of the FIR filter pulse shaper relative to the efficiency of the input signal PSD. While at the same time the optimized pulse fulfills the FCC restriction unlike the input one.

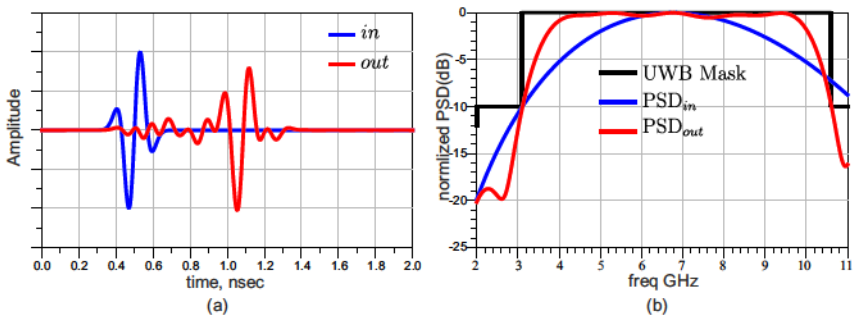

Fig. 5.20: Pulse shaper optimization wit FIR filter, $N = 5$.

FCC mask	Input signal	Optimized pulse
100%	72%	88%

Table 5.1: Computed utilization efficiency compared to FCC mask.

5.4.2 UWB FIR Pulse Shaper Design Exercise

In this section, the design of a UWB pulse shaper based on the manufactured FIR tap characteristics will be presented. As the measurement results are available in frequency domain (S-parameter measurement), the pulse shaper optimization will be done in the frequency domain. The input Gaussian pulse in time domain was Fourier transformed to frequency domain, and inserted as 2-port S-parameter file, which is the input to the shaping FIR filter, where $N = 9$ and delay τ equivalent to the electrical length of 180° at $F = 7.24GHz$. The output signal is optimized to fulfill the frequency spectrum mask of a standard regulation (for example, EC or FCC standards). A frequency-to-time transformation is performed to get the output pulse in time domain. Concept and circuit simulation setup are shown in Fig. 5.21.
First example is to generate a pulse fulfilling the FCC regulation mask and efficiently use the allowed spectrum. The input signal was a Fourier transformed fourth order Gaussian pulse. The output pulse looks like higher order Gaussian pulse with a little bit wider pulse width and small amplitude ringing compared to the peak amplitude of the pulse, this ripple is coming from the non-constant amplitude inside the filter taps. The PSD spectrum of the optimized output pulse showed that the majority of power is concentrated inside the desired frequency mask; in this case the FCC mask beside it fulfills the limitation at edge frequencies, as shown in Fig. 5.22.

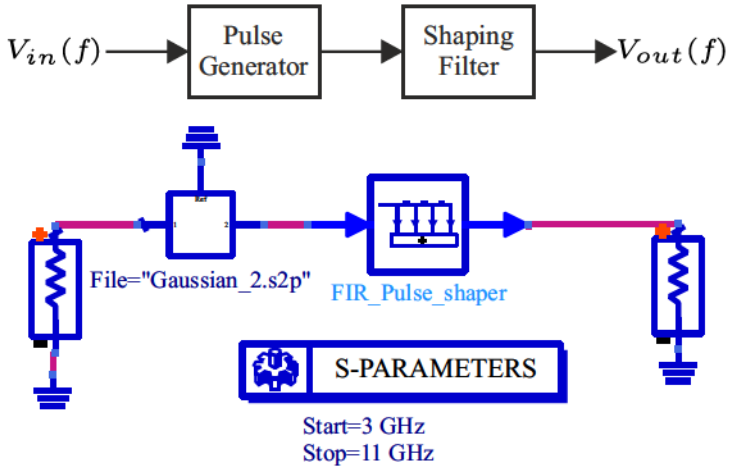

Fig. 5.21: Concept and simulation setup of UWB FIR pulse shaper.

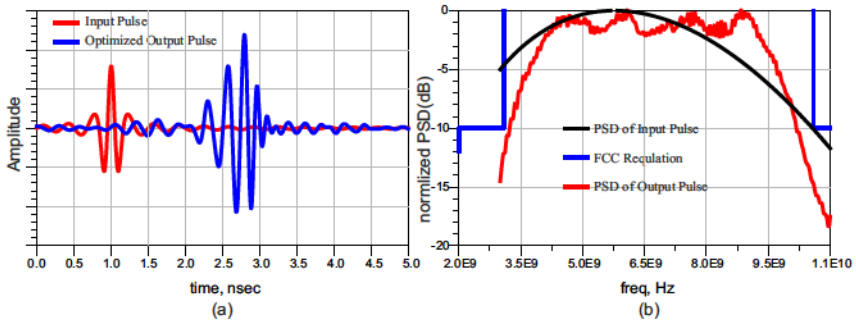

Fig. 5.22: UWB pulse shaper optimized for FCC regulation.

In Fig. 5.23, the EC frequency mask was inserted as goal, so our optimized output pulse showed not only meeting the emission limit according to this regulation, but also efficient use of this mask.

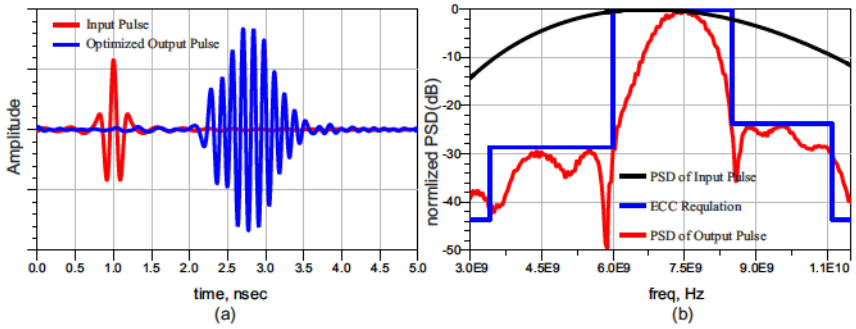

Fig. 5.23: UWB pulse shaper result optimized for ECC regulation.

The optimized output pulse fulfills these regulation but still not efficiently fills the ECC mask as shown in Fig. 5.23. In order to improve the efficient use of the allowed spectrum, a small section compact supplementary BPF (see 4.6.1.2) was added, as shown in Fig. 5.24. The result is shown in Fig. 5.25; although the generated pulse looks wider than the one without this small filter section, it improved the efficient use of the ECC mask by more than 18% as shown in Table 5.2.

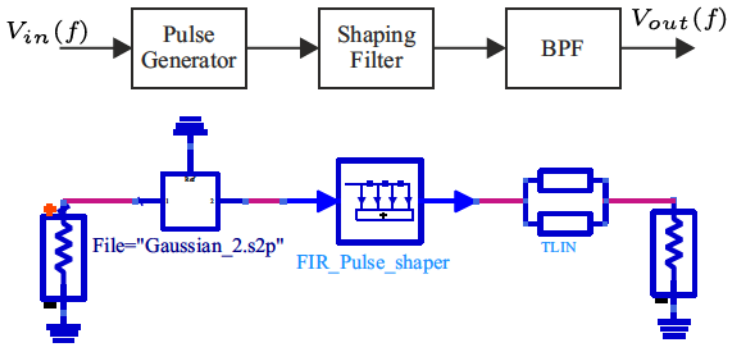

Fig. 5.24: Compact pulse shaper with supplementary section to improve efficient use of ECC mask.

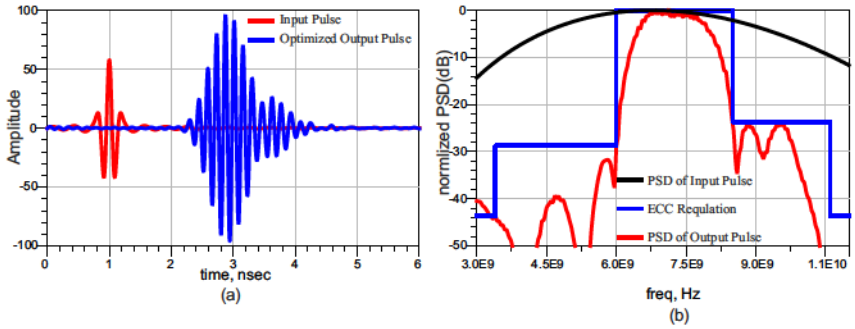

Fig. 5.25: Improved UWB pulse shaper for ECC mask.

ECC mask	w/o BPF	w. BPF
100%	64%	82%

Table 5.2: Computed utilization efficiency for ECC mask.

For a comparison of PSD performance of the pulse shaper with and without compact filter, see Fig. 5.26.

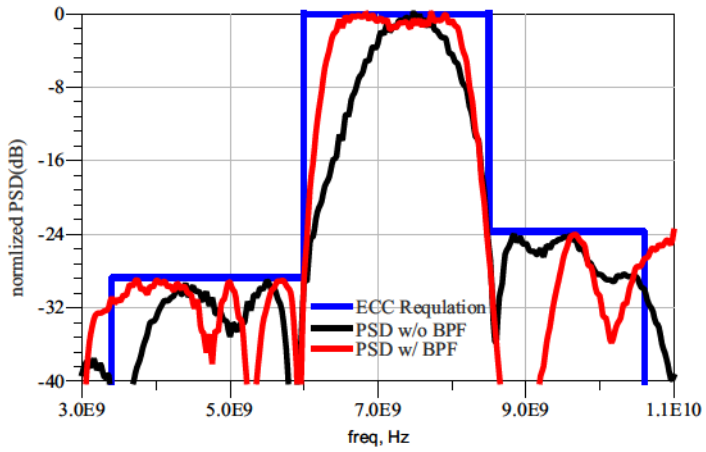

Fig. 5.26: Comparison of PSD performance of pulse shaper with and without the supplementary BPF section.

CHAPTER 6

ANTENNAS AND FIR FILTER

6.1 Introduction

An UWB antenna element/array works together with other RF system components to meet overall system goals. A poorly designed antenna will decrease the overall system performance. Such goals currently drive many workers to join the field of signal processing and smart antennas, where it is assumed that the signals from the elements of an array can be processed digitally in a computer (digital signal processing) and beams are formed digitally. However, digital beamforming seems to be improper for microwave applications in the GHz-range due to an extremely high sampling rate. The topic of this chapter is the integration of FIR filter and UWB antennas, and is organized as follows. First is the introduction of the fundamentals of UWB antennas and antenna arrays, and its mathematical description. The concept of phased array is presented, hence introducing different ways of controlling the antenna array beam pattern, such as amplitude weighting and null steering. Section 6.5 will discuss the concept of beamforming, where the next section will show application and different types of beamforming. The core of this chapter is to use the FIR filter as beamformer and at the same time compensate the distortion which may appear from the antenna element and/or array. Beamforming concept, mathematical description and design example are presented in section 6.6.

6.2 UWB Antenna and Antenna Array

A UWB antenna is distinguished by its large bandwidth. It should provide impedance matching smooth gain and constant phase center across the operation band. The transmitted signal power level in a UWB system must be under a certain limit which is close to noise level, therefore the usage of an effective antenna element or array is important. In narrowband application, the antenna elements are optimized for the system frequency; in UWB application, the antenna shows frequency-dependent behavior in both amplitude and phase, beside a radiation pattern with angle dependence [OHI04]. In general, a UWB pulse system uses short-time duration pulses and the UWB antenna differentiates

these pulses. Very few UWB antennas transmit the input pulse as it is and integrate the received pulse in receiving mode [KRC06]. This causes pulse distortion; in addition, in the case of antenna array, a distortion may appear from the mutual coupling between each antenna. This source of distortion does not count for the distortion which can be produced from the UWB channel.

6.2.1 Polarization

The polarization of a wave is the direction of the electrical field; most antennas radiate either linear or circular polarization, which are both special cases of elliptical polarization. A linearly polarized antenna radiates in one plane containing the direction of propagation, and can be further classified as being vertical, horizontal, or slant. On the other side is the circular polarized antenna, where the electric field rotates around the axis of propagation as a function of time. The polarization can be classified according to the sense of rotation to either Right Hand Circularly Polarized (RHCP) or Left Hand Circularly Polarized (LHCP). Co-polarization or co-pol happen when both the transmitting and receiving antenna have the same polarization, but if the polarization is orthogonal then it will be defined as cross polarization, or x-pol.

6.2.2 Half-Power Beamwidth (HPBW), Sidelobe Level (SLL), and Nulls

Half-Power Beamwidth, or HPBW, is directly related to the radiation pattern, where the radiation pattern refers to the angular dependence of the field strength transmitted/received from an antenna. HPBW is defined where the power level is decreased by 3 dB compared to the main beam at φ_0. In antenna array, the HPBW is proportional to array length Nd where N is the antenna element number and d is the inter-element spacing. The HPBW of a scanned, narrow beam, linear array antenna, broadens approximately inversely to the cosine of the scan angle as shown in equation 6.2.1.

$$\varphi_{3dB(\varphi=\varphi_0)} \approx \frac{\varphi_{3dB(\varphi=0)}}{\cos(\varphi_0)} \tag{6.2.1}$$

Besides the main beam in the radiation pattern, there are also some lobes which are called sidelobes; in general it is desirable to minimize SLL[1], while concentrating the power density inside the main beam. These lobes are separated by nulls, where the radiated signal strength falls to zero.

6.2.3 Directivity and Gain

Directivity D describes the ability of an antenna to concentrate energy in a certain direction (θ_0, φ_0), which can be defined as the ratio of the radiation intensity $U(\theta_0, \varphi_0)$ in a given direction from the antenna to the radiation intensity averaged over all directions U_0.

[1] Sidelobe Level

The average radiation intensity is equal to the total power radiated P_{rad} by the antenna divided by 4π [Bal05].

$$D(\theta_0, \varphi_0) = \frac{U(\theta_0, \varphi_0)}{U_0} = \frac{4\pi\ U(\theta_0, \varphi_0)}{P_{rad}} \tag{6.2.2}$$

And the gain G can be calculated by multiplying the directivity by the radiation efficiency $G = k \cdot D$ where k takes a value $0 \leq k \leq 1$. The efficiency k takes into account losses at the input terminal due to reflection and within the structure of the antenna, such as conduction and dielectric losses. Linear antenna array built from N isotropic radiators with inter-element spacing $d = \lambda/2$ will result in $D_{max} = G_{max} = N$. Here a lossless feeding network was assumed and no losses due to mutual coupling between antenna elements.

6.2.4 Mutual Coupling

Mutual coupling is the electromagnetic interaction between antenna elements in the array. This coupling will affect the performance of the antenna array (such as input matching, gain, SLL, HPBW, and nulls depth and locations). Even if the antenna is not fed by its own, there can be induced surface current by radiation from neighboring antennas. Dependent on the inter-element spacing d, mutual coupling can affect the performance of the whole antenna array. Another factor which can also affect the coupling is the antenna array geometry where uniform circular arrays (UCA) have benefits over the uniform linear array (ULA). Due to the symmetry of the UCA structure, the effect of mutual coupling becomes periodic and symmetric around the array. However, for the ULA, the elements at the edge will have different coupling characteristics from the center. In addition, the direction of the main beam will eventually produce different mutual coupling effects; antenna types also affect the mutual coupling. The easier way to reduce coupling between antennas is to provide shielding with narrow space between elements, but this can also change the behavior of the antenna itself. Another method is to compensate the coupling with modifications in the feed network, or by multiplying the feeding matrix with the inverse coupling matrix. This method works sufficiently, but only for an exact beam direction. A general, adapted method is to use an appropriate predistorter circuit such as using FIR filter [Bal05][NHS07].

6.3 Antenna Array

6.3.1 Introduction

In most wireless communication systems, it is desired to direct power in a certain direction, not only to save power but also so as to not cause interference for other existing systems. Increasing the size of a single antenna can provide a directional beam, but multilobes also are generated; normally these lobes are in undesired directions, which means decreasing the useful power radiated into a specific direction [ADO+06]. There is the need for higher gain to increase the communication ranges; one can do this using a large focus system antenna (for example reflector antenna or horn antenna, but they both suffer from large size and high cost). These factors all led to the use of antenna arrays in order to generate

a desired beam of arbitrary beamwidth, direction and gain. The first area where antenna arrays were used was radar [Van02] and nowadays antenna arrays play an important role not only for radar, but also for many communication systems. The total field of array is a vector superposition of the fields radiated by individual elements. This superposition will be constructive in the main beam and destructive in the remaining directions. Many parameters can affect the overall antenna pattern [Mil05]:

1. The geometrical configuration of the overall array (linear, circular, spherical, rectangular, etc.).
2. The relative placement of the elements.
3. The excitation amplitude of the individual elements.
4. The excitation phase of each element.
5. The individual pattern of each element.

An optimal antenna array design will use this degree of freedom to achieve system requirements.

6.3.2 Array Types

Antenna arrays are built by combining a number of antennas. Typically, antenna elements are configured as an equally spaced linear design, in a planar geometry with equal spacing between adjacent element in each column and row, or antennas are arranged in a circle with equal spacing between adjacent antennas. These antenna elements are normally identical (homogenous array); in a very special case one can use different kinds of antennas or different radiation properties to build up a heterogeneous array [Han09].

6.3.2.1 Linear Array (LA)

The linear Array is the most common antenna array geometry and allows the simplest array synthesizing techniques. It consists of antenna elements spread in a straight line; if the feeding amplitude, phase and antenna inter-element spacing are constant, then this type of array will be referred to as uniform linear array (ULA).
Fig. 6.1 shows a linear array consisting of N-elements positioned along the z-axis. Assuming elements have no coupling between them, and that all elements are fed with the same amplitude and phase (uniform), the total electric far field at distance R_a can be described as the product of the element pattern $E_0(R_a, \varphi)$ and the Array factor (AF).

$$\begin{aligned} E(R_a, \varphi) &= \underbrace{E_0(R_a, \varphi)}_{Element\ Pattern} \underbrace{\{1 + e^{j(kd\ sin\varphi)} + \cdots + e^{j(k(N-1)(d\ sin\varphi)}\}}_{Array\ Factor(AF)} \\ &= E_0(R_a, \varphi) \sum_{n=1}^{N} e^{j(n-1)(kd\ sin\varphi)} \end{aligned} \tag{6.3.1}$$

where $k = (\frac{2\pi}{\lambda})$ is the wave number, and d is inter-element spacing. If the antenna element is isotropic $E_0(R_a, \varphi) = 1$ then the total field is only the array factor

$$AF = \sum_{n=1}^{N} e^{j(n-1)(kd\ sin\varphi)} \tag{6.3.2}$$

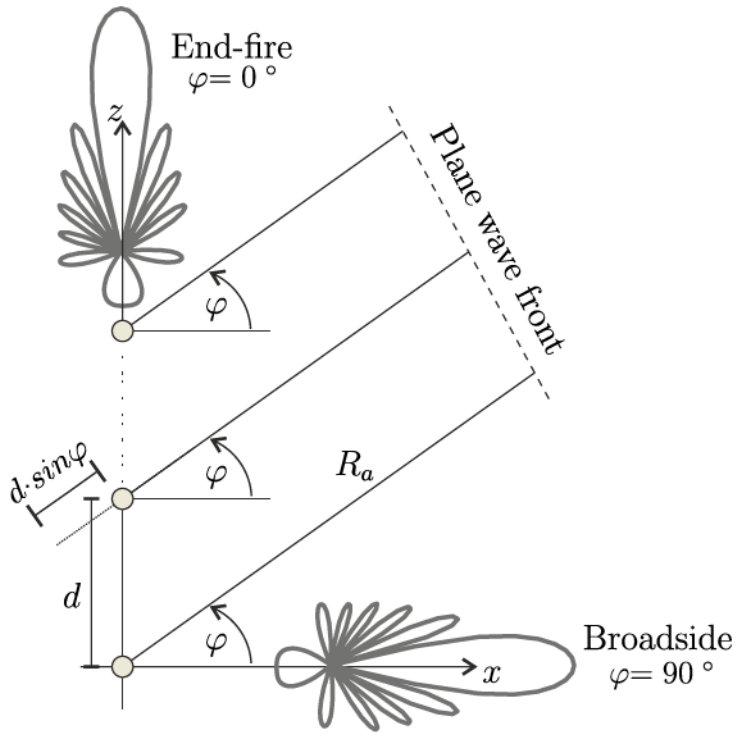

Fig. 6.1: Linear array geometry.

If the excitation phase increment ψ is not zero then the AF will become

$$AF = \sum_{n=1}^{N} e^{j(n-1)(kd\ sin\varphi+\psi)} \tag{6.3.3}$$

If the main beam direction need to be steered towards angle φ_0 then ψ should be selected such that

$$\psi = -kd\ sin\varphi_0 \tag{6.3.4}$$

So φ_0 is only a function of d and ψ and does not depend on N, but null directions will dependent on N, see 6.4.2 for more details. If the excitation amplitude is not uniform, a general formula for the AF can be written as

$$AF = \sum_{n=1}^{N} w_n\ e^{j(n-1)(kd\ sin\varphi)} \quad \text{with} \quad w_n\ = e^{-j(n-1)(kd\ sin\varphi_0)} \tag{6.3.5}$$

where w_n is a complex weighting factor of the nth antenna element. As a general note about LA:

1. Increasing N will reduce the HPBW and increase the number of nulls.
2. Reducing HPBW will increase directivity according to Kraus [KM02] $D_{max} = \frac{41253}{\theta_{3dB} \cdot \varphi_{3dB}}$ where θ_{3dB} and φ_{3dB} are the HPBW in the two planes in degree.
3. The LA is called a broadside array when the radiation pattern is perpendicular to the plane of the array, and End-Fire array when it radiating in the direction of the array.
4. A special case is the broadside ULA of spacing $d = \lambda/2$ with maximum directivity $D_{max} = N$.

6.3.2.2 Circular Array (CA)

The CA provides some advantage over the LA; for example, the ability to scan the beam azimuthaly without limitation, in LA scanning the beam may create a grating lobe dependent on d. In the case of CA, unlike LA, the resulting beamwidth is invariant as the scan angle varies. Another important term is that the compensation of mutual coupling is easier in case of CA, due to its perfect symmetry as the CA has no edge elements [IB05][DPG+98][Fou00].

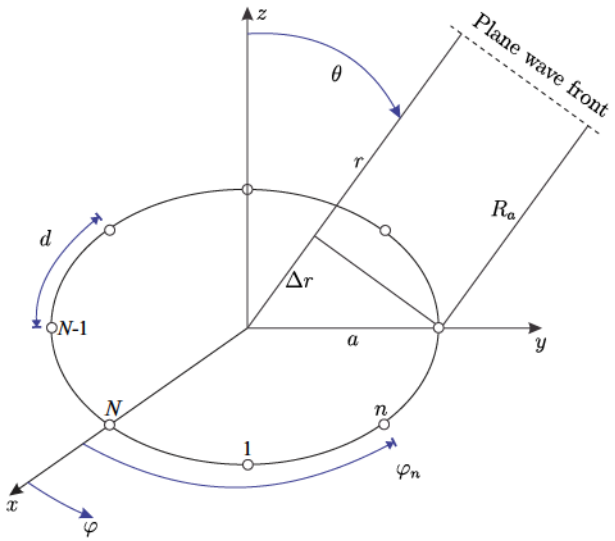

Fig. 6.2: Circular array configuration.

According to Fig. 6.2, a uniform circular array (UCA) with radius a, consisting of N isotropic element in the x-y plane. A plane wave arrives at the antenna from elevation angle θ and azimuthal angle φ. The electric farfield at far distance R_a (which is also the AF in this case) can be calculated as:

$$AF = \sum_{n=1}^{N} w_n \, e^{j \; kasin(\theta)cos(\varphi - \varphi_n)} \tag{6.3.6}$$

where φ_n is the angular position of the nth element of the array and is given by

$$\varphi_n = 2\pi \frac{n}{N} \tag{6.3.7}$$

The radius a results from the element spacing d as:

$$a = \frac{Nd}{2\pi} = \frac{Nc_0}{2\pi f} \qquad \text{where} \quad d = \frac{c_0}{2f} \tag{6.3.8}$$

One can see that a is a function of frequency and N, where assuming d is similar as for the standard ULA which is needed to prevent the appearance of grating lobes. In order to steer the beam in a certain direction (θ_0, φ_0) the weighting coefficient w_n should be selected as:

$$w_n \; = e^{-jkasin(\theta_0)cos(\varphi_0 - \varphi_n)} \tag{6.3.9}$$

A limitation in CA is that the control of SLL is not easy as it is in LA, and element selection is complicated and highly dependent on the dimension of the antenna [Fou00][Nei08]. Fig.6.3 shows the main difference between ULA and UCA under different beam direction $\varphi_0 = [0° \ 60° \ 130°]$: In case of UCA the beam shape is not a function of the steering angle but has high SLL. This can be solved by applying amplitude weighting see 6.4.1. On the other hand, the ULA has lower SLL but the beam shape is a function of the steering angle; as the beam is steered far from 0° it becomes wider, and an additional beam will appear (grating lobe, GL).

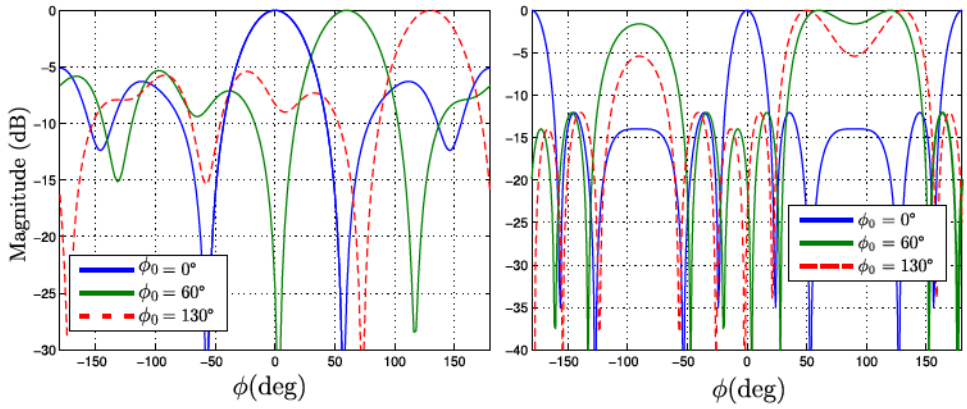

Fig. 6.3: Comparison between ULA (right) and UCA (left) with 5-element $\lambda/2$ spacing and different steering angles.

6.3.2.3 Different Array Geometries

The array geometry is one of many factors which can decide the final performance of an antenna array, as have been discussed in the last sections. In some applications you need to have much higher directivity (narrow main beam), lower SLL, symmetrical patterns, and steer the beam toward any direction in the space. The solution could be using a planar array where antenna elements are placed along a rectangular grid, circular grid, triangular grid, etc. An example of a rectangular patch array and its Three-dimensional radiation pattern is shown in Fig.6.4(a).
One can even put antenna elements in non-planar geometry in a three-dimensional structure; for example, an array whose elements are uniformly distributed on a hemisphere. One example of such a structure is the multi surface conformal patch array shown in Fig.6.4(b), which is used for a satellite communication and navigation ground segment system. For more details about conformal array antenna, see [JP06]. In summary, all other array geometries can be considered as a variation or mixed form of linear, circular and planar array antennas.

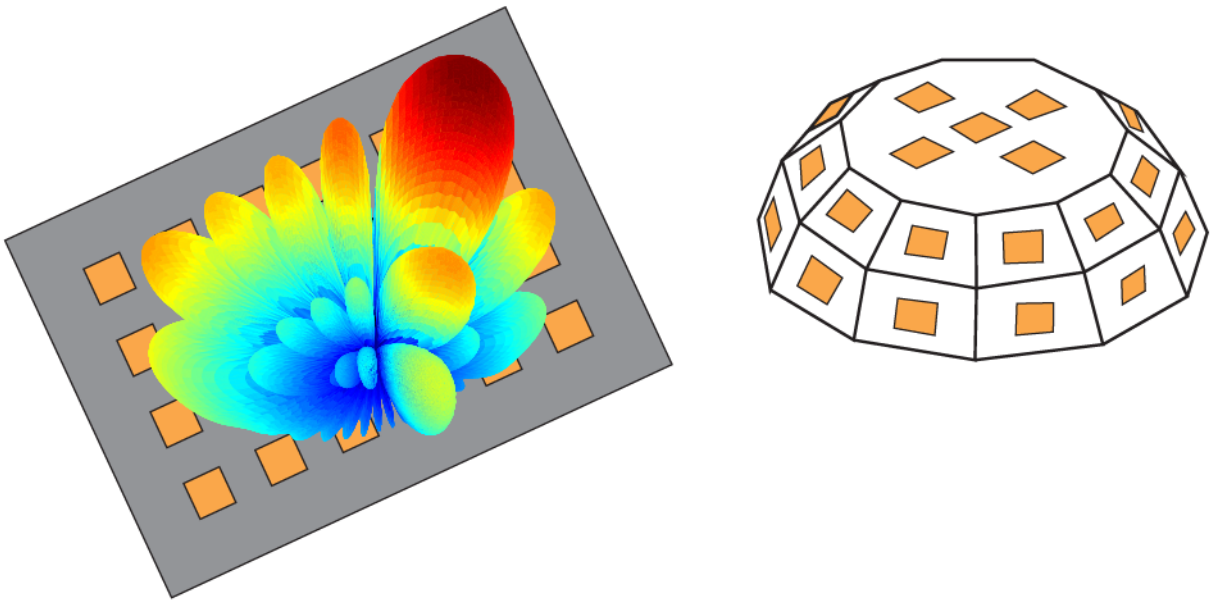

(a) (b)

Fig. 6.4: (a) Three-dimensional radiation pattern for a 6x4 rectangular patch array. (b) Hemispherical 27 patch elements array [GLW98].

6.4 Phased Array

According to section 6.3.2.1, one can steer the main beam electrically by applying a phase shift; these types of antenna arrays are called electronically steered array (ESA), as opposed to a mechanically steered array (MSA) which is too slow for some applications. In this section, the concept of phased array and the way to realize a phase shifter (PS) will be investigated. A linear array with N elements with equal spacing d is shown in Fig.6.5(a). By controlling the phase $\Delta\varphi_i$ (see section 6.4.1) of excitation of each element, one can steer the beam to a desired direction. If there is need to scan the beam in the direction φ_0, the excitation phase $\triangle\varphi_n$ should be as follows:

$$\triangle\varphi_n = (n-1)kdsin\varphi_0 \tag{6.4.1}$$

The phase shift for a given frequency is equivalent to a time delay, which means that the incident wave will arrive at a different time to each antenna, and it will arrive at the first element with time advance with respect to the second element. This spatial time delay between first element (reference element $n=1$) and the nth element can be calculated as:

$$t_{0,n} = (n-1)t_0 \quad \text{where} \quad t_0 = \frac{d}{c_0}\, sin\varphi_0 \tag{6.4.2}$$

where c_0 is the speed of light in a vacuum. This spatial time delay can be compensated by adding a PS in conventional narrowband applications. Note that a conventional PS is assumed to create a fixed phase shift over its frequency band of operation, while Equation 6.4.1 shows that the phase shift need to increase with frequency for a fixed steer angle

φ_0. Or by replacing the PS with true-time delays (TTD) of τ_n as shown in Fig.6.5(b) for wideband applications, which can be calculated as:

$$\tau_n = T_0 + (N-n)t_0 \tag{6.4.3}$$

This means the longest time delay will applied to the first element (the one that will first receive the wavefront), and no delay will be applied for the last antenna element($n = N$); with this, all signals will add constructively. A constant time delay $T_0 \geq (N-1)\frac{d}{c_0}$ is required in order to avoid negative time delay in case $\varphi_0 < 0°$ [AG05]. Or one can use two definitions for τ_n dependent on φ_0 as:

$$t_{0,n} = \begin{cases} (n-1)t_0 & \text{if} \quad \varphi_0 \geq 0 \\ (N-n)t_0 & \text{if} \quad \varphi_0 < 0 \end{cases} \tag{6.4.4}$$

Technically, this desired phase shift can be realized by different methods; for example, by changing the length of a transmission line. The physical length which represents this time delay can be calculated as

$$l_n = \frac{c_0}{\sqrt{\varepsilon_{r,eff}}}\tau_n \tag{6.4.5}$$

where $\varepsilon_{r,eff}$ is the effective dielectric constant [Nei08]. Seeing the PS as two-port component between each antenna and its branch of the feed network its transmission coefficient S_{21} can be represented as:

$$S_{21} \propto e^{-j\beta l} = e^{-j2\pi f l\sqrt{\varepsilon\mu}} \tag{6.4.6}$$

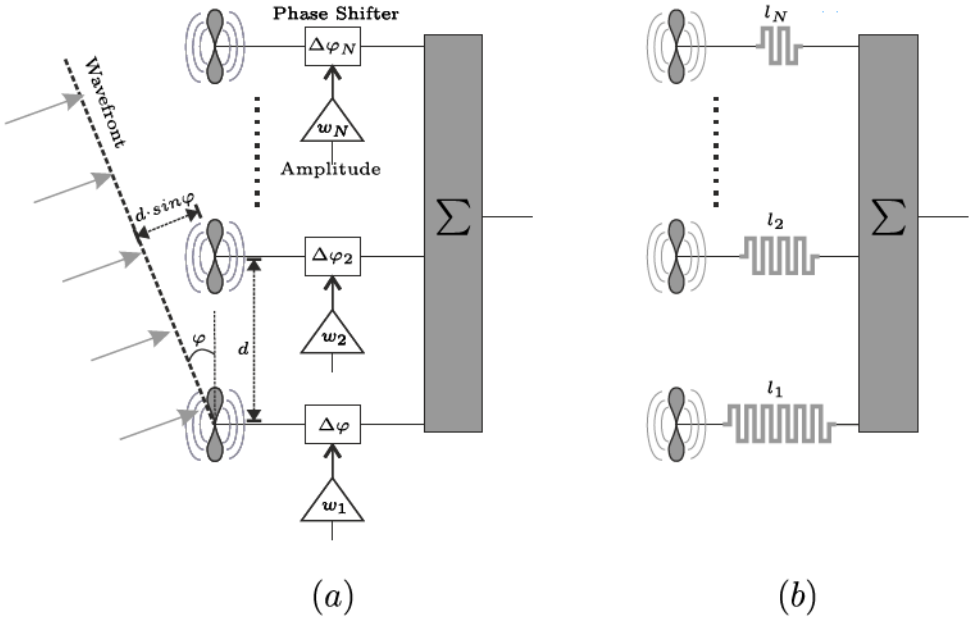

Fig. 6.5: (a)Phased array principle with amplitude weighting (b) Technical realization of PS using meander transmission line.

Equation 6.4.6 shows all parameters which can control the phase of S_{21}; one can produce phase shifting by one of the following means:

1. Phase shifting by changing frequency (f) .
2. Phase shifting by changing length (l).
3. Phase shifting by changing permittivity (dielectric constant) (ε).
4. Phase shifting by changing permeability (μ).

In this thesis will not go into details about these means here; for further discussion of PS, the reader is referred to section 7.4 [Vis06] and to [FS91] for passive or active PS.

6.4.1 Amplitude Weighting:

SLL, HPBW, or both can be controlled using amplitude weighting [AG05]. Table 6.1 summarizes the effect of applying different types of continuous current distribution, where the far field pattern can be directly calculated by applying the Fourier transformation of its current distribution, in the same way as time and frequency are related in signal processing. The same concept can be applied to antenna arrays by using the Fourier transformation of the discrete current distribution.

TYPE OF DISTRIBUTION $-1 \leq x \leq 1$	DIRECTIVITY PATTERN $E(u)$	HALF POWER BEAMWIDTH IN DEGREES	ANGULAR DISTANCE TO FIRST ZERO	INTENSITY OF 1st SIDELOBE dB BELOW MAX.	GAIN FACTOR q_z, q_y
 $f(x) = 1$	$l\dfrac{\sin(u)}{u}$	50.8 (λ/l)	57.3 (λ/l)	13.2	1.0
 $\cos\dfrac{\pi x}{2}$	$\dfrac{\pi l}{2}\dfrac{\cos u}{(\pi/2)^2 - u^2}$	68.8 (λ/l)	85.9 (λ/l)	23	0.810
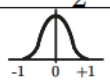 $\cos^2\dfrac{\pi x}{2}$	$\dfrac{l}{2}\dfrac{\sin u}{u}\dfrac{\pi^2}{\pi^2 - u^2}$	83.2 (λ/l)	114.6 (λ/l)	32	0.667
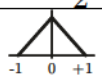 $f(x) = 1 - \lvert x \rvert$	$\dfrac{l}{2}\left(\dfrac{\sin\frac{u}{2}}{\frac{u}{2}}\right)^2$	73.4 (λ/l)	114.6 (λ/l)	26.4	0.750

Table 6.1: Radiation Characteristics for linear antennas with Uniform, Cosine, Cosine-Squared and Triangular Distribution [Sol12]

As shown in Table 6.1, the uniform distribution will provide the maximum directivity (Gain factor =1 compared with other current distributions) and the smallest HPBW, but will provide high SLL. Having smoother current distributions will reduce the SLL, but increase the HPBW, and also reduced gain efficiency as outer antenna elements will contribute less compared to the uniform distribution. The lowest SLL can be achieved by

applying a Cosine- Squared distribution where one can achieve a SLL of around $-32\,\mathrm{dB}$, but at the cost of gain factor and wider HPBW. This table shows a direct relationship between SLL and HPBW, as normally the highest SLL in an antenna array radiation pattern will be close to the main beam. The radiation patterns of different distributions (see Table 6.1) are shown in Fig. 6.6 for an 8-element LA. Again, it is clear that uniform distribution provides the narrowest HPBW and squared cosine provides the lowest SLL. In conclusion, in order to reduce the SLL, the amplitude of outer elements in the array should be smoothly reduced compared with the middle elements. In other words, one can use window functions to control the amplitude weighting.

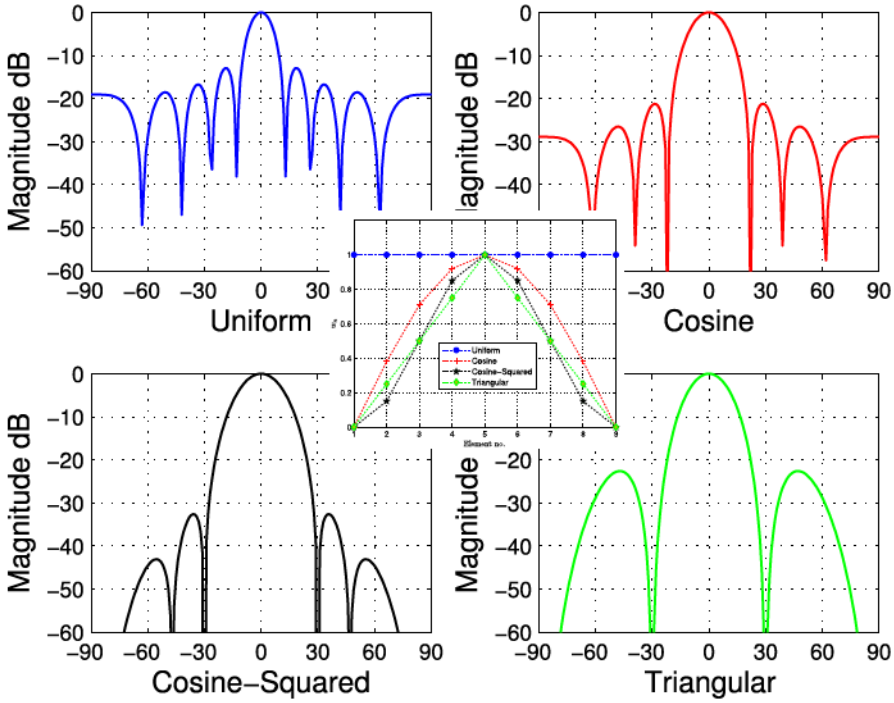

Fig. 6.6: Radiation Pattern for a 9-element LA with Uniform, Cosine, Cosine-Squared and Triangular Distribution.

Window functions are widely used in signal processing. In Fig. 6.7, some common window functions' amplitude weights are plotted. For more details about window functions see [AG05].

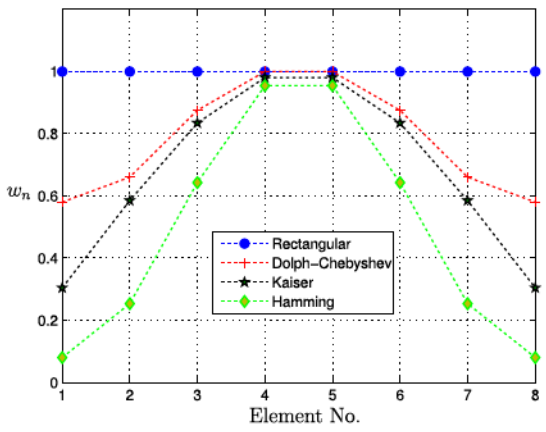

Fig. 6.7: Amplitude weights of 8-element ULA by applying various window functions.

An 8-element ULA was first designed and then the excitation coefficients were multiplied by different window coefficients. The corresponding normalized radiation patterns are depicted in Fig. 6.8. Again, the rectangular window (uniform)provides the smallest HPBW but with high SLL. Different window functions also are implemented: Dolph-Chebyshev with SLL below $-20\,\mathrm{dB}$, Kaiser window with parameter β which controls the sidelobe attenuation (for more details about β see Matlab help under Kaiser window) and last the Hamming window function. The Dolph-Chebyshev window provides the minimum SLL for a given directivity (HPBW) compared to other window functions (see Fig. 6.9).

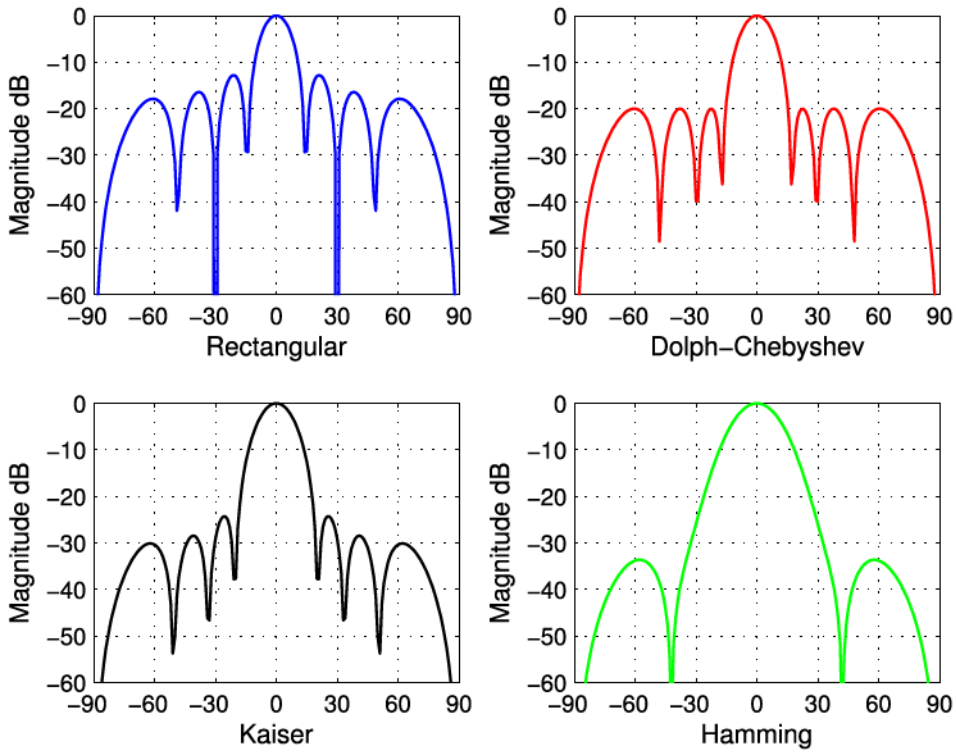

Fig. 6.8: Radiation pattern of 8-element LA under various window functions.

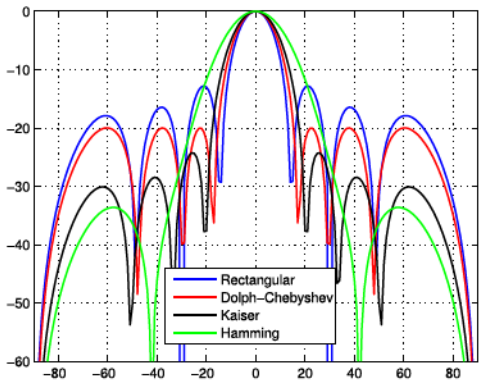

Fig. 6.9: Comparison of radiation patterns of 8-element LA with different window functions.

6.4.2 Null Steering

"Adaptive antenna" and "Adaptive nulling" receive antenna systems are becoming important in communication applications and radar to minimize (null) the received power from one or more interference sources (undesired signal) [Fen08]. This is shown in Fig. 6.10. Not only can the main beam direction be steered to a desired direction, but also the nulls in the array pattern can be steered to a desired direction. This is useful when it is necessary to attenuate a signal arriving from a certain direction, or from a direction other than the main direction. Consequently, this increases the signal-to-interference ratio at the output of the beamformer [AG05]. In narrowband antenna array, obtaining a desired radiation pattern with specific constraints like main beam direction, SLL, HPBW, and null steering is possible by calculating the weight coefficients which satisfy these constraints. To calculate the weight coefficients of N elements and for i different null positions the following equations are to be solved [Nei08]

$$\begin{aligned} w^H S_0 &= 1 \qquad \text{where} \\ S_0 &= [1, e^{-jkd\sin\varphi_0}, \ldots, e^{-jk(n-1)d\sin\varphi_0}]^T, \quad n = 1..N \end{aligned} \tag{6.4.7}$$

$$\begin{aligned} w^H S_i &= 0 \qquad \text{where} \\ S_i &= [1, e^{-jkd\sin\varphi_1}, \ldots, e^{-jk(n-1)d\sin\varphi_i}]^T, \quad i \in \mathrm{N} \end{aligned} \tag{6.4.8}$$

where $(.)^H$ is the Hermitian (complex conjugate) transpose and S_0 is the main beam steering vector with φ_0 the main beam direction and S_i is the steering vector for nulls in φ_i directions. So the weight vector w^H can be solved analytically or numerically [Van02]. As it can be seen from equation 6.4.8, one can insert $N-1$ pattern nulls or minima and at the same time keep steering the antenna beam in a desired direction.

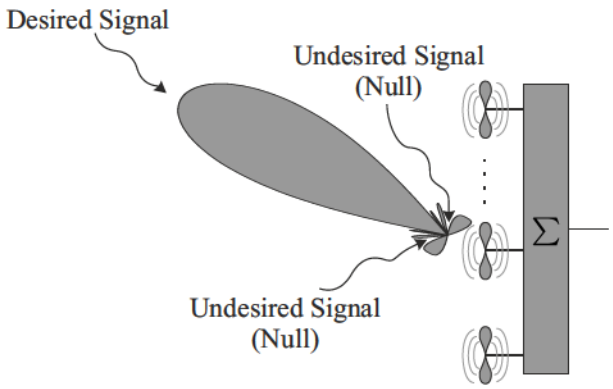

Fig. 6.10: Beamforming and null forming in interference directions.

Schelkunoff's polynomial method can be used to insert nulls in a desired direction in the radiation pattern by having information only about the number of nulls and their position [Bal05], but one cannot control other parameters such as main beam direction and SLL. The linearly constrained minimum variance (LCMV) beamforming method will be used to insert nulls and steer the main beam in a desired direction. The basic idea behind the LCMV beamforming is to constrain the response of the beamformer so signals from the direction of interest are passed with specified gain and phase, while minimizing

contribution from undesired directions [VVB88]. Fig. 6.11 shows the required complex weighting vector w_n to steer the main beam and insert nulls for each frequency. A single vector is only valid to steer the beam of a narrowband frequency and can be realized using PS and/or amplitude control element. In broadband one can use TTD-elements but still provide a frequency dependent radiation pattern which is not sufficient for the UWB frequency band. More details about different beamforming techniques will be presented in section 6.5.2.3. As a result for UWB beamforming and nulls inserting there is need for a frequency dependent weighting vector characteristic respecting amplitude and phase. One solution is to use FIR filter to produce such frequency dependence, more theory and example about using the FIR filter as beamformer are presented in section 6.6. In the following sections a procedure and example for UWB beamforming with nulls inserted in a desired direction will be introduced.

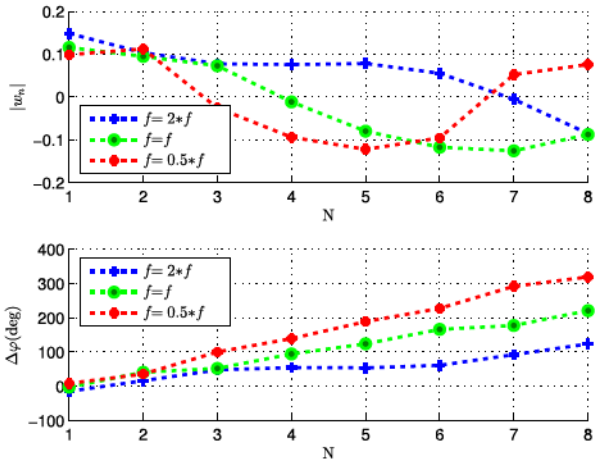

Fig. 6.11: Weighting vector w_n using the LCMV algorithm for wideband.

In Fig. 6.12 a 7-element $\lambda/2$ spaced linear array is designed; the main beam direction is steered to a desired direction φ_0 and two nulls are inserted using the LCMV beamformer. This narrowband pattern will be used in the next section as a reference pattern for designing a wideband null steering array.

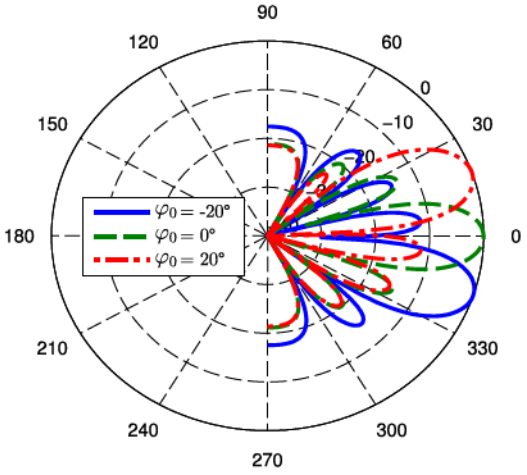

Fig. 6.12: Reference patterns designed using LCMV beamforming with null steering at 60° and −60° and different main beam direction.

6.4.3 Design Procedure for wideband Array

The design procedure will be as follows:

1. Design of a desired radiation reference pattern $H_{Ref}(\varphi)$. This reference pattern could have some specification like: main beam direction, nulls position, SLL, and specific HPBW. Here the LCMV beamforming method is used as array synthesis techniques in order to generate $H_{Ref}(\varphi)$.
2. This desired pattern will be considered to be a frequency independent pattern over the whole desired frequency band $H_{ideal}(f, \varphi)$
3. Chose starting antenna element number N and filter order M.
4. Obtain FIR filter coefficients numerically, e.g. by mathematical optimization like the least squares method or convex optimization [NS11].
5. If the optimization problem in step 4 was not possible to solve then N and M has to be increased and repeated again from step 4; else calculate the overall radiation pattern $H_{tot}(f, \varphi)$ which is based on the array factor and the new optimized filter coefficients.

In this procedure an isotropic radiator is used; one can also include in the procedure the radiation pattern of a real antenna element.

6.4.4 Design Example

In this subsection a design example which implements the steps of the design procedure is presented. The goal is to design wideband beamforming for the ECC frequency band with specific nulls in certain directions. Starting by generating a reference pattern using the LMCV beamforming method having a beam direction at $\varphi_0 = 0°$, and two nulls at $60°$ and $-60°$. The generated pattern is plotted at Fig. 6.13; 5-element was used.

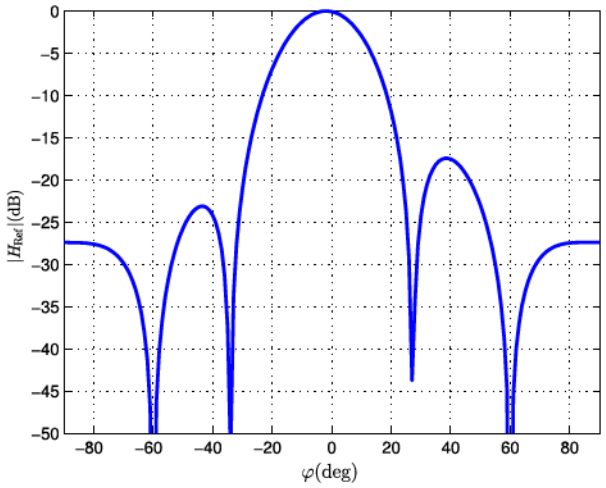

Fig. 6.13: Normalized 5-element reference pattern with two nulls at $60°$ and $-60°$.

The radiation pattern has two deep nulls as desired at $60°$ and $-60°$, with acceptable SLL and HPBW. Then initial values for N and M are selected. Other parameters like distance

d between antenna element was $\lambda/2$ for the highest frequency 8.5 GHz and incremental time delay of the filter $\tau = 1/f_h$. The radiation pattern generated by the above design procedure for $N = 5$ and $M = 5$ is shown in Fig. 6.14. It can be seen that the resulting radiation pattern does not match the desired one. However, the main beam direction does coincide with the desired one. A shift in the nulls far away from the main beam direction can be seen, which can be critical in some applications when the spatial distance between desired direction and interference is small.

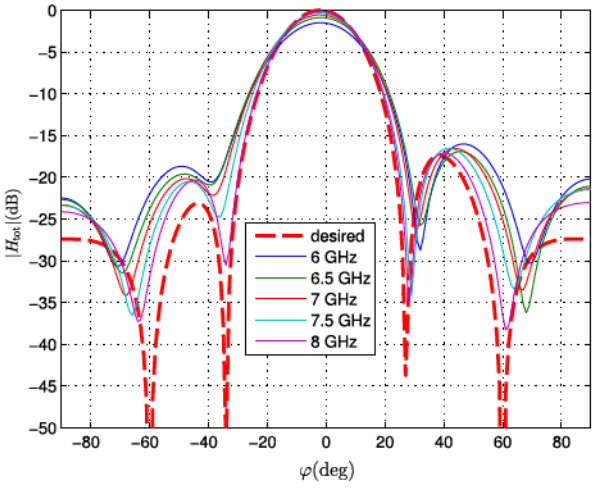

Fig. 6.14: Resulting radiation pattern for $N = 5$ and $M = 5$.

Increasing M to 7, Fig. 6.15, still shows some shift in the nulls, and still does not match with the desired one, although nulls here is slightly deeper. This shows, increasing M alone will not so much improve the design, and therefore a trade off between N and M should be found.

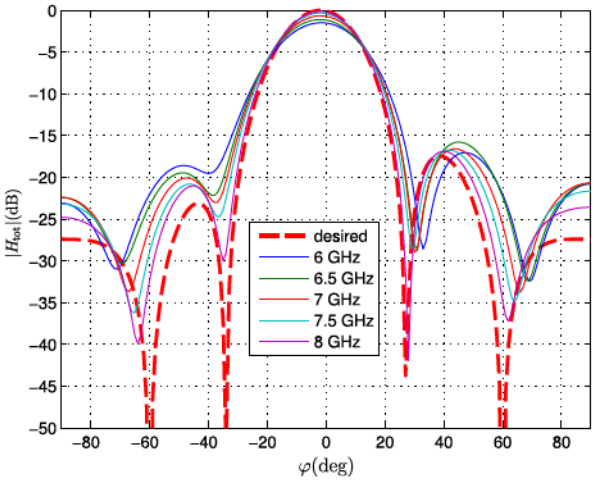

Fig. 6.15: Resulting radiation pattern for $N = 5$ and $M = 7$.

In Fig. 6.16 where $N = 7$ and $M = 5$, the nulls now in the right position and the main beam shape is better matched with the desired one; this is obviously a result of increasing N, which has a higher influence in the main beam direction. Increasing N in a LA tends to narrow the main beam, as well as reduce the First-null beam width (FNBW) therefore enabling nulls to be shifted out to the right position closer to the main beam direction,

while shifting nulls closer to the main beam direction is harder. Also by increasing N, one can increase the available degree of freedom and therefore more nulls can be inserted.

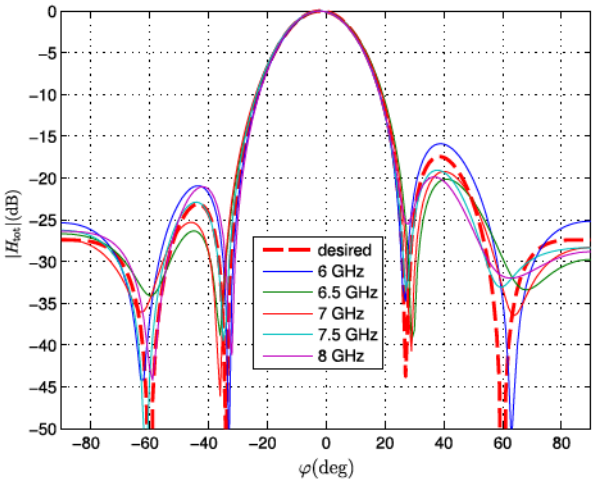

Fig. 6.16: Resulting radiation pattern for $N = 7$ and $M = 5$.

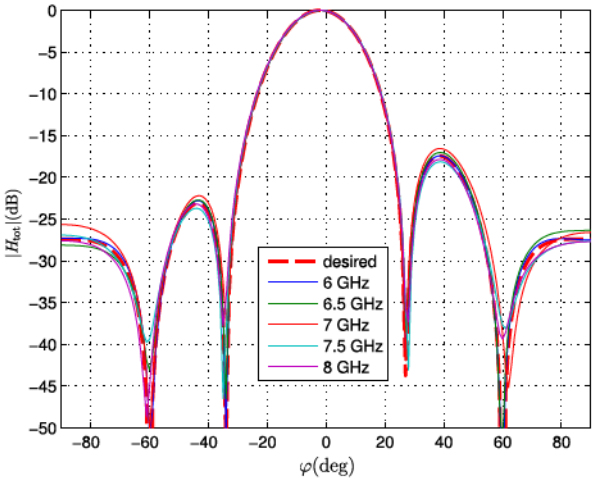

Fig. 6.17: Resulting radiation pattern for $N = 9$ and $M = 9$.

Last, Fig. 6.17 shows result of a design done with $N = 9$ and $M = 9$. A very good match in main beam direction, nulls position, SLL and HPBW can be seen. Also have deep nulls of attenuation in excess of $-35\,\mathrm{dB}$.
In order to quantify the quality of agreement of the optimized wideband pattern and the reference pattern, the pattern correlation is measured and expressed by a correlation coefficient ρ.

$$\rho\left(f_i\right) = \frac{cov(H_{tot}\left(\varphi, f_i\right), H_{Ref}\left(\varphi, f_i\right))}{\sqrt{var(H_{tot}\left(\varphi, f_i\right))} \cdot \sqrt{var(H_{Ref}\left(\varphi, f_i\right))}} \tag{6.4.9}$$

where $cov(\cdot)$ is the covariance and $var(\cdot)$ is the variance and $var\left(\mathrm{x}\right) = cov(\mathrm{x}, \mathrm{x})$ Ideally, the correlation coefficient should be equal to 1, and this happens when an infinite number of antenna elements and infinite filter order are used; however in practice, N and M are limited.

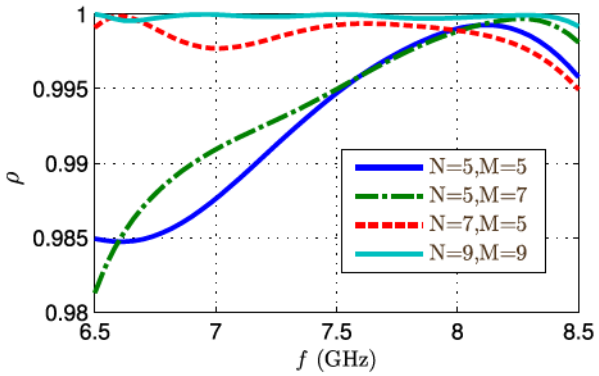

Fig. 6.18: Correlation between reference and optimized pattern at different N and M.

Fig. 6.18 also shows that at higher frequencies the correlation coefficient tend to be better than at lower frequencies; this can be explained by considering τ, which is related to the higher frequency limit, so the overall performance of FIR null steering is better at higher frequency. On the other hand, increasing N will improve the correlation coefficient at lower frequencies as the degree of freedom is increased and the nulls can be realized properly. In reference antenna text books, for example [Bal05], the formula for calculation the FNBW of a broadside array is as follows:

$$FNBW = 2 \cdot \left[\frac{\pi}{2} - \cos^{-1}\left(\frac{\lambda}{Nd} \right) \right] \tag{6.4.10}$$

This formula is plotted in Fig. 6.19: As N increases, the $FNBW$ decreases; eventually inserting a null close to the main beam direction becomes easier.

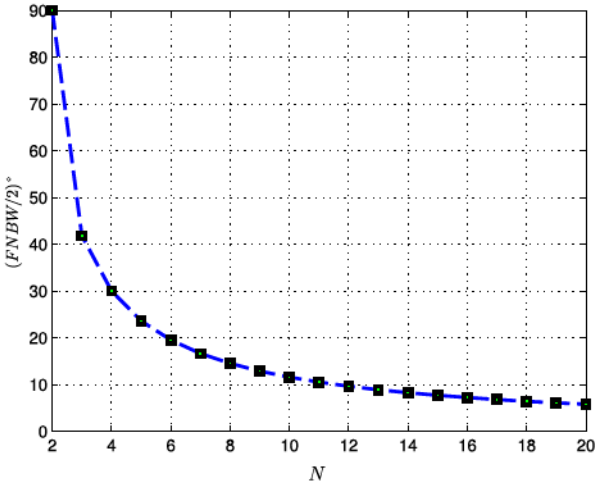

Fig. 6.19: $FNBW/2$ for a ULA as function of antenna element number N and $d = \lambda/2$

The 8-element ULA has its first null (FN) around 15° and adding a null before this FN ($\varphi_{null} = 10°$), see Fig. 6.20, will increase the SLL. If the inserted null angular position is $\geq$ FN, see case $\varphi_{null} = \{15°, 30°\}$, the SLL remains close to the standard $-13.3\,\mathrm{dB}$ of the continuous aperture.

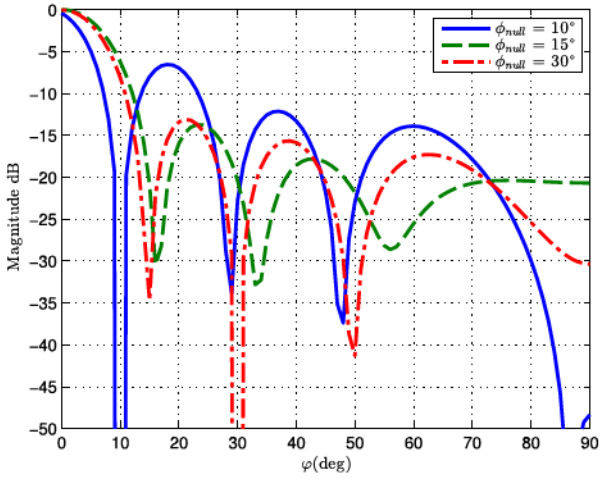

Fig. 6.20: 8-Element ULA with different null position

Nulls have narrow width, and misalignment of nulls could result in too little attenuation of the undesired signal. This can be solved by inserting multiple nulls toward the same direction with small angular shift. In other words, creating a wideband null as shown in Fig. 6.21 by combining two nulls instead of a single one; the two nulls were inserted at 25° and 35°, instead of having only a single null at 30°. In fact, the number of nulls is fixed, so what one can do is shift the second null closer to the first one to create the wideband null. A similar concept was used in [Sol12] for increasing the bandwidth of a patch antenna using double resonator. Using the double null, the bandwidth of the null (maximum−30 dB) can be increased from 2° up to 20°.

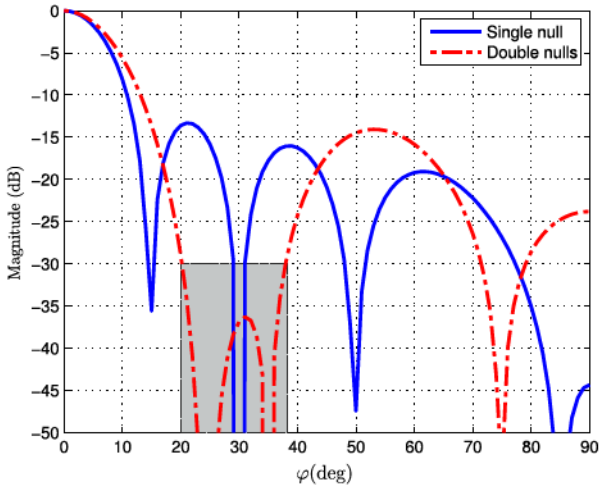

Fig. 6.21: Creating wideband null.

An optimization design for the ECC band frequency invariant ULA radiation pattern, with $N = 11$ and $M = 11$ is shown in Fig.6.22, with a very good match with the reference pattern(red dashed line). Instead of having narrowed null at 30°, one have a wideband null wider than 20°, which can increase the interference suppression. In Fig.6.23, a three-dimensional plot shows the frequency invariant behavior of the 11-element ULA with wideband null steering using an 11-order FIR filter controlling each antenna element. Null placement may be incorporated directly into the beam steering array weights.

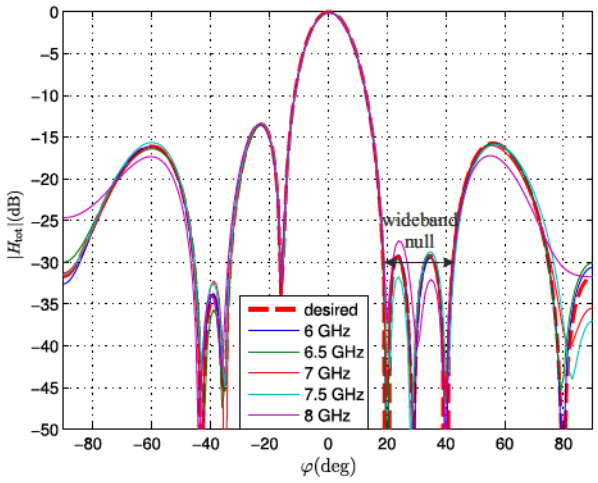

Fig. 6.22: ECC band frequency invariant with wideband null at 30°.

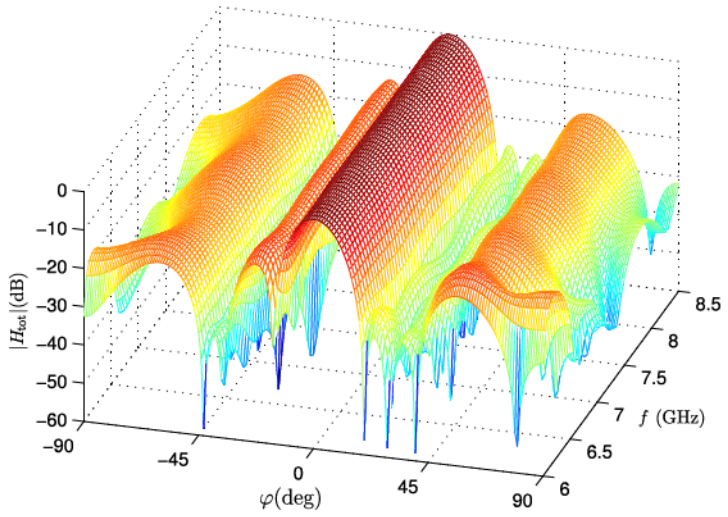

Fig. 6.23: Three-dimensional plot showing the frequency invariant behavior of the design example for the ECC frequency band.

6.5 Beamforming

According to [VVB88], a beamformer is a processor used in conjunction with an array of sensors to provide a versatile form of spatial filtering. Another simple definition of beamforming from [God97] says: beamforming is a process of combining the signals from different elements. This combining is realized by a beamforming network (BFN) between each antenna element and the central summing point, as shown in Fig.6.24. The goal of this BFN is to provide constructive superposition in the main direction, destructive superposition in other directions, compensation of mutual coupling, and pulse equalization. Requirements such as compact size, low insertion losses and low noise figure are also important when one design and manufacture a BFN. Depending on the system requirements, one can optimize some or all of these requirements.

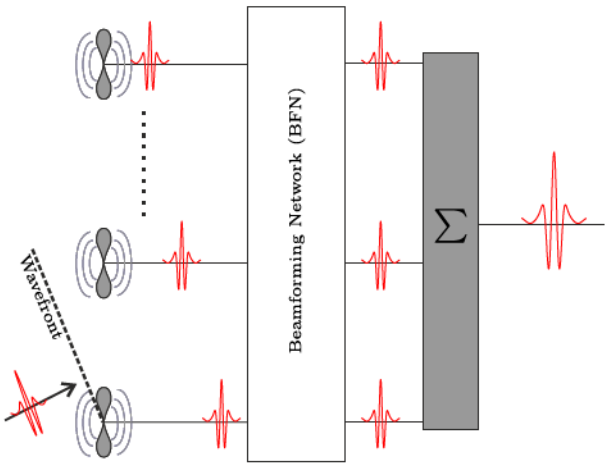

Fig. 6.24: Concept of Beamforming System.

6.5.1 Applications of Beamforming

Beamforming together with UWB technology provides a wide range of different applications; this section will describe some practical applications of array beamforming.

Radar:

The first antenna arrays were used in radar applications. A UWB Radar system can use the advantage of UWB beamforming technology for achieving higher spatial resolution, easier target information recovery from the reflected signal, deeper material penetration, and lower probability of intercept signal than with narrowband signal [Tay95]. Most of the radar industry goes to military applications, such as target identification, target imaging and discrimination, and missiles and weapon control. On the other hand, it also finds its way to very useful commercial applications, such as vehicular collision avoidance radar, remote sensing, aircraft safety and traffic control, space, non-contact measurement, etc. UWB beamforming can be used for localization, thanks to the huge fractional bandwidth provided by UWB, which can provide excellent localization accuracy to closely spaced objects even through walls. Beamformers at both side of a communication link can estimate both Direction of Arrival (DoA) and the Time of Arrival (ToA)[ASA+09].

Biomedical:

During the last few years, UWB technology has received increasing interest not only for communication applications but also for biomedical purposes. UWB technology can be used for biomedical imaging and remote monitoring in the same way as ground penetrating radar (GPR) [GMK07]. The low electromagnetic radiation due to the low power pulse less than -41.3 dBm/MHz has little influence on the environment, which is suitable for hospital application and safe for the human body [MLE09].

Sonar:

Sonar has much in common with radar, except that it operates in water; array beamforming finds its application in sonar, such as the monitoring or tracking of submarines. It is also used for earthquake monitoring and geological exploration [AG05].

Communication:

One popular application of UWB technology is the increasing of wireless communication data rate. Beamforming is able to improve the performance of a mobile communications system in a number of ways, as it provides the capability to reduce cochannel interferences and multipath fading. This results in better quality of services, such as reduced BER and outage probability. Its capability to form multiple beams could be exploited to serve many users in parallel, resulting in an increased spectral efficiency. Its ability to adapt beam shapes to suit traffic conditions is useful in reducing the handoff rate, which may result in increased tracking efficiency [God97].

6.5.2 Beamforming Types

Beamforming can be divided into different groups according to which category is used. Table 6.2 summaries some of these categories. In the next some of them will be discussed in detail.

Frequency Band	Narrowband	Broadband
Implementation (Concept)	Analog	Digital
Adaptation	Fixed or Switched beamforming	Adaptive
Transmitter (TX) or Receiver (RX)	TR or RX	TR or TX or both
Implementation (Components)	Active components	Passive components
Number of Control Beams	Single beam	Multiple beams

Table 6.2: Beamforming Types.

6.5.2.1 Analog or Digital

In analog beamforming (ABF) the BFN directly follow by the antenna element and is realized by passive or active circuits which shift amplitude and phase and combine (add) the signals from individual element (power combiner). In the case of digital beamforming (DBF), the signal from each antenna element is first digitized through an Analog-Digital converter (ADC); in some cases the received signal from the antenna element is down converted to an intermediate frequency (IF) before being digitized. Then it is followed by a digital BFN where the phase shift and amplitude weighting is performed of a sample signal data by digital multiplication by a complex weight. The outputs of Digital BFN are summed up digitally and produce the output of the antenna array response exactly in the same way as with ABF. The popularity of DBF is based on the widespread usage of digital signal processing (DSP) [Fou00]. Some advantages, such as flexibility, reliability, repeatability, and adaptivity make the trend for narrowband beamforming going to DBF [Fou00]. Unfortunately, all of these advantages cannot help us to completely move to DBF, but perhaps this will be possible in the near future. The main disadvantage, beside

power consumption and high cost, is the missing of ADC with a high sampling rate for low cost devices; in order to satisfy the Nyquist criterion, a sampling frequency, $F_s \geq 2f_{max}$ is needed. Working in the UWB frequency band with $f_{max} = 10.6\,\text{GHz}$, which means F_s of at least $21\,\text{GHz}$; such an extremely high sample rate places great demand on ADC and is currently not feasible for low cost mobile devices. In 2012, the state-of-the-art in RF-Sampling was $1.8\,\text{GHz}$ Nyquist bandwidth, which means $f_{max} \leq 1.8\,\text{GHz}$. Therefore analog frequency down-conversion becomes a must, which increases system cost, size, and power. As a result, digital beamforming seems to be improper for UWB short pulse application, since the extremely high bandwidth places great demands on the ADC and is still far from mass-market application [NEHH+06][Tex12][KMO+06]. As an alternative, in this work is chosen to realize the FIR in the analog form.

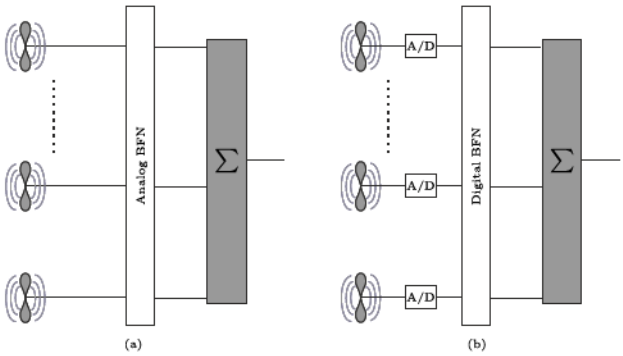

Fig. 6.25: (a) Analog Beamforming (ABF). (b) Digital Beamforming (DBF).

6.5.2.2 Fixed and Adaptive Beamforming.

Adaptive beamforming is able to automatically adapt the radiation pattern from an array to different scenarios based on the environment they were operating in. This can be done by adaptively changing the amplitude and the phase of the signal fed to each antenna element in the array in real time. These new complex weights are computed by signal-processing using an adaptive algorithm [Bal05][God97][BU08].

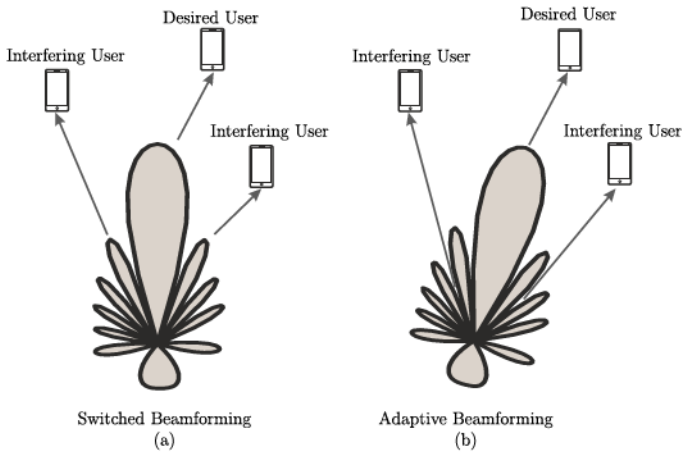

Fig. 6.26: Advantage of using Adaptive beamforming in compare to switched beamforming.

In conventional (fixed or switched) beamforming, a fixed set of complex weights are used,

which need knowledge about the direction of arrival (DOA) in order to steer the beam in this direction. Despite its benefits, this beamforming technique is still independent of the environment and provides no solution for a real time scenario. As shown in Fig.6.26 in the case of adaptive beamforming, the desired user received the maximum signal and nulls is directed to interfering user, while in switched beamforming the desired user is not exactly in the center of the main beam and the interfering user is located in the direction of high SLL instead of null; this, of course, increases the overall interference in the system. The concept of adaptive beamforming is widely used in mobile systems to provide smart antenna systems. This system can increase network capacity and range, reduced susceptibility to multipath effects and provide location awareness [AG05][MM80][Fen10][Bal05]. A small remark provided by [Bal05] is that antennas are not smart; it is the digital signal processing, along with the antenna. In the following, adaptive beamforming using FIR filter in analog mode will be proposed, which can reduce the overall effort compared to a DBF.
Fig.6.27 shows the functional block diagram of adaptive beamforming; part (a) is in digital mode where received signals are down converted to baseband and sampled. The adaptive algorithm, which calculates the complex weight required to steer the beam to the desired user and steer nulls to interfering users. Fig.6.27(b) shows a block diagram of a mixed adaptive beamforming where, in this case, there is no need for down converting and sampling direct after antennas. Applying the optimized weight (in this case, it will be the FIR filter coefficients), which has been calculated by the adaptive algorithm, directly to the analog received signals. By doing so, one reduce computing efforts and decrease the cost and complexity of circuit. This FIR beamforming concept and the calculation of its coefficients will be presented in detail in the following sections.

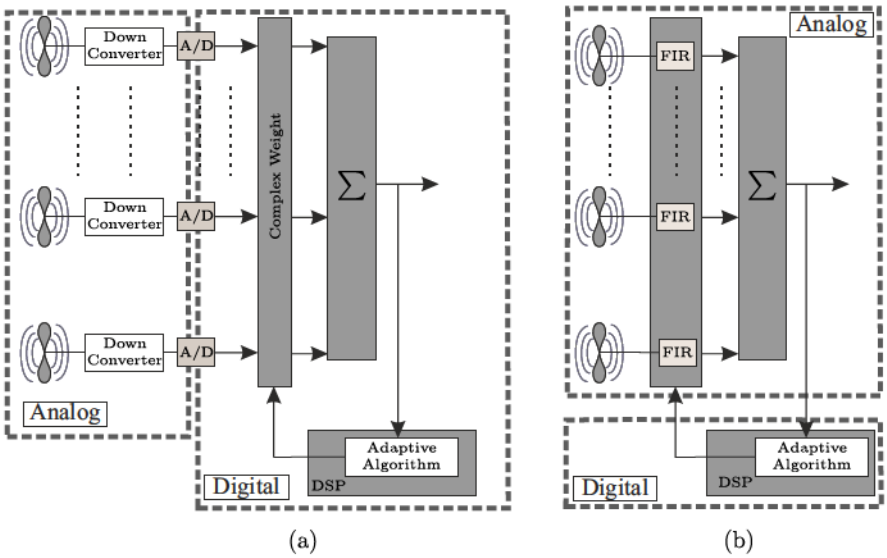

Fig. 6.27: (a) Adaptive Digital beamforming (b) Mixed Beamforming based on Analog FIR Filter.

6.5.2.3 Narrowband and Wideband Beamforming

6.5.2.3.1 Narrowband Beamforming The concept of narrowband beamforming as already studied in detail in section 6.4, is based on adjusting only the phase of each element to steer the beam in a desired direction, while keeping the amplitude of each element the

same. The term narrowband means operating with signals having a fractional bandwidth (FBW) of less than 1% where FBW is defined by equation 2.2.1 [AG05]: where f_h and f_l are the highest and lowest frequencies of the signal respectively. Fig.6.28(a) shows the typical characteristics of a PS which is frequency independent. This PS was used for wideband beamforming, with $FBW = 10\%$ as shown in Fig.6.29. The design used a 5-element ULA, with inter-element spacing $d{=}\lambda/2$, and main beam steered to $\varphi_0 = 30°$. As shown in Fig.6.29(a) (PS case), the beam direction, HPBW, SLL, and nulls positions are all frequency dependent [Nei08]

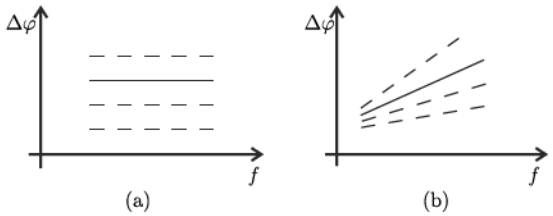

Fig. 6.28: Phase characteristic versus frequency: (a) PS (b) TTD .

6.5.2.3.2 Wideband Beamforming In wideband beamforming, the PS is replaced by a true time delay (TTD) which has a linear phase response versus frequency, Fig.6.28(b). As shown in Fig.6.29(b), the performance is improved compared to the PS-case, in particular in the main beam direction, which still is frequency independent. If the FBW is increased to be 20%, the minimum bandwidth requirement for UWB beamforming, for both beamformers, the frequency dependent performance of SLL, HPBW and null position are clearly visible, especially at lower frequencies, Fig.6.30.

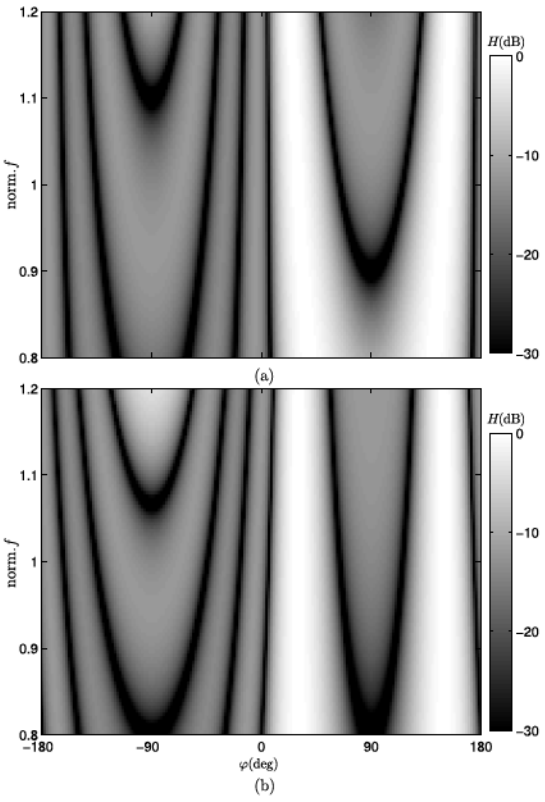

Fig. 6.29: Wideband ($FBW = 10\%$) beamforming using (a) Phase shift by PS frequency independent (b)Frequency dependent phase shift by TTD.

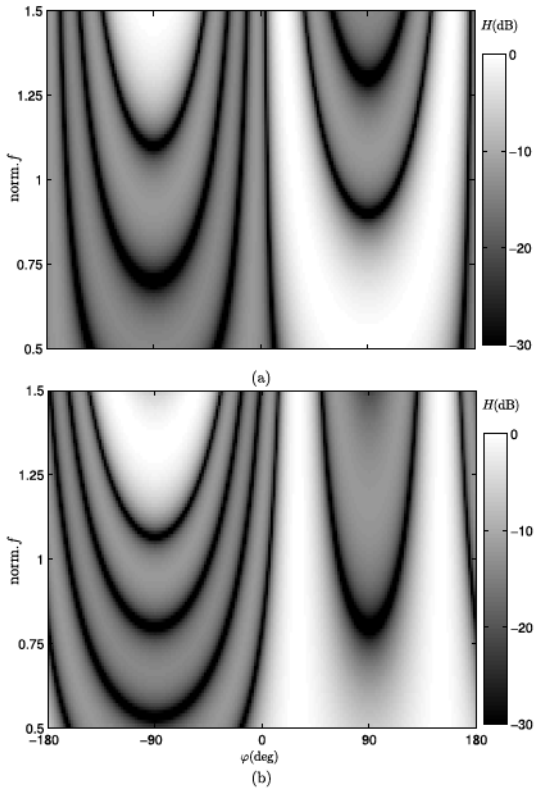

Fig. 6.30: UWB ($FBW = 25\%$) beamforming using (a)Frequency independent phase shift by PS (b)Frequency dependent phase shift by TTD.

6.6 Beamforming using FIR Filter

6.6.1 FIR as Beamformer

The last section 6.5.2.3, showed that for the UWB beamforming the conventional beamforming methods are not able to provide a frequency invariant radiation pattern for the whole UWB, and there is need for a frequency dependent weighting factor in order to make antenna patterns frequency independent. In this section, a beamforming method which can fulfill these requirements will be introduced. By seeing the required frequency response of a BFN as a transfer function, theoretically this transfer function can be realized by a number of filter types. In this work, the analog FIR filter will be used to realize this transfer function by generating a desired frequency dependence of phase and amplitude. An example of a desired response in both amplitude and phase is sketched in Fig.6.31.

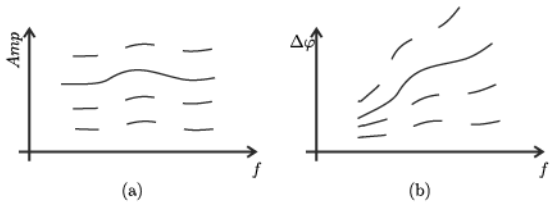

Fig. 6.31: Desired Amplitude and Phase response of weights in a 4-element Array beamformer.

In principle, one can see the FIR filter BFN as an extension of the TTD-BFN with integrated weight control and additional degrees of freedom by inserting several delays at the same time.

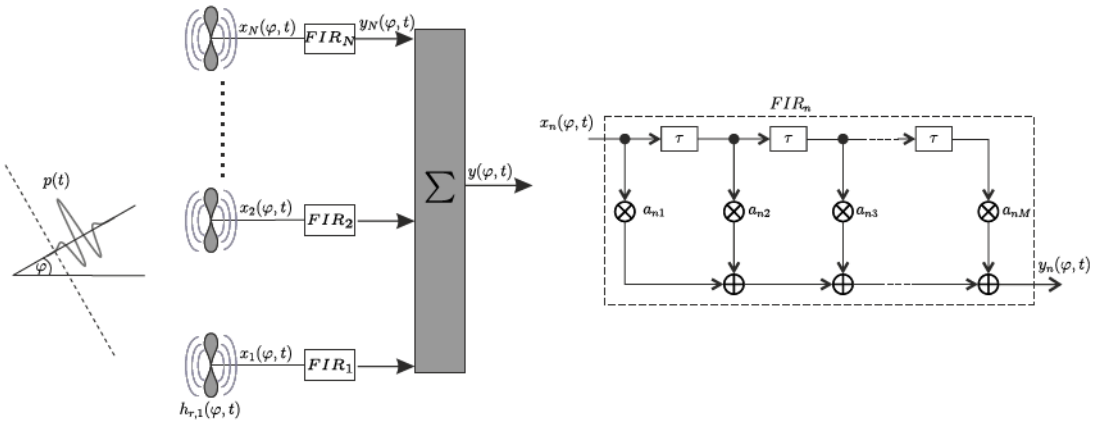

Fig. 6.32: (a) N-element ULA Beamforming Using FIR filter (b) structure of a single M order FIR Filter

In Fig.6.32(a), a ULA is shown with N elements, and inter-element spacing d, with

$$d = \frac{c_0}{2f_h} \tag{6.6.1}$$

and c_0 is the velocity of light, and f_h is the upper limit of the frequency band. Each antenna is connected to M-order FIR filter. Following [Nei08], assuming the received signal from the nth antenna is $x_n(\varphi,t)$ which can be calculated as follows

$$x_n(\varphi,t) = p(t) * h_{r,n}(\varphi,t) * \delta(t - t_{0,n}) \tag{6.6.2}$$

Where $p(t)$ is the transmitted UWB pulse, $(*)$ denotes convolution, $\delta(.)$ is the Dirac delta function. $h_{r,n}(\varphi,t)$ is the angle dependent transient impulse response of the received antenna n. Assuming all antenna elements are identical, then $h_{r,n}(\varphi,t) = h_a(\varphi,t)$. $t_{0,n}$ is the spatial delay of the nth antenna element and can be calculated as follows

$$t_{0,n} = (n-1)\,t_0 = (n-1)\,\frac{d}{c_0}\,sin\varphi \tag{6.6.3}$$

The filter output signal is defined as $y_n(\varphi,t)$ and can be calculated as follows

$$y_n(\varphi,t) = x_n(\varphi,t) * \sum_{m=1}^{M} a_{nm}\delta(t - (m-1)\,\tau) \tag{6.6.4}$$

a_{nm} is a weighting coefficient, where $-1 \leq a_{nm} \leq 1$ and τ is the incremental time delays of the FIR filter and chosen to be equal

$$\tau = \frac{d}{c_0} \tag{6.6.5}$$

The overall output signals $y(\varphi,t)$ can be obtained by summation

$$y(\varphi,t) = \sum_{n=1}^{N} y_n(\varphi,t) \tag{6.6.6}$$

$$y(\varphi,t) = p(t) * h_a(\varphi,t) * \sum_{n=1}^{N}\sum_{m=1}^{M} a_{nm}\delta\left(t-(m-1)\tau\right) * \delta(t-(n-1)t_0) \tag{6.6.7}$$

Applying the Fourier transformation on Equation 6.6.7

$$Y(\varphi,f) = P(f)\cdot H_a(\varphi,f)\cdot \sum_{n=1}^{N}\sum_{m=1}^{M} a_{nm}\ \cdot e^{-j2\pi f((m-1)\tau+(n-1)t_0)} \tag{6.6.8}$$

The frequency response of the overall system $H_{arr}(\varphi,f)$ is

$$H_{arr}(\varphi,f) = \frac{Y(\varphi,f)}{P(f)} = H_a(\varphi,f)\cdot \sum_{n=1}^{N}\sum_{m=1}^{M} a_{nm}\cdot\ e^{-j2\pi f((m-1)\tau+(n-1)t_0)} \tag{6.6.9}$$

For simplicity, antenna elements can be assumed to be an isotropic radiator which means $H_a(\varphi,f) = 1$. With this, the transfer function describes the BFN only and can be calculated as follows

$$H_{BFN}(\varphi,f) = \sum_{n=1}^{N}\sum_{m=1}^{M} a_{nm}\cdot\ e^{-j2\pi f((m-1)\tau+(n-1)t_0)} \tag{6.6.10}$$

Equation 6.6.10 represents a two dimensional summation of time-delayed weighting coefficients. The phase shifts come from the spatial delay in the antenna array and the incremental time delay of the FIR filters. After the math behind the FIR Filter based BFN was introduced, the challenge is be to calculate the FIR filter coefficients related to a desired radiation pattern and frequency range. By selecting the right $\{a_{nm}, N, \text{and } M\}$, almost any desired radiation pattern can be approximately realized. The design procedure will be as follows:

1. Design of a desired radiation reference pattern $H_{Ref}(\varphi,f)$. This pattern will cover specifications such as main beam direction, nulls position, SLL, and specific HPBW. This requirement will be valid for a frequency range between the lower frequency limit f_l and higher frequency limit f_h. One can use any known array synthesis technique for this step.
2. These requirements will limit the group of antenna elements which can be used, and the array geometry which can be applied, where f_h will define the parameters d and τ.
3. Choosing initial values for antenna element number N, and filter order M and calculating the filter coefficients a_{nm}, the next section will discuss this point in details.
4. Using the new calculated filter coefficients the transfer function of the BFN $H_{BFN}(\varphi,f)$ can be calculated.
5. Applying the decision criterium of the cross-correlation between $H_{Ref}(\varphi,f)$ and $H_{BFN}(\varphi,f)$ to be higher than a threshold value. If this condition is fulfilled, then the goal is reached, else one should increase N, M, or both until the goal is achieved.

6.6.2 Calculating the Filter Coefficients:

This section will show the calculation (or approximation) of the filter coefficients which are required to meet the design specifications. Several methods are available, but the most commonly used methods are [Che02]:

1. Window method
2. Frequency sampling method
3. Optimal Method

In this work, the last method will be used, as it is the most flexible and efficient one, although it needs more calculation time compared to the other methods. Filter coefficients can be obtained using different algorithms based on mathematical optimization; for example, least squares method or convex optimization. The idea behind this optimization is to minimize the error difference between the beamforming transfer function and the reference pattern, as shown in equation:

$$\text{minimize} \left\| H_{BFN}(\varphi, f) - H_{Ref}(\varphi, f) \right\| \tag{6.6.11}$$

where $\|\cdot\|$ is the norm of error difference. In this work, the SeDuMi software package (GNU/GPL open source license) in Matlab was used. As this is an optimization problem, meeting the specification is not guaranteed. N, and M can be increased to achieve the optimization goals, As expected, increasing these parameters will minimize the error, but at the same time, there is need to use the minimum required of N and M in order to reduce the size and cost of the final design of the antenna array BFN. In order to control the quality of optimization, the error function can be checked or calculate the correlation coefficient ρ based on equation 6.4.9 , which shows the strength of the correlation of the two transfer functions. As shown in equation 6.4.9, the correlation coefficient is frequency dependent. An average correlation coefficient can be calculated as

$$\overline{\rho} = \frac{1}{N_f} \sum_{f_i}^{N_f} \rho(f_i) \tag{6.6.12}$$

where N_f is number of the frequency points. In this case, the goal is reached when $\overline{\rho} \geq \rho_{Ref}$ and ρ_{Ref} is a predefined threshold value. Ideally, the correlation coefficient should be equal to 1, and this happens when an infinite number of antenna elements and infinite filter order are used; however in practice, N and M are limited. Fig.6.33, shows a plot of average correlation coefficients as a function of N and M for an example array. By increasing M, $\overline{\rho}$ increases and comes close to 1, until at a certain value of M , no improvement appears in $\overline{\rho}$. This shows clearly that both N and M are important to increase $\overline{\rho}$ and in this case N should be increased. From Fig.6.33, one can also read the minimum value of N and M which are needed to achieve a certain correlation coefficient. For example, $N = 7$ and $M = 7$ is enough to produce $\overline{\rho} \geq 0.9$.

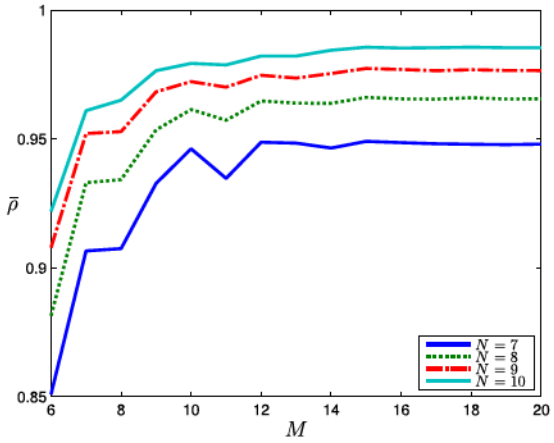

Fig. 6.33: Example average correlation coefficient as a function of array element number N and filter order M.

6.6.3 Design Example

In this section a broadband beamforming array for the EU UWB frequency band will be designed. The design procedure starts with generating a reference pattern $H_{Ref}(\varphi, f)$ under some specification. A 7-element ULA was used to generate this pattern, as shown in Fig.6.35 (red dashed line). Table 6.3, shows parameters which will control the algorithm for the calculation of the filter coefficients.

f_l	f_h	$d = c_0/(2f_h)$	$\tau = 1/(2f_h)$	N	M
6 GHz	8.5 GHz	1.76 cm	58.82 ps	9	9

Table 6.3: Design Parameter for EU-UWB beamforming.

The final optimization results are shown in Fig.6.35, where the radiation patterns for selected frequencies are plotted. There is very good agreement between the reference pattern and the optimized one, although an exception appears at the higher frequency edge ($f = 8.5\ GHz$) ; but because only one SLL is higher than expected, there is still good agreement in the main beam direction. This error is dependent on the main beam direction.

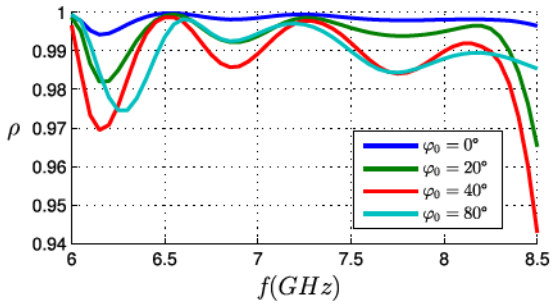

Fig. 6.34: Correlation Coefficient as a function of frequency at different beam direction, optimization is done for frequency band [6 - 8.5]GHz.

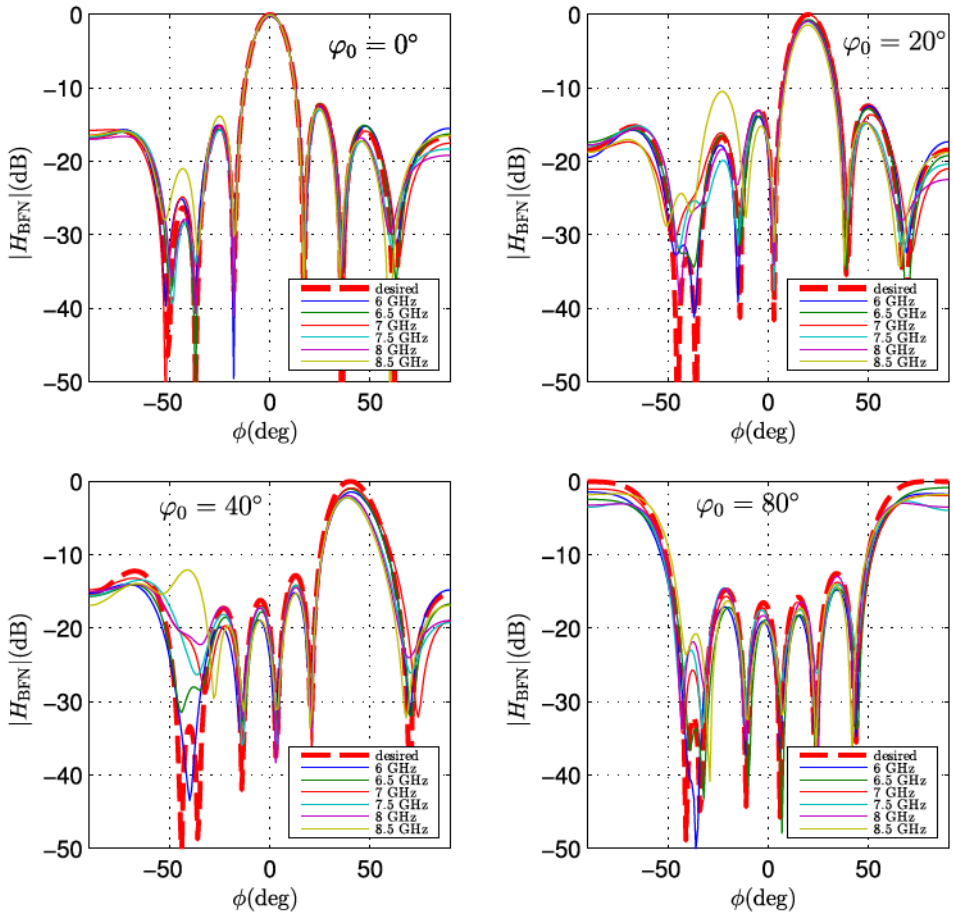

Fig. 6.35: Radiation Pattern of 9-element ULA using FIR BFN with $M = 9$ at different main beam directions.

As shown in Fig.6.34, the correlation coefficient ρ is close to 1 inside the frequency band, and decreases rapidly at the higher edge. This decrease can be explained by the optimization algorithm, in which it is hard to achieve the goal at frequency edges. In Fig.6.36, the frequency band was extended to [5.5 - 9]GHz and run the optimization algorithm again. ρ becomes smoother, and there is no sharp decrease, but still the worst case level is not improved.

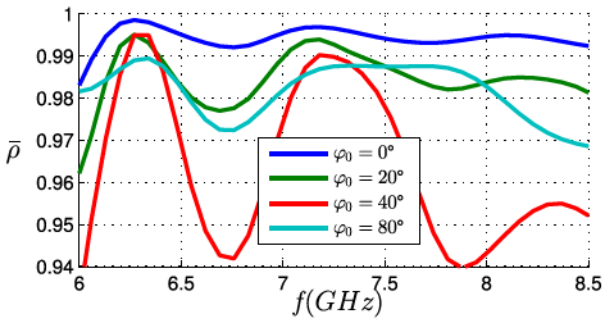

Fig. 6.36: Correlation Coefficient as a function of frequency at different beam direction, optimization are done for frequency band [5.5 - 9]GHz.

In order to improve ρ, the filter order M and/or the antenna element N should be increased. Fig.6.37 shows the relation between N and M for a fractional bandwidth

$f_h/f_l = 2$. It is clear that increasing N and M will produce a beamforming pattern closer to the reference one (ρ close to 1). The goal in this design example is to determine the minimum N and M that will achieve this specification, in order to reduce the size and cost of the BFN. As N and M are dependent on too many parameters, $\{d, \tau, BW, HPBW, SLL, \varphi_0, \text{etc.}\}$ design, a general formula for N and M is not possible.

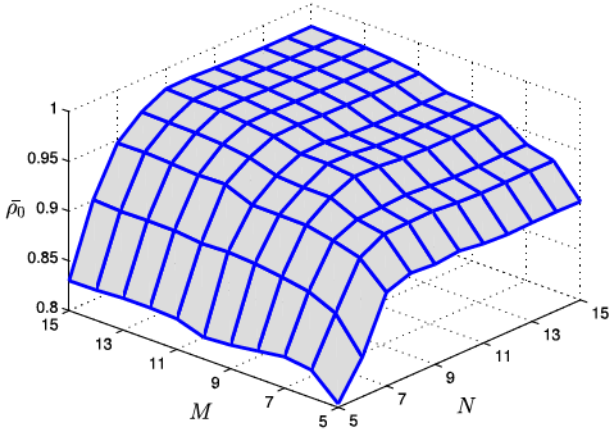

Fig. 6.37: Correlation factor as a function of antenna element N and filter order M with fractional bandwidth $f_h/f_l = 2$.

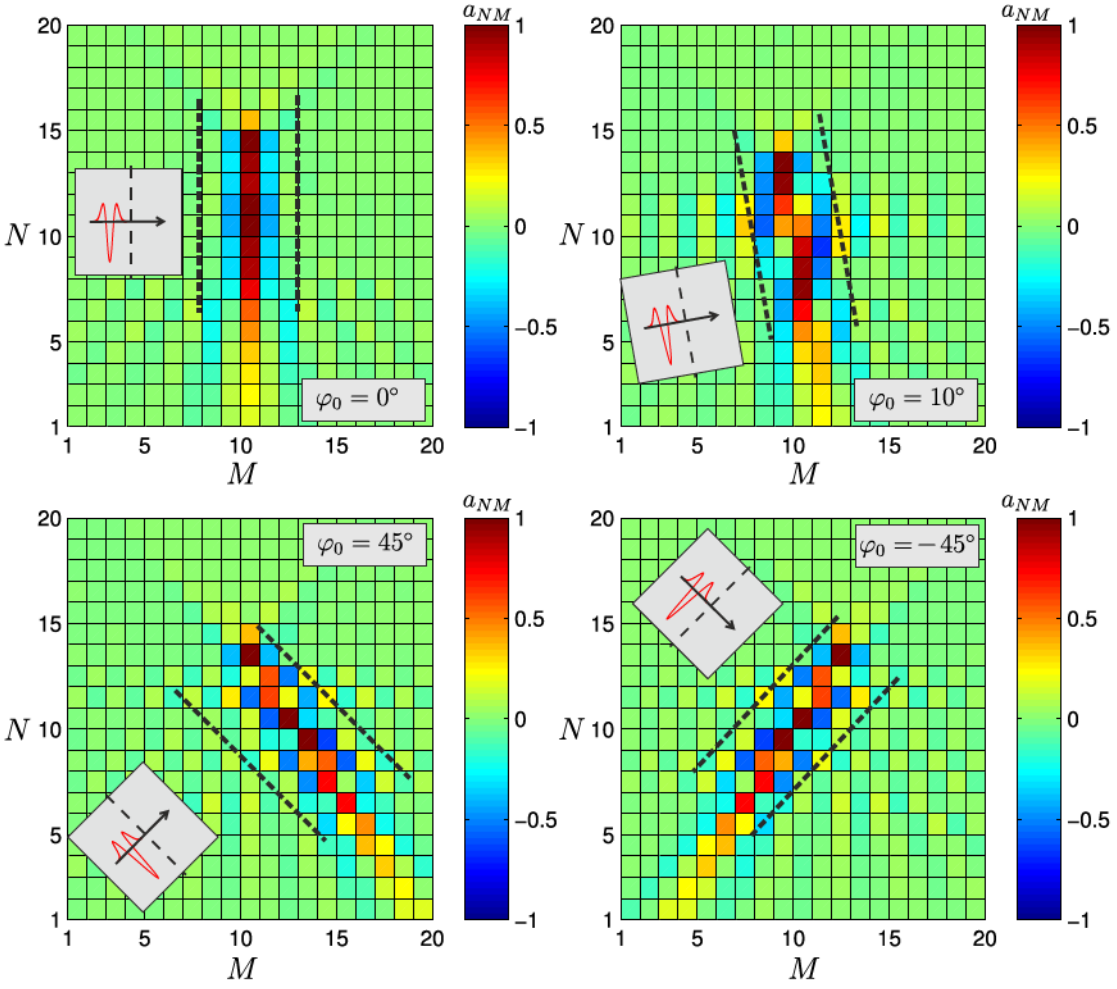

Fig. 6.38: Filter coefficients for *N=20* and *M=20* for a ULA at different beam direction.

Fig.6.38, shows a plot of the weighting coefficients a_{nm} for a 20-element ULA and FIR filter order $M = 20$. The major filter coefficients ($a_{nm} \cong \pm 1$) are located in a line which indicates the beam direction. In case $\varphi_0 = 0°$, the filter coefficients are symmetrically distributed around the center filter order $M = 10$, and these coefficients then rotate as a function of the beam direction see, $\varphi_0 = \{10°, 50°, -50°\}$. The other coefficients are much smaller than 1 but these coefficients are necessary to realize good agreement of the transfer function with the reference pattern over the frequency band, as proven by Fig.6.33. As the beam direction moves from broadside, $\varphi_0 = 0°$, the required delay is increased. In the main beam direction φ_0 , the distribution of coefficients looks similar to a simple true-time delay BF, where the received signals are delayed and summed constructively; for other angles, the superposition is more complex and the result is a partly destructive superposition.

CHAPTER 7

CONCLUSION AND FUTURE WORK

In this chapter we conclude the thesis by summarizing our contributions and discussing some guidance for future work. In this thesis, we have focused on developing an analog FIR filter in MIC technology for the UWB frequency band, and an implementation of the filter is demonstrated based on the new active node concept. The measurement results proved the new concept and also validated the simulation result.
Based on this measurement result different application designs for the analog FIR filter have been presented such as:

- Adaptive analog filtering
- Pulse shaping circuits
- Beamforming network

These applications support new services to coexist with current radio systems with minimal or no interference, as well as promise greater functionality, better channel selectivity, reduced size, lower power consumption, and at the end lower cost. Using FIR filters in a beamforming network we were able to design a broadband beamforming array for the EU UWB frequency band. The final optimization results produce a very good agreement between the reference and optimized pattern as well as a high (close to 1) average correlation coefficient $\overline{\rho}$ for the whole frequency band. Different ways of controlling the antenna array beam pattern are discussed, such as amplitude weighting and null steering. Adaptive antenna and adaptive nulling receive antenna systems are becoming important in communication applications and Radar to minimize (null) the received power from one or more interference sources (undesired signal). The concept of adaptive nulling using FIR filters is proven by example of a wideband beamformer for the EU UWB frequency band with insertion of specific nulls in certain direction.

The results of this dissertation point to several interesting directions for future work:

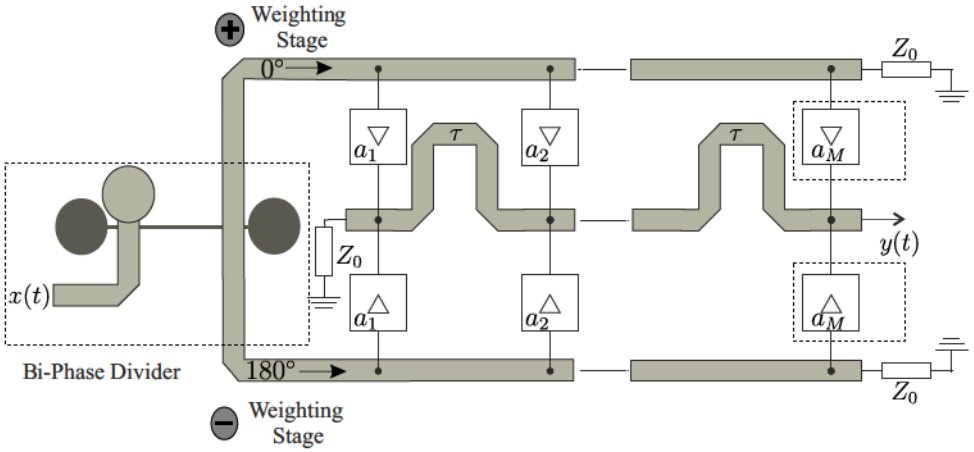

Fig. 7.1: Transpose Triple Line Analog UWB FIR Filter

A compact circuit size is always a desire in microwave circuits. A way to reduce the overall size of a triple line FIR filter could be to apply the delay line in the output line instead of in two parallel delay input lines. The new design of the Transpose Triple Line Analog UWB FIR filter is shown in Fig. 7.1. Another improvement may be achieved by reducing the filter order as done in section 4.5.2 by defining a threshold value and replacing all filter coefficients within this threshold by zero. The weighting stages with zero coefficients are omitted, but the delay line goes on for the next nonzero coefficients.
This thesis showed that analog UWB FIR filter is technically feasible in MIC technology using the active node concept. On the other hand, the travelling wave concept is feasible using MMIC technology. However, for both concepts practical implementation would require small size and low cost and this requires MMIC technology. In addition, all the other MMIC technology advantages can be used such as flexibility, broadband performance, reproducibility, and reliability.

Currently, there are no existing examples or designs of MMIC analog FIR filter circuits, which operate over the complete UWB band. As a result, a great deal of research will need to be spent on the creation of new circuits and the modification of existing circuits to design and evaluate a future MMIC analog UWB FIR filter and achieve a proven design model.

BIBLIOGRAPHY

ABH+11 Ashby, D. ; Baker, B. ; Hickman, I. ; Kester, W. ; Pease, R. ; Williams, T. ; Zeidman, B.: *Circuit Design: Know It All: Know It All.* Elsevier Science, 2011 (Newnes Know It All). – ISBN 9780080949659

ABS+05 Allen, Ben ; Brown, Tony ; Schwieger, Katja ; Zimmermann, Ernesto ; Malik, Wasim ; Edwards, David ; Ouvry, Laurent ; Oppermann, Ian: Ultra wideband: Applications, technology and future perspectives. In: *International Workshop On Convergent Technologies (IWCT)*, 2005

ACDB06 Arslan, H. ; Chen, Z.N. ; Di Benedetto, M.G.: *Ultra Wideband Wireless Communication.* Wiley, 2006. – ISBN 9780470042380

ADO+06 Allen, B. ; Dohler, M. ; Okon, E. ; Malik, W. ; Brown, A. ; Edwards, D.: *Ultra Wideband Antennas and Propagation for Communications, Radar and Imaging.* Wiley, 2006. – ISBN 9780470056820

AG05 Allen, Ben ; Ghavami, Mohammad: *Adaptive array systems - fundamentals and applications.* John Wiley & Sons, Inc., 2005

AGG04 Allen, B. ; Ghorashi, S.A. ; Ghavarm, M.: A review of pulse design for impulse radio. In: *Ultra Wideband Communications Technologies and System Design, IEE Seminar on*, 2004, S. 93–97

Agi10 Agilent Technologies, Inc. (Hrsg.): *User's Manual for ADS.* Agilent Technologies, Inc., July 2010

Agi12 Agilent: *Applying the 8510 TRL Calibration for Non-Coaxial Measurements*, 2012

ASA+09 Adamiuk, Grzegorz ; Sczyslo, Sebastian ; Arafat, Saeed ; Wiesbeck, Werner ; Zwick, Thomas ; Kaiser, Thomas ; Solbach, Klaus: Infrastructure-Aided Localization with UWB Antenna Arrays. In: *Frequenz, Journal of RF-Engineering and Telecommunications* 63 (2009), S. 210–213

Ava12 Avago, Technologies.: *Gain Blocks and Drivers.* `http://www.avagotech.com/pages/en/rf_microwave/amplifiers/gain_block_and_drivers/2503/`. Version: September 2012

BA07 Bialkowski, M.E. ; Abbosh, A.M.: Design of a Compact UWB Out-of-Phase Power Divider. In: *Microwave and Wireless Components Letters, IEEE* 17 (2007), Nr. 4, S. 289–291. – ISSN 1531–1309

Bal05 Balanis, Constantine A.: *Antenna theory - analysis and design*. 3rd. John Wiley & Sons, Inc., 2005

BU08 Bevelacqua, P.J. ; University, Arizona S.: *Antenna Arrays: Performance Limits and Geometry Optimization*. Arizona State University, 2008. – ISBN 9780549452782

Che02 Chen, W.K.: *The Circuits and Filters Handbook, Second Edition*. Taylor & Francis, 2002 (Circuits & Filters Handbook 3e). – ISBN 9781420041408

CIW06 Chong, Chia-Chin ; Inamura, H. ; Watanabe, F.: Potential of UWB Technology for the Next Generation Wireless Communications. In: *Spread Spectrum Techniques and Applications, 2006 IEEE Ninth International Symposium on*, 2006, S. 422–429

CR90 Cornett, F. ; Reynolds, D.K.: Continuous-time adaptive signal processing. In: *Southeastcon '90. Proceedings., IEEE*, 1990, S. 929–933 vol.3

DBG04 Di Benedetto, M.G. ; Giancola, G.: *Understanding Ultra Wide Band Radio Fundamentals*. Pearson Education, 2004. – ISBN 9780132441834

DPG+98 Drabowitch, S. ; Papiernik, A. ; Griffiths, H. ; Encinas, J. ; Smith, B. L.: *Modern antennas*. Chapmann & Hall, 1998

Eur07 European, Union: Official Journal of the European Union, 23.2.2007, L.55/33-36. 2007. – Technical Report

Fed02 Federal Communication Commission: Revision of part 15 of the commission's rules regarding ultra wideband transmission systems / ET Docket 98-153, FCC 02-48. 2002. – First Report and Order

Fen08 Fenn, A.J.: *Adaptive Antennas and Phased Arrays for Radar and Communications*. Artech House, Incorporated, 2008 (Artech House radar library). – ISBN 9781596932739

Fen10 Fenn, Alan J.: *Adaptive Antennas and Phased Arrays*. `http://ocw.mit.edu`. Version: 2010.. – RES.LL-002

Fou00 Fourikis, N.: *Advanced Array Systems, Applications and Rf Technologies*. Academic Press [Imprint], 2000 (Electronics & Electrical). – ISBN 9780122629426

Fre94 Frerking, Marvin: *Digital Signal Processing in Communications Systems*. Springer, 1994. – ISBN 9780442016166

FS91 Feldle, H.-P. ; Solbach, K.: Passive and active phased arrays using solid state technologies. In: *Phased Arrays, IEE Colloquium on*, 1991, S. 3/1–3/4

Fu09 Fu, Jia-Shiang: *Adaptive Impedance Matching Circuits Based on Ferroelectric and Semiconductor Varactors* -. Ann Arbor : ProQuest, 2009. – ISBN 978–1–109–11488–1

GLW98 Gschwendtner, E. ; Loffler, D. ; Wiesbeck, W.: Conformal Microstrip Antenna Array with Hemispherical Coverage for Mobile Users of Future Satellite Systems. In: *Microwave Conference, 1998. 28th European* Bd. 1, 1998, S. 535–539

GMK07 Ghavami, Mohammad ; Michael, Lachlan B. ; Kohno, Ryuji: *Ultra Wideband - Signals and systems in communication engineering.* 2nd. ed. John Wiley & Sons, Inc., 2007

God97 Godara, Lal C.: Application of antenna arrays to mobile communications, part II: beam-forming and direction-of-arrival considerations. In: *IEEE Proceedings* 85 (1997), Aug., Nr. 8, S. 1195–1245

GRA03 G. Robert Aiello, Gerald R.: Ultra Wide-Band Wireless Systems. In: *IEEE Microwave Magzine* (2003), S. 36–47

Han09 Hansen, R.C.: *Phased Array Antennas.* Wiley, 2009 (Wiley Series in Microwave and Optical Engineering). – ISBN 9780470529171

Hit14 Hittite, Microwave C.: *Tunable Filter.* `https://www.hittite.com/products/index.html/category/342`. Version: Juli 2014

IB05 Ioannides, P. ; Balanis, C.A.: Uniform circular arrays for smart antennas. In: *Antennas and Propagation Magazine, IEEE* 47 (2005), Aug., Nr. 4, S. 192–206

Ims12 Imst GmbH (Hrsg.): *User's Manual for EMPIRE.* Imst GmbH, July 2012

INT07 INTEL: Ultra-Wideband (UWB) Technology / INTEL. 2007. – Technical Report

JP06 Josefsson, L. ; Persson, P.: *Conformal Array Antenna Theory and Design.* Wiley, 2006 (IEEE Press Series on Electromagnetic Wave Theory). – ISBN 9780471780113

KM02 Kraus, J.D. ; Marhefka, R.J.: *Antennas for all applications.* McGraw-Hill, 2002 (McGraw-Hill series in electrical engineering). – ISBN 9780072321036

KMO+06 Kaiser, Thomas ; Molisch, Andreas F. ; Oppermann, Ian ; Benedett, Maria Gabriella D. ; Porcino, Domenico: *UWB Communication Systems - A Comprehensive Overview.* Hindawi Publishing Corporation, 2006. – ISBN 978–9–775–94510–5

KRC06 Karumudi Rambabu, Kevin Khee-Meng C. Adrian Eng-Choon Tan T. Adrian Eng-Choon Tan ; Chia, Michael Yan-Wah: Study of Antenna Effect on UWB Pulse Shape in Transmission and Reception. In: *International Symposium on Antennas and Propagation* (2006)

Ksh09 Kshetrimayum, R.S.: An introduction to UWB communication systems. In: *Potentials, IEEE* 28 (2009), Nr. 2, S. 9–13. – ISSN 0278–6648

KZ10 Kaiser, T. ; Zheng, F.: *Ultra Wideband Systems with MIMO.* Wiley, 2010 `http://books.google.de/books?id=D15M_FLNPGwC`. – ISBN 9780470740002

LKM06 Li, Keren ; Kurita, D. ; Matsui, T.: UWB Bandpass Filters with Multi Notched Bands. In: *Microwave Conference, 2006. 36th European*, 2006, S. 591–594

mic12 microwaves101.: *Owen resistive splitter.*. `http://www.microwaves101.com/encyclopedia/Resistive_splitter2.cfm`. Version: September 2012

Mil05 Milligan, Thomas A.: *Modern antenna design*. 2nd edition. John Wiley & Sons, Inc., 2005

Mix09 Analog Devices: Mixers and Modulators. Version: 2009. `//www.analog.com/static/imported-files/tutorials/MT-080.pdf`. 2009. – Technical Report

MLE09 Mukhopadhyay, S.C. ; Lay-Ekuakille, A.: *Advances in Biomedical Sensing, Measurements, Instrumentation and Systems*. Springer Berlin Heidelberg, 2009 (Lecture notes in electrical engineering). – ISBN 9783642051678

MM80 Monzingo, R.A. ; Miller, T.W.: *Introduction to Adaptive Arrays*. Scitech, 1980. – ISBN 9781891121241

MR90 Mokari, M.E. ; Rubin, M.: Design and realization of transversal microwave bandpass filters. In: *Circuits and Systems, 1990., IEEE International Symposium on*, 1990, S. 1513–1516 vol.2

MSF07 Maxwell, E.N. ; South Florida, University of: *Ultra-wideband Electronics, Design Methods, Algorithms, and Systems for Dielectric Spectroscopy of Isolated B16 Tumor Cells in Liquid Medium*. University of South Florida, 2007. – ISBN 9780549553007

NEHH+06 Neinhüs, Markus ; El-Hadity, Mohammed ; Held, Sebastian ; Kaiser, Thomas ; Solbach, Klaus: An ultra wideband linear array beamforming concept considering antenna and channel effects. In: *European Conference on Antennas and Propagation*. Nice, France, Nov. 2006

Nei08 Neinhüs, Markus: *FIR-Filter basierte Steuerung von ultrabreitbandigen Gruppenantennen*, Fakultät für Ingenieurwissenschaften der Universität Duisburg-Essen, PhD Thesis, 2008

Nek11 Nekoogar, Faranak: *Ultra-Wideband Communications - Fundamentals and Applications*. New Jersey : Prentice Hall PTR, 2011. – ISBN 978–0–132–78223–4

NGM+05 Nath, J. ; Ghosh, D. ; Maria, J-P ; Kingon, Angus I. ; Fathelbab, W. ; Franzon, P.D. ; Steer, M.B.: An electronically tunable microstrip bandpass filter using thin-film Barium-Strontium-Titanate (BST) varactors. In: *Microwave Theory and Techniques, IEEE Transactions on* 53 (2005), Sept, Nr. 9, S. 2707–2712. `http://dx.doi.org/10.1109/TMTT.2005.854196`. – DOI 10.1109/TMTT.2005.854196. – ISSN 0018–9480

NHS07 Neinhus, M. ; Held, S. ; Solbach, K.: FIR-filter based equalization of ultra wideband mutual coupling on linear antenna arrays. In: *Antennas, 2007. INICA '07. 2nd International ITG Conference on*, 2007, S. 115–119

NS11 Neinhus, M. ; Solbach, K.: Finite impulse response-filter-based RF-beamforming network for wideband and ultra-wideband antenna arrays. In: *Microwaves, Antennas Propagation, IET* 5 (2011), Nr. 7, S. 844–851. – ISSN 1751–8725

OHI04 Oppermann, Ian ; Hämäläinen, Matti ; Iinatti, Jari: *UWB Theory and Applications*. John Wiley & Sons, Inc., 2004

Pan09 Pancera, Elena: *Strategies for Time Domain Characterization of UWB Components and Systems.*, Universitätsverlag Karlsruhe, PhD Thesis, 2009

Pat03 Pattan, Bruno: A BRIEF EXPOSURE TO ULTRA-WIDEBAND SIGNALING. In: *MICROWAVE JOURNAL* (2003), S. 104–108

Ram01 Ramsden, Ed: *An Introduction to Analog Filters*. `http://www.sensorsmag.com/sensors/electric-magnetic/an-introduction-analog-filters-1023`. Version: July 2001

Rau85 Rauscher, C.: Microwave Active Filters Based on Transversal and Recursive Principles. In: *Microwave Theory and Techniques, IEEE Transactions on* 33 (1985), Nr. 12, S. 1350–1360. – ISSN 0018–9480

RB08 Rulikowski, P. ; Barrett, J.: Adaptive Arbitrary Pulse Shaper. In: *Microwave and Wireless Components Letters, IEEE* 18 (2008), Nr. 5, S. 356–358. – ISSN 1531–1309

Ree05 Reed, Jeffrey H. ; Reed, Jeffrey H. (Hrsg.): *An Introduction to Ultra Wideband Communication Systems*. Prentice Hall, 2005 (Prentice Hall Communications Engineering and Emerging Technologies)

RFSL04 Roy, S. ; Foerster, J.R. ; Somayazulu, V.S. ; Leeper, D.G.: Ultrawideband radio design: the promise of high-speed, short-range wireless connectivity. In: *Proceedings of the IEEE* 92 (2004), Nr. 2, S. 295–311. – ISSN 0018–9219

RMP75 Rabiner, L. ; McClellan, J.H. ; Parks, T.W.: FIR digital filter design techniques using weighted Chebyshev approximation. In: *Proceedings of the IEEE* 63 (1975), Nr. 4, S. 595–610. – ISSN 0018–9219

Roh14 Rohde&Schwarz: *MB-OFDM UWB*. `http://www.rohde-schwarz.fr/fr/Produits/Test_Mesure/Signal_Generators/AFQK264.html`. Version: 2014. – Rohde&Schwarz

Ros07 Rosas, Bill: *Optimizing Test Boards for 50 GHz End Launch Connectors*. `http://mpd.southwestmicrowave.com/showImage.php?image=439`. Version: 2007. – Southwest Microwave, Inc

SOH+03 Sheng, Hongsan ; Orlik, P. ; Haimovich, A.M. ; Cimini, L.J. ; Zhang, Jinyun: On the spectral and power requirements for ultra-wideband transmission. In: *Communications, 2003. ICC '03. IEEE International Conference on* Bd. 1, 2003, S. 738–742 vol.1

Sol12 Solbach, Prof. Dr.-Ing. K.: *Antennas for Communications*. University Lecture. `http://www.uni-due.de/hft/ant.php`. Version: 2012

Sta07 Standard ECMA-368 2nd edition: *High Rate Ultra Wideband PHY and MAC Standard*. December 2007

Tay95 Taylor, J.D.: *Introduction to Ultra Wideband Radar Systems*. CRC Press, 1995. – ISBN 9780849344404

Tex12 Texas, Instruments: RF-Sampling and GSPS ADCs Breakthrough ADCs Revolutionize Radio Architectures / Texas Instruments. 2012. – Technical Report

TJ06 Tsai, Chih-Yung ; Jeng, Shyh-Kang: Design of an ultra-wideband waveform shaping network using an analog microwave differentiator array fed by a Gaussian pulse signal. In: *Antennas and Propagation Society International Symposium 2006, IEEE*, 2006, S. 1307–1310

Van02 Van Trees, Harry L.: *Optimum array processing - part IV of detection, estimation and modulation theory*. John Wiley & Sons, Inc., 2002

Vis06 Visser, H.J.: *Array and Phased Array Antenna Basics*. Wiley, 2006. – ISBN 9780470871188

VVB88 Van Veen, B.D. ; Buckley, K.M.: Beamforming: a versatile approach to spatial filtering. In: *ASSP Magazine, IEEE* 5 (1988), Nr. 2, S. 4–24. – ISSN 0740–7467

ZM07 Zhang, R. ; Mansour, R.R.: Novel digital and analogue tunable lowpass filters. In: *Microwaves, Antennas Propagation, IET* 1 (2007), June, Nr. 3, S. 549–555. – ISSN 1751–8725